The role of OTULIN in skin inflammation and cell death

Inaugural-Dissertation
zur
Erlangung des Doktorgrades
der Mathematisch-Naturwissenschaftlichen Fakultät
der Universität zu Köln

vorgelegt von
Hannah Schünke

aus Bergisch Gladbach

Köln, 2021

Berichterstatter:	Prof. Dr. Manolis Pasparakis
	Prof Dr. Hamid Kashkar
	Prof. Dr. Ulrich Baumann

Tag der mündlichen Prüfung: 16.04.2021

Zusammenfassung

Das Hautepithel bildet eine physikalisch und immunologisch aktive vielschichtige Barriere, welche vor Pathogenen und Umweltfaktoren schützt und gezielte Immunantworten zu externen und internen Stimuli aktiviert. Eine besondere Rolle zur Instandhaltung der Haut-Homöostase spielen hierbei Mechanismen, die das Überleben oder den Tod einer Zelle regulieren. Entzündungs- und Zelltod-Signalwege, die angeborene Immunantworten auslösen können, werden mit Hilfe von linearen Ubiquitin-Ketten reguliert, die von der E3-Ligase LUBAC (Linear ubiquitin assembly complex) gesteuert werden. OTULIN (OTU deubiquitinase with linear specificity) hingegen ist ein deubiquitinierendes Enzym, welches spezifisch lineare Ubiquitin-Ketten degradiert. Maus-Studien konnten bereits zeigen, dass der Verlust von OTULIN zu einem zusätzlichen Ausfall der LUBAC Komponenten und somit zu Zelltod-vermittelten Entzündungsreaktionen führt. Außerdem führen Mutationen im OTULIN-Gen zu der pathologisch komplexen humane Erkrankung ORAS, welche zu systemischen Entzündungen führt, die viele Organe und im Besonderen die Haut betreffen. Die Rolle, die OTULIN in der Regulierung der Haut-Homöostase bei Entzündungsreaktionen und im Zelltod spielt, bleibt jedoch bis heute unverstanden. Das Ziel dieser Arbeit war es herauszufinden, welche biologische Funktion OTULIN in der Haut hat und welche zellulären Prozesse dieser zugrunde liegen. Die Studie zeigt, dass OTULIN vor Hautentzündungen schützt, in dem es den Tod von Keratinozyten verhindert. Die Deletion von OTULIN in der Epidermis führt bei Mäusen zu Bildung von Hautläsionen, die auch die Schwanz-Haut betreffen. Diese veränderten Hautstrukturen ähneln Papillomen und sind mit einem Genexpressions-Profil versehen, welches auf Entzündungen hinweist. Die genetischen Studien dieser Arbeit zeigen zusätzlich, dass die Hauterkrankung durch TNFR1-vermittelten, RIPK1-Kinase-abhängigen Zelltod ausgelöst wird. Außerdem wird deutlich, dass Nekroptose die Hauptursache für die Entwicklung der Hautläsionen in OTULIN$^{E\text{-}KO}$-Mäusen ist, da der Verlust von RIPK3 und MLKL dies verhindert, wohingegen FADD-abhängige Apoptose nur eine kleine Rolle zu spielen scheint. Des Weiteren scheinen auch Reaktionen auf die bakterielle Haut-Flora zur Pathogenese in OTULIN$^{E\text{-}KO}$-Mäusen beizutragen, da der Verlust von MyD88 die Entwicklung der Hauterkrankung stark verzögert und abschwächt. Zusammenfassend verdeutlichen die Daten in dieser Studie, dass OTULIN eine Schlüsselrolle in der Epidermis innehat, da es vor Zelltod, sowie Entzündung schützt und dadurch die Erhaltung der Hauthomöostase bestimmt.

Abstract

The skin epithelium provides a physical and immunologically active multilayered barrier that protects the body from environmental factors and mediates cellular immune responses. Especially mechanisms regulating the cell survival and cell death of epidermal keratinocytes play a crucial role in maintaining tissue homeostasis. Inflammatory and cell death signalling is tightly controlled by linear ubiquitination, mediated via the E3 ligase Linear Ubiquitin Assembly Complex (LUBAC) to initiate innate immune responses. LUBAC itself is controlled by OTU deubiquitinase with linear specificity (OTULIN), a deubiquitinating enzyme that specifically degrades linear ubiquitin chains. Mouse model studies suggested that OTULIN deficiency results in loss of LUBAC components and cell death-mediated inflammation. Interestingly, mutations in the gene encoding OTULIN cause the OTULIN-related autoinflammatory syndrome (ORAS), a human genetic disease presented with complex pathological features and systemic inflammation affecting multiple organs, including the skin. The role of OTULIN in regulating skin homeostasis, inflammation and cell death is poorly understood and remains to be elucidated. The aim of this study was to investigate the biological function of OTULIN in the skin and to unravel the underlying cellular processes. The results acquired in this thesis reveal that OTULIN prevents skin inflammation by inhibiting keratinocyte necroptosis. In detail, deleting OTULIN in the mouse epidermis causes skin lesions that develop in different parts of the skin, including the tail. Those lesions resemble papilloma-like structures and are displayed with an inflammatory gene expression profile. Our genetic studies demonstrate that this skin pathology is driven by TNFR1 mediated RIPK1 kinase-dependent cell death. Furthermore, RIPK3 and MLKL deficiency strongly protect mice lacking OTULIN in keratinocytes from skin inflammation, thereby identifying necroptosis as a key driver, whereas FADD-dependent apoptosis plays a minor role in the skin disease development. Additionally, MyD88 deficiency strongly delayed and ameliorated skin pathology, implying that microbiota-dependent stimuli contribute to the pathogenesis in $OTULIN^{E\text{-}KO}$ mice. Taken together, the data presented in this study uncover a key role for OTULIN in the epidermis in preventing cell death and inflammation to maintain skin homeostasis.

Table of content

Table of figures

List of tables

List of Abbrevations

ABC	Avidin-biotin-complex
ABIN	A20-binding inhibitor of NF-κB activation 1
AKT	Protein kinase B
APAF-1	Apoptotic protease activating factor 1
A20	Tumor necrosis factor alpha-induced protein 3
BAFF	B-cell activating factor of the TNF family
BAK	Bcl-2 homologous antagonist/killer
BCL-2	B-cell lymphoma 2
Bid	BH3 interacting domain death agonist
BSA	Bovine serum albumin
CC3/8/9	Cleaved caspase-3/8/9
CC	Coiled-coiled
CD40L	Cluster of differentiation
cDNA	Complementary DNA
cFLIP	Cellular FLICE-like inhibitory protein
CHX	Cycloheximide
cIAP1/2	Cellular inhibitor of apoptosis protein 1/2
Cre	Causes recombination
CYLD	Cylindromatosis (protein)
Cpdm	Chronic proliferative dermatitis
DAB	Diaminobenzidine
DAMP	Damage-associated molecular pattern
DD	Death domain
ddH2O	Double-distilled water
DED	Death effector domain
Del	Deleted
DISC	Death-inducing signaling complex
DMEM	Dulbecco's modified eagle medium
DMSO	Dimethyl sulfoxide
DNA	Desoxyribonucleic acid
dNTPs	Desoxyribonucleotides
DR	Death receptor
ds	Double stranded
DTT	Dithiothreithol
DUB	Deubiquitinase
ECL	Enhanced chemiluminescence
EDTA	Etylene diamine tetraacetate
E-KO	Epidermis specific knockout
ERK	Extracellular signal related kinases
FADD	Fas (TNFRSF6)-associated via DD
FasL	Fas ligand/ CD95
FCS	Fetal calf serum
GO	Gene ontology
GSEA	Gene set enrichment analysis
HECT	Homologous to the E6-AP carboxyl terminus
H&E	Hematoxylin and eosin
Het	Heterozygous

HEPES	4-2-hydroxyethyl-1-piperazineethanesulfonicacid
HOIL-1L	Heme-oxidized IRP2 ubiquitin ligase 1 homolog
Hom	Homozygous
HOIP	HOIL-1L- interacting protein
HRP	Horseradish peroxidase
ID	Identification number
IFN	Interferon
IHC	Immunohistochemistry
IκBα	Inhibitor of NF-κB alpha
IKK1	Inhibitor of κB kinase 1
IKK2	Inhibitor of κB kinase 2
IKKε	Inhibitor of κB kinase epsilon
IL	Interleukin
IRAK	interleukin-1 receptor associated kinase
IRF	Interferon regulatory factor
ISG	Interferon stimulated gene
IVC	Individually ventilated cages
JNK	c-Jun N-terminal kinase
K6/10/14	Keratin 6/10/14
KO	Knockout
LPS	Lipopolysaccharide
LRR	Leucine rich repeat
LoxP	Locus of X-over P1
LUBAC	Linear ubiquitin chain assembly complex
MAPK	Mitogen-activated protein kinases
MEF	Murine embryonic fibroblasts
MK2	MAPK-activated protein kinase 2
MLKL	Mixed-lineage kinase domain like
mRNA	Messenger RNA
mTOR	Mammalian target of rapamycin
MyD88	Myeloid differentiation primary response gene 88
NAP1	Nucleosome assembly protein 1
NGS	Normal goat serum
Nec-1	Necrostatin-1
NEMO	NF-κB essential modulator
NF-κB	Nuclear factor kappa light polypeptide gene enhancer in B-cells
NIK	NF-κB inducing kinase
NP-40	Nonidet P40
NZF	Npl4 zinc finger
ORAS	OTULIN-related autoinflammatory syndrome
OTULIN	OTU deubiquitinase with linear linkage specificity
p	Phosphorylated
P38	MAPK p38
PAMP	Pathogen associated molecular pattern
PBS(T)	Phosphate Buffered Saline (Tween)
PFA	Paraformaldehyde
PIM	PUB interaction motif
PUB	Protein-ubiquitin binding
rb	Ribosomal

RBR	RING-between-RING
RHIM	RIP homotypic interaction motif
RING	Really interesting new gene
RIPK1	Receptor (TNFRSF)- interacting serine-threonine protein kinase 1
RIPK3	Receptor (TNFRSF)- interacting serine-threonine protein kinase 3
RNA	Ribonucleic acid
RT	Room temperature
SD	Standard deviation
SDS	Sodium dodecyl sulfate
SEM	Standard error of the mean
SHARPIN	SHANK-associated RH domain interacting protein SI
SMAC	Second mitochondria derived
SPATA2	Spermatogenesis associated 2
SPF	Specific pathogen free
ss	Single stranded
TAB1	TAK1-binding protein 1
TAB2	TAK1-binding protein 2
TAK	TGF-β-activated kinase 1
TE	Tris EDTA buffer
TEMED	N,N,N',N' Tetra Methylenediamine
TANK	TRAF family member-associated NF- κB activator
TBK1	TANK-binding kinase 1
Tbp	TATA-binding protein
Tg	Transgene
TIR	Toll-Interleukin receptor
TIRAP	TIR domain containing adaptor protein
TLR	Toll-like receptor
TNF	Tumor necrosis factor
TNFR1/2	TNF receptor 1/2
TRADD	Tumor necrosis factor receptor type 1-associated DD
TRAF	TNF receptor-associated
TRAIL	Tumor necrosis factor related apoptosis inducing ligand
TRIF	TIR-domain-containing adapter-inducing interferon-β
TWEAK	TNF-like weak inducer of
UBA	Ubiquitin associated
UBAN	Ubiquitin binding to ABIN and NEMO
UBD	Ubiquitin binding domain
UBL	Ubiquitin-like
WT	Wildtype
zVAD-fmk	Carbobenzoxy-valyl-alanylaspartyl-[O-Methyl]-fluoromethylketone
ZBP1/DAI	Z-DNA binding protein 1

Abbreviations of units

bp	Base pair	**mM**	Millimol
cm	Centimeter	**µM**	Micromol
µm	Micrometer	**nM**	nNnomol
cm	Centimeter	**mA**	milliampere
nm	Nanometer	**mol**	Mole
g	Gram	**rpm**	Revolutions per
mg	Milligram	**V**	Volt
µg	Microgram	**W**	Watt
ng	Nanogram	**°C**	Degree Celsius
kda	Kilo Dalton	**%**	Percentage
l	Liter	**h**	Hours
ml	Millimeter	**min**	Minutes
µl	Microliter	**s**	Seconds
M	Mole	**x *g***	G force

1. Introduction

1.1 Ubiquitination und deubiquitination

1.1.1 The post-translational modification ubiquitination

The regulation of signaling cascades is critical for cellular processes that control immune responses. Especially ubiquitination is a reversible post-translational modification that can mediate cellular processes including immunity, cell differentiation, cell survival and cell death [1, 2]. The protein Ubiquitin is evolutionarily conserved and was discovered to mark proteins for degradation via the 26S proteasome [3]. Ubiquitin molecules are being coupled to lysine residues on target proteins and being read by proteins containing Ubiquitin-binding domains (UBDs) [4, 5]. This mechanism is characterized by the transfer of a single Ubiquitin molecule with its C-terminus to a substrate lysine, called mono-ubiquitination, or of several Ubiquitin molecules to other Ubiquitin molecules, termed poly-ubiquitination. The enzymatic reaction is carried out by activating (E1), conjugating (E2) and ligating (E3) enzymes acting sequentially (Figure 1). In the human genome there are more than 600 Ub E3 ligases known and being identified as homologous to the E6-AP Carboxyl Terminus (HECT) ligases, Really interesting new gene (RING)/U-box ligases, or RING-between-RING (RBR) ligases, differing in their Ubiquitin transfer mechanisms [4]. HECT ligases form thioester intermediates to catalytic cysteine residues to bind Ubiquitin moieties and attach it to a lysine residue of the target substrate. In comparison, RING ligases directly transfer Ubiquitin from the E2 conjugating enzyme to the substrate via binding to the RING1 domain. Similarly, RBR ligases bind to an E2 enzyme and transfer the Ubiquitin molecule to the RING2 domain, forming a thioester intermediate, like HECT ligases, and couple it to the target substrate [4, 5]. It became well established that ubiquitination serves crucial functions in signaling processes.

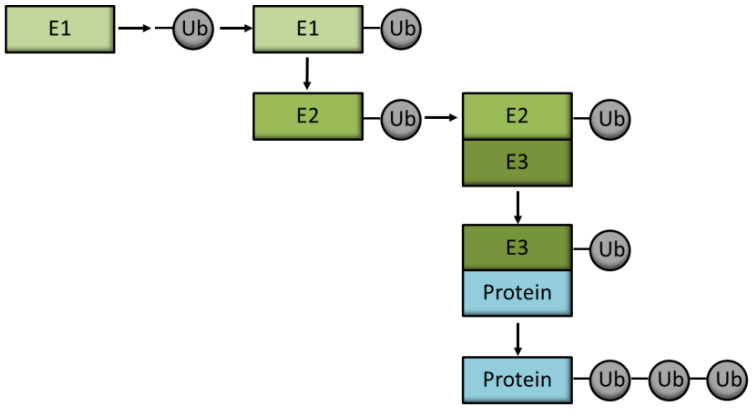

Figure 1: The Ubiquitin cascade.

E1 adenylates Ubiquitin and forms an Ubiquitin thioester intermediate. E1 transfers Ubiquitin to E2, followed by subsequent transfer of the Ubiquitin molecule onto E3. Finally, E3 transfers Ubiquitin to the target protein.

1.1.2 Types of ubiquitination

Ubiquitin allows poly-Ubiquitin chains on itself by conjugation of Ubiquitin moieties on its existing seven lysine residues (K6, K11, K29, K33, K48 and K63). Furthermore, it permits the head-to-tail linkage of Ubiquitin molecules via the C-terminal carboxyl group of the donor Ubiquitin and the N-terminal methionine residue (M1) of the acceptor Ubiquitin [2, 6]. On the one hand, these Ubiquitin chains are recognized, dependent on their position and conformation, by proteins that contain UBDs, thereby allowing specific activation of cellular pathways. On the other hand, more than 100 deubiquitinating enzymes called deubiquitinases (DUBs) are known to recognize and hydrolyze isopeptide-bonds between Ubiquitin molecules or between Ubiquitin and substrate [7-9]. Importantly, regulating and balancing Ubiquitin linkages is implicated in several cellular processes like proteosomal degradation, autophagy, DNA repair, multi-protein complex formation, receptor internalization and signaling, intracellular trafficking, inflammation and by providing a platform for further post-translational modifications [5, 10]. Thus, ubiquitination and deubiquitination are key specified cellular responses and crucial for cell fate.

1.2 TNFR1 induced pro-inflammatory and pro-survival signaling

1.2.1 TNFR1 induced complex I formation

Innate immune receptors are highly regulated by post-translational modifications to trigger signaling pathways upon binding by their respective ligands. Activation of the cytokine receptor Tumor necrosis factor receptor 1 (TNFR1) induces the formation of signaling complexes that heavily rely on Ubiquitin conjugation events. Binding of the soluble pro-inflammatory cytokine Tumor necrosis factor (TNF) to its membrane-bound receptor TNFR1 induces rapid receptor trimerization resulting in the assembly of the TNFR1-associated multi-protein signaling complex, which is referred to as complex I [11-13] (Figure 2).The activation of TNFR1 signaling and stabilization of complex I leads to induction of downstream Nuclear factor `κ-light-chain-enhancer´of activated B-cells (NF-κB) and Mitogen-activated protein kinase (MAPK) signaling to pro-survival and pro-inflammatory gene expression. In complex I initially the adaptor proteins TNFR1-associated DEATH domain (TRADD) and Receptor-interacting serine/threonine-protein kinase 1 (RIPK1) are recruited via homotypic death domain (DD) interactions to TNFR1 [14-17]. TRADD further attracts the E3 Ubiquitin ligase TNFR-associated factor 2 (TRAF2) via interaction of its TRAF binding domain that allows the

engagement of the E3 ligases cellular inhibitors of apoptosis 1 and 2 (cIAP1/2) [16, 18-22]. The recruitment of cIAP1/2 to complex I promotes K11-, K48- and K63 Ubiquitin chains conjugated to themselves and RIPK1 and supports the engagement of the Linear Ubiquitin assembly complex (LUBAC) via Ubiquitin binding [20, 22-24]. This Ubiquitin ligase complex is composed of Heme-oxidized IRP1 Ubiquitin ligase 1 (HOIL-1L), HOIL-1L- interacting protein (HOIP) and SHANK-associated RH-domain interactor (SHARPIN). LUBAC exclusively generates linear (M1-linked) Ubiquitin chains on target proteins like TNFR1, TRADD and RIPK1 in complex I [23-27]. However, complex I formation and signaling does not only rely on the action of different Ubiquitin ligases, but is also regulated by DUBs. Besides negative regulation of Ubiquitin linkages, these DUBs appear to have distinct roles in TNFR1 signaling. TNFα - induced protein 3 (A20) controls complex I more by binding than by hydrolyzing linear Ubiquitin chains, whereas Cylindromatosis (CYLD) and OTU deubiquitinase with linear specificity (OTULIN) are critical in regulating linear Ubiquitin linkages [28-36]. In detail, CYLD binds LUBAC to control further Ubiquitin events in complex I, whereas OTULIN regulates cytosolic LUBAC activity by preventing its auto-ubiquitination, thereby promoting its E3-ligase activity [29, 30, 34]. Hence, it is not only of great importance to balance Ubiquitin chains within complex I but also to counteract LUBAC ubiquitination to mediate TNFR1 signaling.

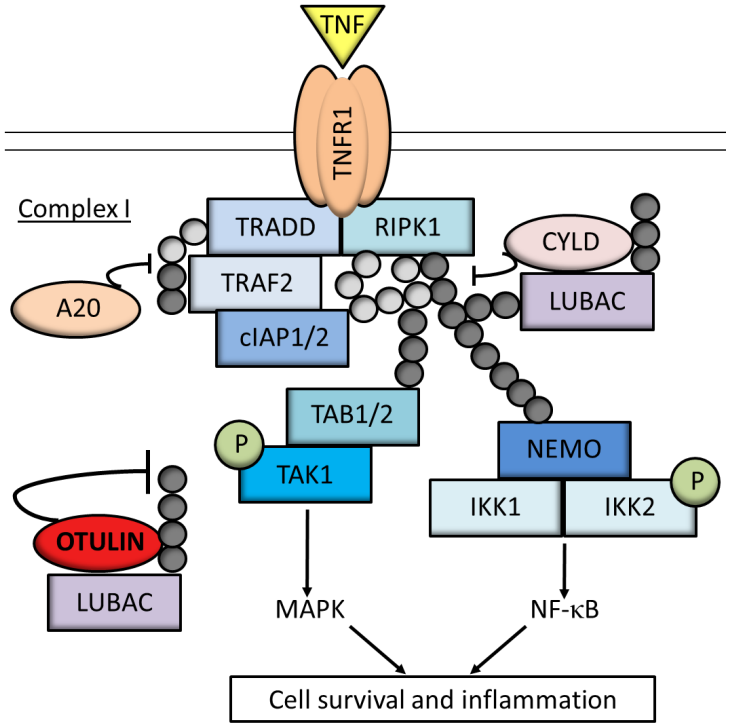

Figure 2: Complex I formation upon TNF binding to TNFR1.

TNF binding to TNFR1 induces the assembly of cytosolic, membrane-bound complex I. Herein, Ubiquitin ligases cIAP1/2 and LUBAC conjugate Ubiquitin chains to RIPK1. This leads to recruitment of TAK1 and the IKK complex, composed of IKK1/2 and NEMO. TAK1 phosphorylates IKK2 and activates downstream MAPK signaling and the IKK complex induces downstream NF-κB signaling pathway, resulting in pro-survival and pro-inflammatory signaling. The DUBs A20, CYLD and OTULIN stabilize Ubiquitin linkages in complex I signaling.

1.2.1.1 TNFR1 induced complex I signaling

The ensemble of poly-Ubiquitin chains attached to proteins in complex I provide a signaling platform for the recruitment of further kinase complexes. On the one hand, K63-linked Ubiquitin chain binding is preferred by the Ubiquitin binding Transforming growth factor β-activated kinase 1 (TAK1) binding protein 1 and 2 (TAB1/TAB2) with their associated kinase TAK1 that undergoes autophosphorylation. The subsequent activation of the MAPK pathway leads to further activation of JNK, p38 and ERK and results in the translocation of Activator protein 1 (AP-1) to the nucleus and subsequent induction of target genes [21, 37, 38]. On the other hand, NF-κB essential modulator (NEMO) is engaged via its UBAN (Ubiquitin binding to the A20-binding inhibitor of NF-κB activation 1 (ABIN) and NEMO) domain that binds M1-linked Ubiquitin chains with higher affinity compared to K63 linkages [39-42]. These Ubiquitin-binding events lead to the recruitment of TRAF family member-associated NF-kappa-B activator (TANK)-binding kinase 1 (TBK1)/ Inhibitor of nuclear factor kappa-B kinase subunit epsilon (IKKε) to complex I via TANK/ Nucleosome assembly protein 1 (NAP1) [40, 43, 44]. NEMO further binds as a regulatory subunit to Inhibitor of kappa B kinase 1 (IKK1) and 2 (IKK2) via its Coiled-coiled-1 (CC1) domain, thereby forming the IKK-complex that induces the activation of the NF-κB signaling pathway [14, 38, 45, 46]. Taken together, TNFR1 signaling and its regulation are critical for downstream pro-inflammatory and pro-survival pathway activation.

1.2.2 NF-κB pathway activation

In resting cells the NF-κB transcription factors p50/p105, p52/p100, p65 (RelA), c-Rel and RelB remain as heterodimers or homodimers in an inactive state in the cytoplasm, inhibited by IκBs [14, 47]. In order to activate the NF-κB subunits, the binding of the inhibitors need to be terminated. The release of the NF-κB subunits promotes its transcription factor function to target genes involved in survival and inflammation. This is induced by two major signaling cascades in the cell: the canonical and non-canonical NF-κB pathway [14] (Figure 3).

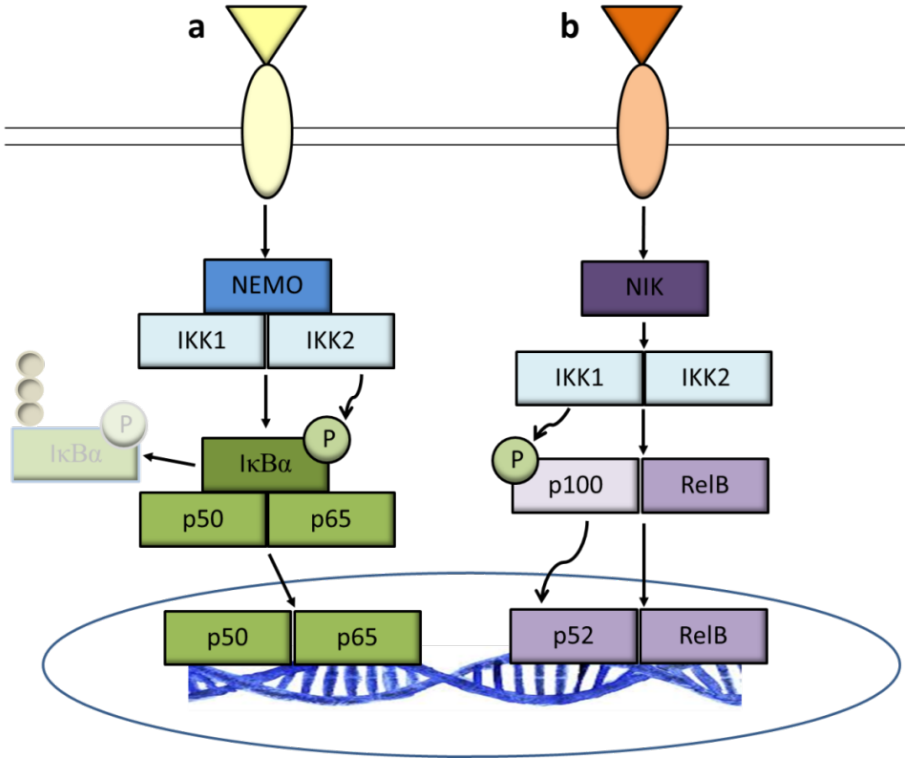

Figure 3: Canonical and non-canonical pathways of NF-κB activation.

In canonical NF-κB signaling, binding of a ligand to its receptor activates the IKK complex that induces the degradation of IκBa through phosphorylation. Thereby, p50:p65 NF-κB subunits are released, translocate to the nucleus and activate target gene expression. In non-canonical NF-κB signaling, binding of a ligand to its receptor activates NIK which induces IKK1 induced phosphorylation of NF-κB subunit p100. The processed p52:RelB subunits translocate to the nucleus and activate target gene expression.

1.2.2.1 The canonical NF-κB cascade

The canonical NF-κB pathway is activated upon binding of ligands like TNF, Interleukin-1 (IL-1) or Lipopolysaccharide (LPS) to their cognate receptors. This triggers the formation of a complex containing K63-ubiquitinated RIPK1 at Ser379 or Ser377 that serves as a signaling platform for further recruitment of the IKK complex [21, 48]. The inductions of the catalytic subunits IKK1 and IKK2 via TAK1 lead to the phosphorylation of Iκba on Ser32 and Ser36, thereby targeting it for K48-ubiquitination and mediating its subsequent proteosomal degradation [38, 45, 46, 49]. The resulting release of the NF-κB p65:p50 heterodimer permits its translocation to the nucleus, thus activating the transcription of pro-survival and pro-inflammatory target genes, including Tnf, Il-6 and A20 [14, 47, 49].

1.2.2.2 The non-canonical NF-κB cascade

In contrast, interaction of Binding of B cell activating factor of the TNF family (BAFF), TNF-like weak inducer of apoptosis (Tweak) and Cluster of differentiation (CD40L) to their corresponding receptors induces the non-canonical NF-κB pathway [50]. The binding of these

TNF family members to their respective receptors is followed by the subsequent degradation of TRAF2/3 and cIAP1/2. Independently of RIPK1, this leads to IKK1 phosphorylation by stabilized NF-κB inducing kinase (NIK), allowing further processing of the NF-κB precursor p100 to p52. The immediate formation of a transcriptionally active p52:RelB complex drives nuclear translocation and targets specific gene expression [50, 51]. Collectively, NF-κB pathway activation is key for gene transcription and the expression of corresponding pro-inflammatory and pro-survival proteins in response to immune signaling.

1.3 TNFR1-induced cell death signaling

1.3.1 Hallmarks of apoptosis

Apoptotic cell death is morphologically distinguished by cell shrinkage, plasma membrane blebbing, apoptotic body formation [52]. The cell death event is executed in a regulated way and therefore noted to be a programmed form of cell death. Apoptosis can be initiated extrinsic or intrinsic, dependent on the origin of induction [12, 53]. Furthermore it is biochemically characterized by nuclear fragmentation as a result of chromatin condensation. In brief, a cascade of pro-apoptotic stimuli leads to the activation of caspases that cleave downstream cellular substrates, thereby promoting internucleosomal fragmentation of DNA and formation of apoptotic bodies that are cleared by phagocytosis [12, 54].

1.3.2 TNFR1-induced apoptosis

The switch from pro-survival signaling to cell death is another possible outcome of TNF sensing. On a molecular level, destabilization of membrane bound complex I results in the formation of cytosolic complexes IIa and IIb that induce apoptosis (Figure 4). The formation of complex I or complex IIa/b is controlled by several post-translational modifications of key signaling molecules [12, 55]. Wether both complexes originate from membrane-bound complex I or assemble from cytoplasmic proteins and if they exist independently or have different kinetics, remain elusive. Nonetheless, inhibition of the translational machinery promotes complex IIa mediated cell death, whereas inhibition of different proteins within complex I results in RIPK1-kinase dependent cell death [56, 57]. Moreover, IKK1/2 dependent phosphorylation of RIPK1 on Ser25 inhibits autophosphorylation of RIPK1 on Ser166 in the kinase domain thereby suppressing its enzymatic activity. These data show that specific phosphorylation events prevent RIPK1 kinase activation and therefore its cytotoxic potential

[58, 59]. The IKK related kinases TBK1/IKKε were shown to protect cells from undergoing RIPK1 kinase-dependent apoptosis by directly phosphorylating RIPK1, independent of IKK1/2 and NF-κB activation [60, 61]. Apart from direct inhibition within complex I, RIPK1 phosphorylation by MAPK-activated protein kinase 2 (MK2), a downstream substrate of p38, appears to be important for inhibiting the association of RIPK1 and Fas-associated protein with death domain (FADD) and thereby for preventing apoptosis [62-64]. Moreover, inhibitory cleavage of RIPK1 at D325 executed by caspase-8 further restricts RIPK1 activation and cell death induction [65].

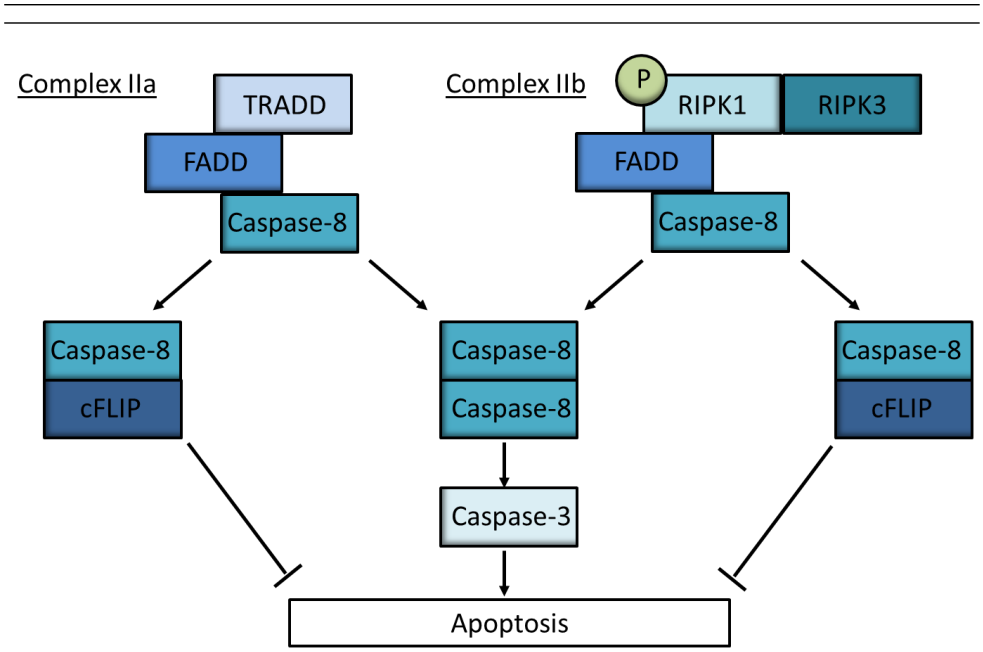

Figure 4: Formation of the apoptotic complexes IIa and IIb.

Under certain conditions, TNF stimulation induces the formation of two apoptotic complexes. In complex IIa TRADD and in complex IIb RIPK1 kinase activity mediate FADD and caspase-8 activation of downstream caspase-3, resulting in apoptotic cell death.

1.3.2.1 TRADD-dependent apoptosis (complex IIa)

Inhibition of protein translation, such as by Cycloheximide (CHX), switches TNFR1 complex I formation to the formation of complex IIa. In complex IIa FADD associates with TRADD via DD interactions and recruits initiator caspase-8 via Death effector domain (DED) interactions that further activates effector caspase-3. In detail, the attraction of pro-caspase-8 homodimers induces a conformational change that results in an autocatalytic cleavage at Asp374 and Asp216. Thereby, p10/p18 cleavage products that form a catalytically active caspase-8 heterotetramer and cleavage fragments p43/42, p30 are generated [66-68]. The further processed p10/p18 homodimers induce the cleavage and activation of caspase-3, -6

and -7 that mediate apoptotic cell death. Caspase-8 activity is regulated via interaction with its catalytically inactive homolog cellular FLICE-like inhibitory protein (cFLIP) in a concentration and isoform-specific manner [69-71]. In fact, the heterodimerization of caspase-8 and cFLIP results in production of a p10-cleavage fragment but not in the generation of the active p18 fragment. Therefore, cFLIP binding to caspase-8 inhibits caspase-8 activity and cleavage of downstream executioner caspases, however allows for negative regulation on necroptosis [72-74].

1.3.2.2 RIPK1 kinase activity-dependent apoptosis (complex IIb)

Inhibition of cIAP1/2, TAK1 or the IKK complex leads to complex I destabilization and RIPK1 induced deubiquitination resulting in release from complex I to the cytosol initiating complex IIb formation that relies on RIPK1 kinase activity. The autophosphorylation events on several autophosphorylation sites are believed to induce conformational changes in RIPK1 and to result in the exposure of its DD. RIPK1 auto-activation via auto-phosphorylation on Ser166 allows RIPK1 to associate with FADD and RIPK3 and causes further attraction of caspase-8 and cFLIP, thereby mediating complex IIb composition [55, 59]. In here, RIPK1, FADD and caspase-8 interact and trigger RIPK1 kinase-dependent apoptosis, whereas RIPK3 is not required for complex IIb activity [12, 17].

1.3.3 Intrinsic apoptosis

Besides numerous internal stimuli, TNFR1 signaling is further connected to cell intrinsic apoptosis via caspase-8 activity [75, 76]. Caspase-8 is not only capable of processing caspase-3 and caspase-7 but also of cleaving pro-apoptotic BH3 interacting domain death agonist (Bid) into truncated Bid (tBid) [77]. Bid induction leads to Bcl-2 associated X (BAX) - Bcl-2 homologous antagonist/killer (BAK) heterodimerization at the mitochondrial outer membrane, resulting in Mitochondrial outer membrane permeabilization (MOMP) [78, 79]. In consequence, cytochrome C and Second mitochondrial derived activator of Caspases (SMAC) are released into the cytosol. SMAC inhibits X-linked inhibitor of apoptosis (XIAP), whereas cytochrome C induces the Apoptotic protease activating factor 1 (APAF-1)-dependent apoptosome formation and the recruitment of pro-caspase-9 [80-82]. Finally, activated caspase-9 cleaves and activates effector caspase-3, -6 and -7, thereby amplifying the apoptotic signal in a cell intrinsic manner [83-85].

1.3.4 Hallmarks of necroptosis

In contrast to apoptosis as a controlled type of cell death, necrosis had been considered an accidental form of cell death until recently. However, several studies could define necroptosis as a regulated form of cell death that is associated with morphological signs of cellular swelling, swelling of organelles, disrupture of the cell membrane and release of Damage-associated molecular patterns (DAMPS) [12, 86, 87]. Necroptotic inhibitors that specifically target RIPK1 demonstrated necroptosis to be molecularly controlled [88]. The sudden release of cellular content upon membrane rupture is considered to be highly inflammatory and may be immunogenic, thereby suggesting immunomodulatory properties of necroptosis that are distinct from apoptotic cell death [12, 89].

1.3.5 TNFR1-induced necroptosis

TNFR1 ligation under conditions of inactive caspase-8 also activates the formation of a third multiprotein complex, referred to as complex III (or necrosome) leading to necroptosis. Genetic or chemical inhibition of caspase-8 or destabilization of complex I through deubiquitination of RIPK1 by CYLD promotes the formation of complex III, which induces necroptotic cell death [12, 90, 91] (Figure 5).In contrast, active caspase-8 cleaves RIPK1 during development, thereby preventing apoptosis and necroptosis [65]. However, the exact mechanisms by which cFLIP and caspase-8 prevent complex III formation, thereby determing if a cell survives or undergoes apoptosis or necroptosis, remain elusive. Nevertheless, TNF-induced necroptotic cell death is dependent on the kinase-dependent activity of RIPK1 and its autophosphorylation on Ser161 or S166 [59, 92, 93].

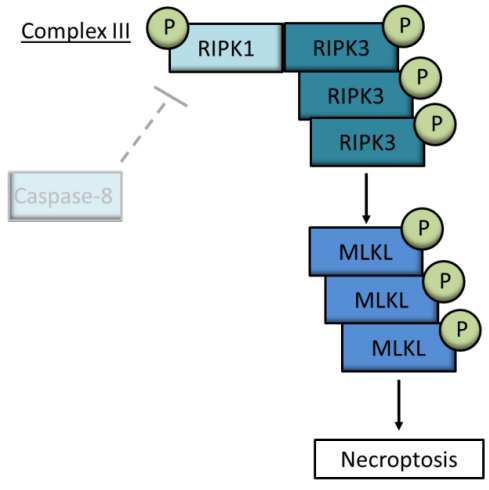

Figure 5: Formation of the necroptotic complex III.

Destabilization of complex I can result in the formation of complex III, where RIPK1 and RIPK3 assemble via RHIM domain interaction. The RIPK1 kinase activity dependent phosphorylation and oligomerization of RIPK3 further promotes MLKL phosphorylation and thereby activation.

1.3.5.1 RIPK1 kinase activity-dependent necroptosis (complex III)

Phosphorylation of RIPK1 is believed to result in conformational changes allowing the interaction with RIPK3 via their Receptor (TNFRSF)-Interacting Protein Homotypic Interaction Motif (RHIM) domains to form amyloid structures [59, 92-95]. In detail, the formation of RIPK1-RIPK3 heterodimers results in the recruitment of additional RIPK3 molecules, leading to further phosphorylation events [94, 96-99]. Phosphorylation of RIPK3 on Ser232 is essential for the recruitment of its substrate Mixed lineage kinase domain-like (MLKL), followed by RIPK3 mediated phosphorylation of MLKL on Ser345 and Ser347 [94, 100-105]. These precise modifications induce a conformational change of MLKL resulting in the exposure of a 4-helical bundle domain, allowing its oligomerization and leading to plasma membrane rupture through mechanisms that are not yet fully understood [106-111]. Collectively, the composition and procession of proteins involved in TNFR1 signaling, as well as their decoration with posttranslational modification, is not only determing cell survival and cell death, but also the type of death cells undergo.

1.4 Pattern recognition receptor signaling

1.4.1 Pattern recognition receptors

Cell survival and cell death are not only considered to control developmental processes, but also to mediate immune responses and thereby secure homeostasis and prevent inflammatory diseases [12, 112]. The innate immune system represents the first line of defense against invading pathogens that is mediated by pattern recognition receptors (PRRs) and cytokine receptors. These innate immune receptors recognize molecular patterns or cytokines on the cell surface or in the cytoplasm and trigger downstream signaling pathways, thereby mediating an inflammatory response [11, 113].

1.4.2 TLR signaling

Toll-like-receptors (TLRs) and receptors for IL-1 cytokine family members have been found to be critical in regulating and initiating an immune response in host-microbe interactions by signaling through the adaptor proteins MyD88 (Myeloid differentiation primary response gene 88) and TRIF (TLR3/TLR4 - IR-(TIR)domain-containing adapter-inducing interferon-β) [114] (Figure 6). The TLR receptor family was shown to serve as critical components in recognizing specific Pattern-associated molecular patterns (PAMPs) and DAMPs, to elucidate differential

signaling cascades [115-117]. To date, 13 TLRs have been identified in humans and 10 in mice that initiate host immune-responses after parasitic, viral and bacterial infection [118]. At the plasma membranes TLRs 1, 2 and 6 detect bacterial lipoproteins, TLR4 detects LPS and TLR5 detects flagellin [119-125]. Moreover, TLRs in endosomes sense nucleic acids such as dsRNA by TLR3, ssRNA by TLR7 and TLR8, ssDNA by TLR9 and bacterial rbRNA by TLR13 [126-131]. TLRs detect pathogens or damage via a leucine-rich repeat (LRR) ectodomain and transduce signals via interaction of a conserved cytoplasmic TIR domain and TIR domain-containing adaptors such as MyD88 and TRIF [122].

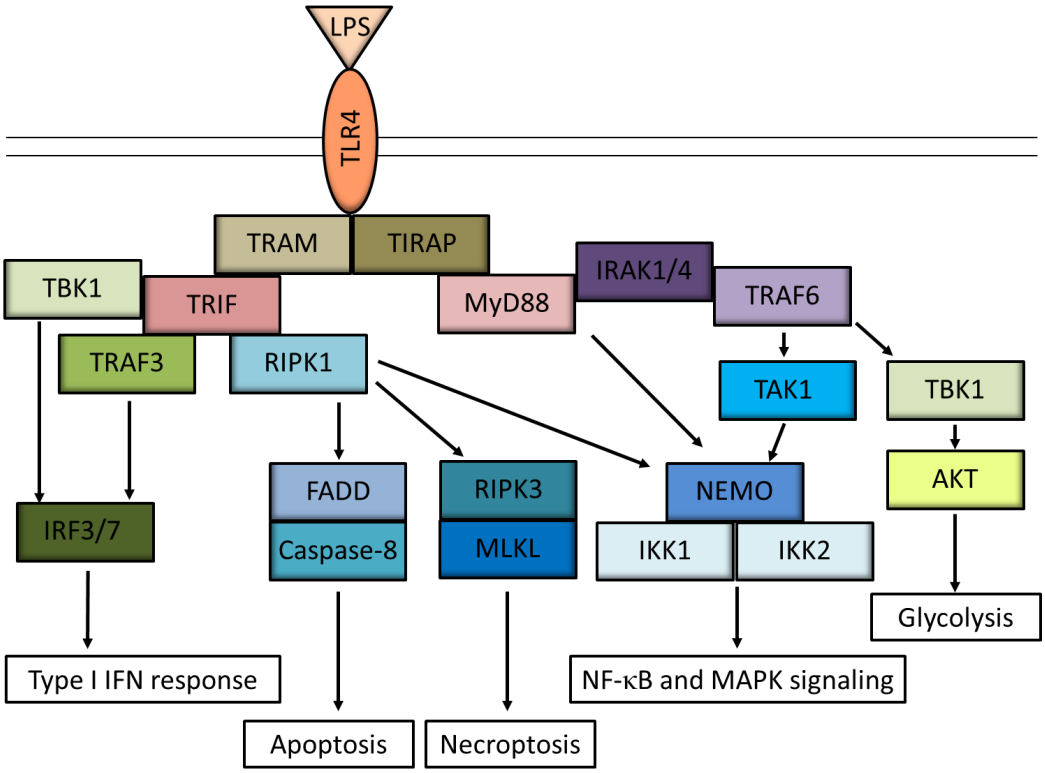

Figure 6: LPS-mediated TLR4 signaling activation.

LPS binding to TLR4 induces the recruitment of TIRAM/TRIF and TIRAP/MyD88. TRIF signals via TBK1 and TRAF3 to activate type I IFN response and via RIPK1 to activate apoptosis, necroptosis and NF-κB and MAPK signaling. MyD88 engages IRAK1/4 and TRAF6 that further activate NF-κB and MAPK signaling and glycolysis.

1.4.2.1 TRIF-dependent TLR pathway

Unlike MyD88, which is involved in the signaling induced by all TLRs except for TLR3, TRIF is only important for TLR3 and TLR4 signaling [118]. TLR4 and TLR3 activation induces TRIF recruitment via TIR domain-containing adapter protein (TIRAP) / Translocating chain-associated membrane (TRAM) and subsequent association with TBK1 and Interferon regulatory factor3 (IRF3). This results in activation of type I Interferon (IFN) gene expression or the interaction with RIPK1, resulting in NF-κB and MAPK signaling or even RIPK1 kinase-

activity dependent apoptosis and necroptosis [56, 71, 132-135]. However, it has also been demonstrated that RIPK3 competes with RIPK1 for the binding to TRIF via their RHIM domains and thereby prevents NF-κB activation [136, 137]. Interestingly, RIPK3 is sufficient to mediate TLR3/4 induced necroptosis in the absence of RIPK1 while the presence of a kinase inactive version of RIPK1 prevents necroptosis downstream of TLRs [56, 138].

1.4.2.2 MyD88-dependent TLR pathway

In contrast to TRIF mediated signaling, the domain structure of the adaptor protein MyD88 does not allow the recruitment of RIPK1 or other cell death molecules. However, upon LPS sensing, TLR4 also interacts with the C-terminal TIR domain of MyD88, thereby initiating the recruitment of IL-1 receptor associated kinases (IRAKs) via the N-terminal death domain, thus driving IRAK auto-phosphorylation and subsequent recruitment of TNF receptor associated factor 6 (TRAF6) [139-141]. E3 ligase activity of TRAF6 activates TAK1 resulting in the IKK-mediated NF-κB and MAPK pathway activation. Furthermore, recruitment of TBK1 to TRAF6 stimulates Protein kinase B (AKT) activation followed by glycolysis induction [142-144].

1.4.3 IL-1 signaling

IL-1 signaling is crucial for mediating both local and systemic responses upon activation of microbial pathogens and cytokine family members of the interleukin receptors. Especially IL-1 induces the expression of adhesion molecules and the release of chemokines to promote the recruitment of inflammatory cells [145]. Upon stimulation of the IL-1 receptor, MyD88 is recruited and further transduces the signaling through the IRAK-TRAF6 cascade, thereby activating the formation of K63/M1-hybrid Ubiquitin linkages [146]. Interestingly, these posttranslational modifications specify the signaling process during TLR and IL-1 signaling [24, 25, 40, 147]. Moreover, LUBAC is recruited to K63-Ubiquitin chains that are attached to TRAF6 in the MyD88 signaling complex and further conjugates M1-Ubiquitin molecules to the K63-Ubiquitin molecules, thereby generating branched Ubiquitin chains [148, 149]. However, the details of the specific regulation of ubiquitination in TLR and IL-1 signaling remain relatively unexplored. In summary, the function of the adaptor protein MyD88 downstream of the TLR and IL-1 pathways highlight the importance of these innate immune signaling processes in response to exogenous and endogenous stimuli.

1.5 The linear Ubiquitination Machinery

1.5.1 LUBAC function and regulation

Among protein modifications by Ubiquitin that regulate numerous cellular functions, linear ubiquitination has been demonstrated to be crucial for inflammatory signaling. LUBAC is the only known E3 ligase that exclusively produces and conjugates linear Ubiquitin chains. It is composed of the three subunits HOIP, HOIL-1L and SHARPIN that all contain UBDs of varying specificity [6, 23, 25, 148]. Mass-spectrometry-based analysis found that the three subunits are closely coordinated, leading to destabilization and impaired LUBAC function if any of the LUBAC components is lost [24, 25, 150, 151]. To form this multiprotein-complex, HOIP and HOIL-1L interact via their respective Ubiquitin-associated (UBA) and Ubiquitin-like (UBL) domains, while SHARPIN employs its UBL to bind to HOIP via the UBA or the Npl4 Zinc Finger 2 (NZF2) domain in HOIP [24-26, 33]. HOIL-1L is required for the assembly and stabilization of the LUBAC complex, whereas HOIP is the catalytically active subunit [152, 153]. Additionally, binding of the N-terminal PUB domain in HOIP to PUB interaction motifs (PIMs) in the DUBs OTULIN and Spermatogenesis Associated 2 (SPATA2)/CYLD complex mediate the activity of LUBAC [29, 30, 34] (Figure 7).

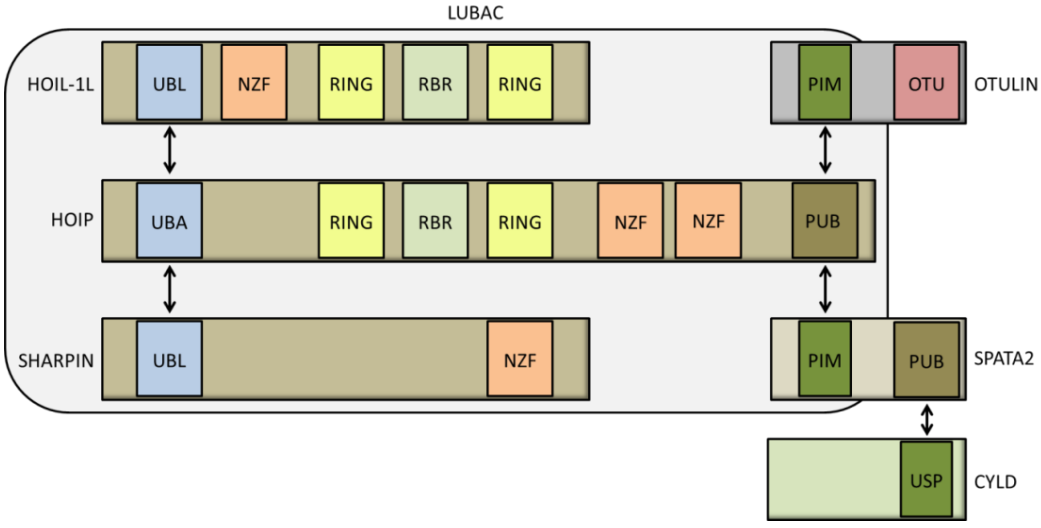

Figure 7: Schematic representation of the interaction and domain structures of HOIL-1L, HOIP, SHARPIN, OTULIN, CYLD and SPATA2.

The UBL domain of HOIL-1L and SHARPIN bind the UBA domain of HOIP, thereby forming LUBAC. CYLD binds to its adaptor SPATA2 via USP-PUB interaction. SPATA2 and OTULIN compete for binding the PUB domain of HOIP via their PIM motifs.

1.5.1.1 LUBAC regulation via deubiquitination

To date, OTULIN is the only known DUB that exclusively hydrolyzes M1-linked Ubiquitin chains while CYLD edits Ubiquitin chains by trimming K63 Ubiquitin chains and mediates K63-M1-hybdrid linkages [32, 33, 35, 36, 149]. Surprisingly, although OTULIN is located in the cytosol and constitutively interacts with HOIP via a PIM-PUB domain interaction, it could not be found in TNFR1 complex I [154-157]. OTULIN exclusively interacts directly with HOIP, thereby being active as a DUB itself, whereas CYLD needs SPATA2 as an adaptor to interact with LUBAC. It has been demonstrated, that SPATA2 contains a PUB domain itself that mediates the interaction with CYLD to associate it to the LUBAC complex [29, 30, 158]. However, studies on the crystal structures of the PUB-PIM interaction have shown mutually elusive interaction of OTULIN and SPATA2 with HOIP. Especially a conserved tyrosine residue within the PIM motif of HOIP reveals that the competition between OTULIN and SPATA2 binding to HOIP is regulated via phosphorylation on OTULIN and SPATA2 [29, 30, 156].

1.5.1.2 LUBAC generates hybrid linkages

HOIP is not only serving as the catalytic machinery to synthesize linear Ubiquitin linkages with high specificity, but is also using its NZF1 domain to bind to other Ubiquitin linkage types, similar to the respective NZF domains in HOIL-1L and SHARPIN [23, 25, 148, 153]. Consequently, it was proposed that conjugation of K63-linked Ubiquitin moieties to target proteins can result in extension with M1-linked Ubiquitin chains by LUBAC. In TNFR1 signaling LUBAC connects K63-linked generated chains by cIAP1/2 with M1-linked chains, thereby producing hybrid chains attached to RIPK1. The resulting Ubiquitin chain network acts as a signaling platform that allows the recruitment of further Ubiquitin binding proteins. Hence, mixed chains are assembled to provide localization and substrate specificity [40, 149, 159].

1.5.1.3 LUBAC attracts ubiquitin binding proteins

Several M1 Ubiquitin specific UBD containing proteins being involved in TNFR1 signaling have been reported, such as NEMO and A20. The UBAN domain in NEMO allows it to interact with M1 linkages and, albeit with much lower affinity, to K63-linked Ubiquitin chains, to serve as a signaling platform [40-42, 149]. Furthermore, recent studies demonstrated the importance of NEMO to bind to Ubiquitin molecules, since the mutation of the UBAN domain in NEMO prevented binding to Ubiquitin oligomers and decreased formation of the IKK complex in cells. In addition, phosphorylation of IKK2 on Ser177 by TAK1 was abolished

in cells expressing inactive HOIP or NEMO mutant MEFs. These data demonstrate that both, conjugation of M1 Ubiquitin chains and serving as a signaling interaction platform for NEMO, is crucial for activating NF-κB signaling via IKK complex formation [39, 149, 160]. The DUB A20 is rather binding and stabilizing, than hydrolyzing Ubiquitin molecules and thereby balancing complex I in TNFR1 signaling. A20 interacts via ZFN7 domains with M1 and K63 Ubiquitin linkages, thereby regulating TNF-dependent NF-κB signaling and preventing cell death [161-165]. A20 was also described to remove K63 Ubiquitin chains from RIPK1 and conjugate K48 chains to RIPK1 via its ZF4 domain to inhibit NF-κB signaling in a feedback mechanism [31, 161, 166]. Thus, the regulatory capacity of A20 is even more important to not only protect cells from undergoing cell death, but also to negatively regulate NF-κB signaling [154, 161, 164, 167].

1.5.2 LUBAC in tissue homeostasis and disease

LUBAC plays a key role in TNFR1 signaling thereby mediating immune responses and tissue homeostasis[168]. However, besides LUBAC promoting TNFR1 complex stabilization and thereby pro-survival and pro-inflammatory signaling by M1 ubiquitination, it also recruits A20 and CYLD which support cell death complex formation[154]. Furthermore, mice with impaired LUBAC components display severe inflammation or embryonic lethality due to aberrant cell death[169-171]. Interestingly, damaging the single LUBAC components results in disease development with distinct characteristics[168].

1.5.2.1 SHARPIN in tissue homeostasis and disease

SHARPIN serves as an adaptor protein to stabilize LUBAC. Independent from HOIP and HOIL-1L, it was shown to be overexpressed in different human cancer types to promote tumor formation [172]. Furthermore, SHARPIN-deficient mice (*cpdm*) exhibit severe chronic proliferative dermatitis, with epidermal hyperplasia, multisystemic inflammation and lymphoid development defects that is alleviated by additional deletion of TNF or TNFR1 [169, 170, 173]. Genetic ablation of caspase-8 and RIPK3 prevents *cpdm*-mice from developing pathology demonstrating that cell death, rather than reduced NF-κB activation, drives inflammation in the absence of SHARPIN. Furthermore, deletion of MyD88 has also been reported to have protective effects on SHARPIN deficient mice, indicating TLR signaling to contribute to disease development in *cpdm*-mice [169, 170, 174].

1.5.2.1 HOIP and HOIL-1L tissue homeostasis and disease

Patients with loss-of function mutations in the N-terminal region of HOIL-1L display an auto-inflammatory syndrome with immunodeficiency that results in premature death during infancy [150]. In contrast, patients with mutations in the C-terminus of HOIL-1L develop muscle weakness and cardiomyopathy without immune disease, indicating different functions for the protein domains of HOIL-1L [175, 176]. Similarly, homozygous missense mutations in the gene RNF31 encoding for HOIP give rise to multi-organ inflammation and recurrent bacterial and viral infections in human patients [177]. Furthermore, the ablation of LUBAC components results in reduced LUBAC activity and NF-κB signaling, respectively [150, 177]. In contrast to the deletion of SHARPIN, ablation of the LUBAC subunits HOIP or HOIL-1L in mice results in embryonic lethality during midgestation at E.10.5 due to defects in vascularization of the yolk sac and abnormal heart development [151, 171]. This phenotype is caused by TNF-dependent apoptosis in endothelial cells because the embryonic lethality is prevented from E.10.5 to E.15.5 by genetic deletion of TNF or TNFR1. On the one hand, embryonic lethality in HOIL-1L$^{-/-}$ mice is not protected by caspase-8 and RIPK3 deletion alone but with co-deletion of RIPK1 [171]. On the other hand, embryonic lethality of HOIL-1L$^{-/-}$ and HOIP$^{-/-}$ mice is also not fully prevented by deletion of TNFR1 or TNF, indicating only the partial contribution of TNFR1 signaling and that LUBAC has additional functions in developmental processes [151, 178]. Thus, LUBAC is a key mediator of pro-survival and cell death signaling *in vivo*.

1.5.3 OTULIN function and regulation

OTULIN (FAM105B, Gumby) is the unique member out of 14 OTU DUBs that specifically hydrolyzes M1-Ubiquitin chains, thereby controlling LUBAC activity [32, 33]. Although, M1-Ubiquitin and K63-Ubiquitin are structurally very similar, OTULIN solely cleaves M1 linkages with its high-affinity Ubiquitin binding site. OTULIN is auto-inhibited in the absence of Ubiquitin and especially, the Glu16 of the proximal Ubiquitin is necessary for the organization of the catalytic center that is determined by Cys129, Asn341 and His339. Upon binding of M1-linked Ubiquitin, the side chain of Glu16 inserts into the catalytic center and activates the triad that allows Ubiquitin-mediated substrate-assisted catalysis of active OTULIN towards M1-Ubiquitin. Therefore, the conformation of the Ubiquitin binding pocket in OTULIN determines its interaction specificity and binds to K63 Ubiquitin linkages with 100-fold reduced affinity [32, 179]. The exceptional specificity of OTULIN for linear ubiquitin linkages indicates an important role for linear ubiquitination and its regulation. Indeed, OTULIN

functions as a regulator of LUBAC activity by hydrolyzing linear Ubiquitin chains on LUBAC itself via PIM domain binding to HOIP [34, 155, 156] (Figure 8). Thus, it is believed that OTULIN tightly controls LUBAC auto-ubiquitination, which is crucial for the assembly of the TNFR1 complex and downstream NF-κB activation, while it is not part of the TNFR1 complex I itself [34, 154, 179].

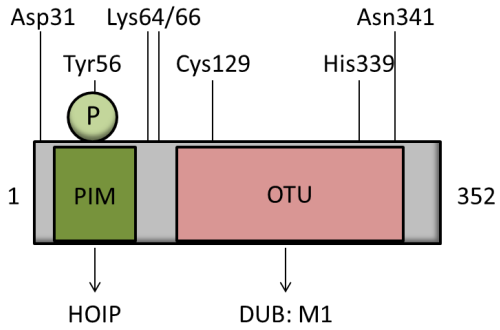

Figure 8: Schematic representation of OTULIN.

N-terminal PIM is essential for HOIP interaction and phosphorylation site on Tyr56. OTU domain is crucial for M1 specific DUB activity and contains catalytic His339, Asn341 and Cys129 that is processed by caspase-8. Asp31 is a caspase-3 cleavage site and Lys64/66 is targeted by TRIM32.

1.5.3.1 OTULIN regulation

OTULIN was originally believed to inhibit LUBAC activity and thereby to promote cell death, however the overexpression and knockdown of OTULIN sensitizes cells to TNF-induced cell death [32]. OTULIN itself is located in the cytosol and interacts with HOIP via its PIM, which binds to the N-terminal PUB domain of HOIP. A phosphorylation event on Tyr56 during necroptosis prevents the interaction of OTULIN and HOIP. This results in HOIP auto-ubiquitination without affecting the catalytic activity of OTULIN [155, 156]. Furthermore, during necroptosis Tyr56 is phosphorylated which is counteracted by Dual specificity protein phosphatase 14 (DUSP14) thereby limiting cell death [155, 156, 180]. Moreover, E3 ligase Tripartite motif-containing protein 32 (TRIM32) interacts with the OTU domain in OTULIN and conjugates non-proteolytic K63-poly-Ubiquitin molecules to the PIM motif. Upon TNF stimulation promotes TRIM32 binding to OTULIN and therefore its regulatory ubiquitination. This event results in reduced interaction with HOIP and enhanced NF-κB activation [181]. Furthermore, it was shown that OTULIN is cleaved into a C-terminal fragment at Asp31 by caspase-3 that restricts caspase activation during apoptosis [180]. Additionally, OTULIN is not transcriptionally regulated in contrast to A20 and CYLD which counteract NF-κB activation in a negative feedback loop [154, 182, 183]. Moreover, OTULIN deficiency results in spontaneous inhibitory phosphorylation of CYLD, thereby limiting CYLD activity, which can be rescued by LUBAC inhibition [180]. Thus, regulation of OTULIN and its activity is critical for TNFR1 signaling.

1.5.4 OTUIN in tissue homeostasis and disease

Human patients carrying OTULIN mutations develop a severe inflammatory disease termed OTULIN-related autoinflammatory syndrome (ORAS)/Otulipenia, similar to patients with impaired LUBAC function. So far, Leu272Pro, Tyr244Cys, Gly281Arg and Gly174Asp mutations in *OTULIN* have been identified to cause symptoms of systemic inflammation with recurrent fevers and panniculitis in human patients. This autoinflammatory disorder leads to episodes of multi-organ inflammation that can be treated with the anti-TNF neutralizing antibody Infliximab [184-186]. Fibroblasts isolated from these patients with the missense mutation Leu272Pro reveal reduced stability and activity of OTULIN, increased linear ubiquitination, increased NF-κB signaling and enhanced cytokine and chemokine production [185, 186]. Intriguingly, these patients closely resemble patients with mutations in *RNF31* (HOIP) and *RBCK1* (HOIL-1L), indicating the importance of balancing levels of linear Ubiquitin linkages in epithelial tissues to maintain homeostasis [150, 177]. Previous studies in mice could show that both, hypomorphic (OTULIN D336E, W96R) and catalytically inactive (OTULIN C129) OTULIN mutants are embryonically lethal at E.12.5-E14 due to reduced craniofacial vasculature [32, 33]. It was shown that impaired Wnt-signalling due to insufficient interaction between OTULIN and Dishevelled (Dvl/Dsh) and increased linear Ubiquitin linkages are causative for defective angiogenesis [33]. The defects in vascularization in the OTULIN C129 mutant were demonstrated to be a consequence of decreased NF-κB signaling and exacerbated cell death that could be prevented by co-ablation of RIPK3 and caspase-8. However, OTULIN/RIPK3/caspase-8 knockout (KO) mice die after birth due to aberrant type I IFN production that is rescued by heterozygosity of RIPK1 implying RIPK1 mediated inflammatory processes [34]. Also a conditional deletion in adult mice or specific ablation in myeloid cells of OTULIN largely recapitulates the clinical features of human ORAS patients and is lethal due to systemic inflammation [185]. Surprisingly, loss of OTULIN in myeloid cells does not affect LUBAC protein levels, whereas OTULIN ablation in T-cells and B-cells correlates with proteosomal degradation of LUBAC, uncovering a cell type specific role for OTULIN [184, 185]. Indeed, the hepatocyte-specific ablation of OTULIN causes the onset of chronic liver disease resulting in hepatocellular carcinoma development. On a molecular level, loss of OTULIN in hepatocytes leads to decreased LUBAC levels, increased M1 Ubiquitin chains and sensitivity to FADD and RIPK1 kinase-dependent apoptosis, without affecting NF-κB signaling [187, 188]. Furthermore, these experiments support a role for type I IFN

signaling in contributing to liver fibrosis and cancer development [188]. In contrast to CYLD-deficiency induced TNFR1-mediated liver disease, liver-specific OTULIN knockout results in liver pathology independent of TNFR1 [187, 189]. Moreover, this study associated OTULIN with mTOR signaling, as treatment with the mTOR inhibitor rapamycin could ameliorate the liver pathology [187]. OTULIN is further connected to autophagy since M1 Ubiquitin chains are conjugated to bacteria to recruit p62 and Optineurin to induce clearance by autophagy. In addition, these Ubiquitin chains attract NEMO that promotes NF-κB pathway activation [190, 191]. In addition, NOD2 receptor signaling was demonstrated to induce RIPK2 poly-ubiquitination by different E3 ligases, leading to the recruitment of LUBAC and further linear ubiquitination on RIPK2. Interestingly, overexpression of OTULIN inhibits M1-Ubiquitin chains on RIPK2 and recruitment of NEMO, while knockdown of OTULIN results in increased NEMO recruitment and enhanced NF-κB signaling, correlated with aberrant pro-inflammatory signaling [179, 192]. Thus, linear Ubiquitin linkages and its regulation by OTULIN have pleotropic effects in cellular signaling processes that are crucial to mediate cellular response mechanisms.

1.6 Inflammation and cell death in the skin

1.6.1 Structure and function of the skin

The skin is the largest organ in humans and serves as an important barrier between the body and the environment. It is constructed of two compartments, an upper layer called the epidermis and the lower layer called dermis [193] (Figure 9). These two layers protect not only the host from external factors like defending from microbial, mechanical and chemical stress, but also allow thermoregulation and the exchange of lipids [194]. The epidermis is an epithelial tissue that contains the intrafollicular epidermis, hair follicles, sebaceous glands and sweat glands and is mainly composed of terminally differentiated keratinocytes. In detail, the intrafollicular epidermis is the protective interface between host and environment and contains important architectural structures to support skin homeostasis [194, 195]. In here, multiple stem cell populations that self-renew and give rise to cells that undergo terminated differentiation have been identified to organize specifically the destination of different cell types. Those cell populations are distinguished by their gene expression profile, location within the epidermis and formation of different layers. The total epidermis is built by the basal layer, spinous layer, granular layer and stratum corneum [193,

[194]. In comparison, the dermis is separated from the epidermis by a basement membrane and forms a reticular layer containing sweat glands, sebaceous glands and a reticular layer containing muscles, nerves and blood vessels. Besides different immune cell populations, the main resident cell type in the dermis is the fibroblast and ensures interaction between the layers, especially between the intrafollicular epidermis and the papillary layer of the dermis. Furthermore, the reticular dermis contains fibroblasts that appear as the collagenous extracellular matrix that contribute to the structural support, whereas the hypodermis is highly vascularized and supports immune cell recruitment [193, 196]. Together with immune cells, these cells form a barrier for host defense in response to pathogens, mediate the pathogenesis of skin inflammation and support wound healing [197]. Considering, that epithelial tissues are constantly challenged by external factors as well as internal stress signals that need a defined cellular response, it is critical for the skin tissue to maintain homeostasis. In summary, the skin epithelium is a highly structured tissue with different cell populations having unique functions to guarantee specified host-environment interaction.

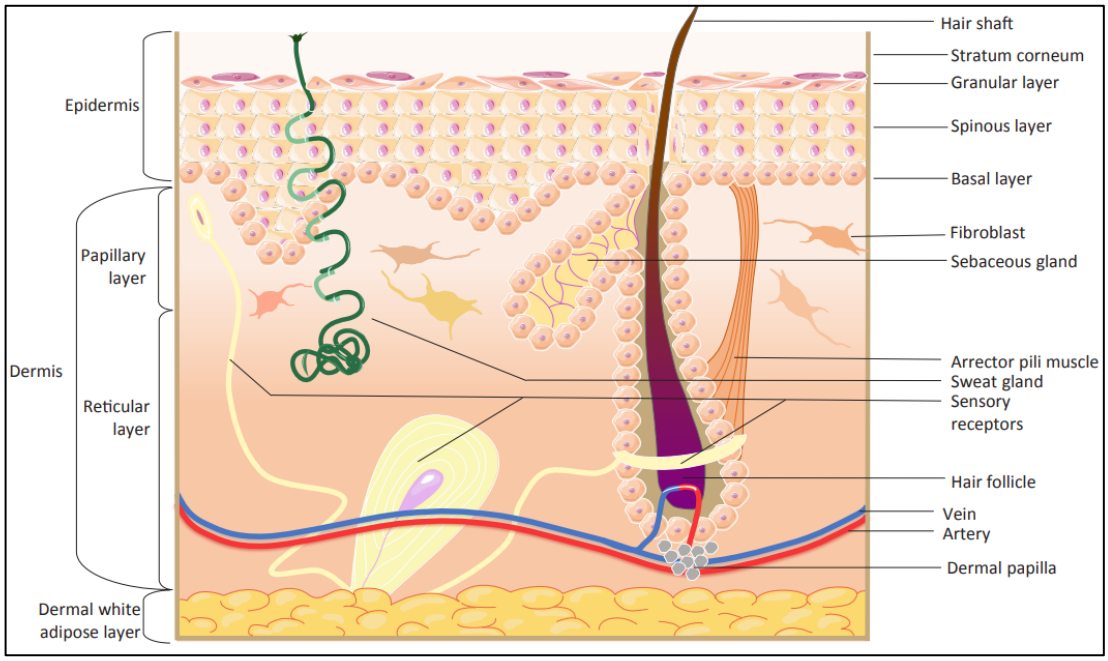

Figure 9: Schematic representation of the skin epithelium.

The skin consists of the two layers epidermis and dermis. The dermis contains mainly keratinocytes that form the basal, spinous, granular and cornified layer. The dermis consists of fibroblasts, immune cells and keratinocytes that form the adipose tissue and the reticular and papillary layer. Throughout the skin structures like hair follicle, sebaceous glands, sweat glands, blood vessels, sensory nerves and muscle fibers can be found. [193]

1.6.2 TNFR1 signaling in the skin

The skin as an outer cover of the body is tightly controlled to prevent tissue damage and disease. The balance between proliferation and differentiation of epidermal keratinocytes and a tightly regulated cross-talk between epithelial, stromal and immune cells is required to maintain its homeostasis[194, 195]. The disturbance of this highly organized system results in the pathogenesis of skin diseases. Therefore, the regulation of inflammatory and cell death signalling in keratinocytes has evolved as a key mechanism in maintaining skin immune homeostasis. These highly controlled networks are not only crucial to fight against pathogens and other environmental dangers, but also to support internal processes such as wound healing [11, 197, 198]. During the last decades, TNF and its cognate receptor TNFR1 were highlighted for being major regulators of the inflammatory response by further activating downstream signaling cascades to promote inflammatory gene expression or cell death [11, 12]. Interestingly, the TNFR1 signaling pathway is tightly regulated by multiple proteins and a series of posttranslational modifications that mediate immune responses in health and disease [55, 199]. Consequently, interference in these cellular processes can result in obstructed signaling and disturbed skin homeostasis.

1.6.2.1 Pro-survival signaling in the skin

In vivo studies in mouse models have helped to uncover the mechanisms that regulate survival and cell death, thereby contributing to the understanding of tissue homeostasis and inflammation. Mutations in the X-chromosomal linked master regulator gene NEMO cause the immune disease Incontinentia Pigmenti (IP) or Ectodermal dysplasia with/without Immunodeficiency (EDA-ID) that lead to embryonic lethality in males and skin lesions in heterozygous females. Mice carrying mutations in NEMO resemble the human phenotype by developing a transient skin phenotype early after birth, due to the presence of mosaic keratinocytes being either wildtype or deficient for NEMO [200, 201]. Since additional knockout of TNFR1 prevents the development of postnatal skin lesions, it is likely that TNF-induced killing of the NEMO-deficient keratinocytes mediates the skin phenotype in mice. Similarly, mice with IKK2 deficiency in keratinocytes develop postnatal skin lesions that are dependent on TNFR1 signaling because the knockout of TNFR1 prevents the skin phenotype in these mice [202, 203]. Yet, it remains to be seen if these defects are caused by defective IKK-complex formation and downstream signaling or a sensitization to TNF induced cell death.

Nevertheless, these studies demonstrate the consequences of disturbed pro-survival signaling in the skin.

1.6.2.1 Cell death signaling in the skin

Cell death is not only considered to affect tissue homeostasis and repair, but also to influence immune responses in the skin [168, 197, 204]. Keratinocyte-specific knockout of caspase-8 causes severe skin inflammation in mice by itself, driven by p38-MAPK-mediated production of IL-1α from keratinocytes triggering inflammation or RIG-I activation triggered enhanced IRF3 signaling [205, 206]. Moreover, keratinocyte-specific deletion of FADD, as an essential protein for apoptotic cell death, causes a similar phenotype. However, the phenotype of both mouse models is fully rescued by additional RIPK3 deletion, providing experimental evidence that RIPK3-dependent cell death of FADD or caspase-8-deficient keratinocytes causes skin inflammation [207]. Furthermore, mice with keratinocyte specific deletion of RIPK1 develop a skin phenotype one week after birth that is partially dependent on TNFR1 signaling, since the additional knockout of TNFR1 prevents the disease up to 4 weeks. In addition, the deletion of RIPK3 or MLKL fully protects the $RIPK1^{E\text{-}KO}$ mice up to 1 year, indicating a new role for RIPK1 as an inhibitor of RIPK3-MLKL dependent necroptosis. Similar Besides, RIPK1 and RIPK3, TRIF and Z-DNA-binding protein 1 (ZBP1) are the only known proteins identified with a RHIM domain [208-212]. However, additional deletion of TRIF only mildly ameliorates the skin phenotype in $RIPK1^{E\text{-}KO}$ mice. In contrast, ZBP1 deletion protects $RIPK1^{E\text{-}KO}$ mice up to 5 months, demonstrating that ZBP1 dependent necroptosis drives the phenotype in $RIPK1^{E\text{-}KO}$ mice. Particularly, the RHIM domain of RIPK1 prevents ZBP1 from activating RIPK3-mediated necroptosis and thereby inhibits inflammation. This was confirmed by the prevention of skin inflammation in mice that possess heterozygous expression of a mutated RHIM domain in combination with a RIPK1 epidermis-specific knockout allele through additional deletion of ZBP1, RIPK3 or MLKL [211, 212]. Collectively, these skin specific mouse studies highlight the importance of cell death and immunity in the skin.

1.6.3 TNFR1 associated ubiquitination in the skin

Recently, several studies have reported the power of balancing and dysbalancing linear Ubiquitin chains especially for complex formation, signal transduction and protein targeting [150, 177, 184, 185]. Recruitment of all LUBAC components HOIP, HOIL-1L and SHARPIN to the TNFR1 complex is crucial for sufficient conjugation of linear Ubiquitin chains to target

proteins, like NEMO and RIPK1 [24, 40]. Ubiquitin chains formed at the NEMO-UBAN domain are critical for the formation of the IKK complex and subsequent NF-κB and MAPK activation [23, 41]. Importantly, interaction of the NEMO-UBAN domain with M1-linked chains is clearly preferred over K63-linked chains and mutations that interrupt linear Ubiquitin binding are enough to suppress NF-κB activation [39, 41, 213]. Patients with mutations in the coding region of *IKBKG* (NEMO) that are critical residues for the recognition of linear Ubiquitin chains, were associated with EDA-ID or IP [214, 215]. Furthermore, epidermis-specific RIPK1 deletion causes skin inflammation that is triggered by keratinocyte apoptosis and necroptosis [216]. Also RIPK1 is heavily ubiquitinated in complex I by the E3 ligases cIAP1, cIAP2 and LUBAC. While the IAPs conjugate K63-linked chains to RIPK1, LUBAC attaches M1-linked chains to stabilize RIPK1 in complex I, thus regulating RIPK1 kinase activity, inducing the recruitment of further adaptors and inhibiting cell death [217-220]. These findings further support the importance of ubiquitination in TNFR1 signaling to promote complex I stabilization and prevent cell death in the skin.

1.6.3.1 The role of LUBAC in the skin

The linear ubiquitination machinery is believed to be crucial for various cellular processes associated to tissue homeostasis [168, 199]. In a skin specific mouse model, were HOIL-1L and HOIP are specifically deleted in keratinocytes, mice develop severe skin inflammation due to TNFR1-driven caspase-8 mediated cell death during the early post-natal period and young age. Surprisingly, in older mice the onset of RIPK3-MLKL dependent cell death is only prevented by combined deletion of TNFR1, TRAIL and CD95L [221]. In contrast, inflammatory skin lesion development in *cpdm* mice is solely driven by TNFR1-induced, RIPK1 and FADD-caspase-8-dependent keratinocyte apoptosis [169, 170]. Interestingly, conditional ablation of SHARPIN in epidermal keratinocytes is sufficient to trigger the *cpdm* phenotype, demonstrating that keratinocyte-intrinsic SHARPIN deficiency causes the cutaneous inflammatory response [222]. The fact, that loss of one of the two subunits HOIP or HOIL-1L results in destabilization of the LUBAC complex, lack of linear ubiquitination, blocked NF-κB signaling and aberrant cell death, is contrary to loss of the third subunit SHARPIN that causes only decreased protein levels of the LUBAC subunits, thereby explaining the phenotypical differences [150, 151, 171, 177, 221].

1.6.4 TNFR1 associated deubiquitination in the skin

The DUBs A20, CYLD and OTULIN influence tissue homeostasis and immune responses by regulating TNFR1 complex I formation, stability and signaling outcome. Interestingly, keratinocyte-specific deletion of A20 results in epidermal hyperproliferation, ectodermal defects and systemic profinflammatory changes [223, 224]. However, A20 mediates TNFR1 signaling more via its binding activities, rather than its catalytic properties, which distinguishes it from CYLD [154, 165]. Indeed, contrary to keratinocyte-specific deletion of A20, mice with epidermal keratinocyte-specific expression of a catalytically deficient CYLD do not develop skin pathology. However, these mice are prone to the development of highly malignant and metastatic skin tumors upon topical challenges with 7,12-Dimethylbenzanthracene/12-O-tetradecanoylphorbol-13-acetate (DMBA/TPA) [225, 226]. Hence, these studies demonstrate an important role for DUBs in regulating TNFR1 signaling and skin homeostasis, but without considering Ubiquitin linkage specificities and DUB function that mediate the outcome. However, especially linear ubiquitination mediated by LUBAC and its counteraction by both, CYLD/SPATA2 and OTULIN, are proposed to control TNFR1 signaling [29, 30, 154, 156]. Similar to CYLD, overexpression of OTULIN was shown to downregulate NF-κB signaling but also to hyperactivate NF-κB signaling, in a cell type and TNF dependent fashion [32, 35, 179]. Furthermore, OTULIN was demonstrated to be crucial for tissue homeostasis in mice, thereby resembling human ORAS patients. In this context, human patients with mutations in the OTULIN gene were treated with α-TNF neutralizing antibodies to prevent aberrant TNFR1 signaling and improve on their symptoms, including chronic skin inflammation. Even though panniculitis was ameliorated in ORAS patients upon Infliximab treatment, the underlying mechanisms resulting in skin pathology remain elusive [185]. Thus, OTULIN is important for the regulation of tissue homeostasis in a TNFR1 dependent fashion, however the exact functions of OTULIN in the skin remain unknown.

1.7 Aim of the project

OTULIN is a key deubiquitinase in the TNFR1 pathway that regulates TNFR1 complex formation and signaling outcome. Regulations of linear ubiquitination events by OTULIN are crucial to balance pro-survival signaling and cell death and to prevent auto-immunity and inflammation, while supporting tissue and immune homeostasis [32-34, 155, 179, 185]. Homozygous hypomorphic mutations in the *OTULIN* gene cause the autoinflammatory disease ORAS in

human patients with symptoms of recurrent fevers, arthritis, diarrhea and panniculitis [184-186]. However, the function of OTULIN *in vivo* in epithelial tissues and its role in especially skin homeostasis remains poorly understood. This study aimed to investigate the biological significance of OTULIN in the mouse skin epithelium during tissue homeostasis and to decipher the role of OUTLIN in initiation, development and progression of skin inflammation.

2. Results

2.1 OTULIN maintains skin homeostasis

2.1.1 Epidermis-specific OTULIN deficiency causes skin inflammation

Deubiquitination by OTULIN has been demonstrated to be crucial during embryonic development [32, 33]. Accordingly, patients with hypomorphic mutations in OTULIN develop the inflammatory disease ORAS with symptoms of recurrent fevers, arthritis, diarrhea and panniculitis [185, 186]. Hence, liver specific deletion of OTULIN results in hepatocellular carcinoma (HCC) development in mice [187, 188]. However, cell type specific mechanisms leading to the disease development remain elusive. To study the role of OTULIN in skin homeostasis, *Otulin*$^{fl/fl}$ mice were crossed with *K14-Cre* transgenic mouse line that expresses Cre recombinase under the control of the keratinocyte specific promoter keratin 14 (K14), which mediates Cre recombination specifically in keratinocytes [227] (Figure 10).

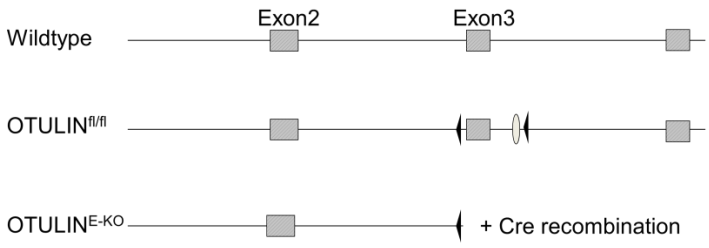

Figure 10: Targeting strategy for OTULIN^{E-KO} mouse generation.

Schematic representation of the targeting strategy showing the LoxP-flanked (floxed) and OTULIN keratinocyte specific knockout (KO) allele generated through K14Cre-mediated recombination. The box indicates exons and LoxP sites are indicated by arrowheads.

Mice with the keratinocyte specific deletion of OTULIN (hereafter referred to as OTULIN^{E-KO}) were born at normal Mendelian ratio and during the first postnatal days were macroscopically indistinguishable from their *Otulin*$^{fl/fl}$ littermates that did not express Cre recombinase (hereafter referred to as wildtype (WT)). OTULIN^{E-KO} mice started to developed spontaneous cutaneous back and tail skin lesions about 6 days after birth that progressed into papilloma-like structures at the age of 3weeks. The back skin was presented with inflammatory foci that were mainly localized to the neck and head area. Similarly, the tail phenotype started at the base and progressed to inflamed ulcers affecting the whole tail with age (Figure 11).

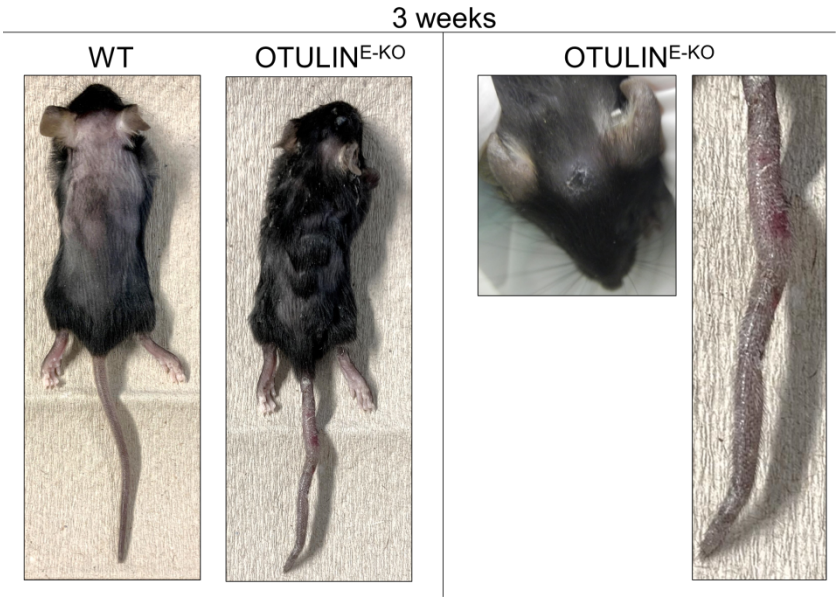

Figure 11: Mice lacking OTULIN in the epidermis develop skin pathology.

Photographs of mice with the indicated genotypes at the age of 3 weeks. Images shown are representative of n > 25 OTULIN^{E-KO} mice.

About 50% of the mice were culled by the age of 3 weeks because of reaching pre-determined severity criteria. OTULIN^{E-KO} mice that did not develop inflammatory tail skin lesions during the first weeks of life could be maintained up to 14 weeks of age. However, all mice developed skin lesions localized to the back skin that progressed to papilloma-like structures with increasing size during ageing (Figure 12).

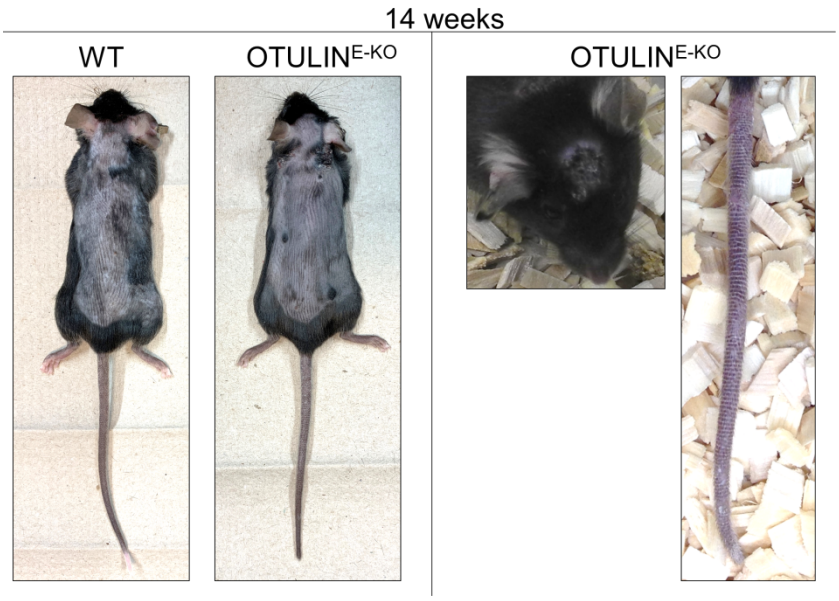

Figure 12: Skin lesions progress to papilloma-like structures during aging in OTULIN^{E-KO} mice.

Photographs of mice with the indicated genotypes at the age of 14 weeks. Images shown are representative of n > 25 OTULIN^{E-KO} mice.

In the macroscopic skin score mice were characterized based on their phenotypic appearance. No macroscopic skin phenotype was detected in WT mice until the age of 50 weeks, therefore all WT mice appeared score 0. In contrast, OTULIN$^{E\text{-}KO}$ mice showed a variable phenotype with a macroscopic skin score of 1, 2 and 3 depending on severity and affected area of the skin lesions (

Figure 13). Taken together, the epidermis-specific deletion of OTULIN mice triggers the development of hyperplastic skin lesions.

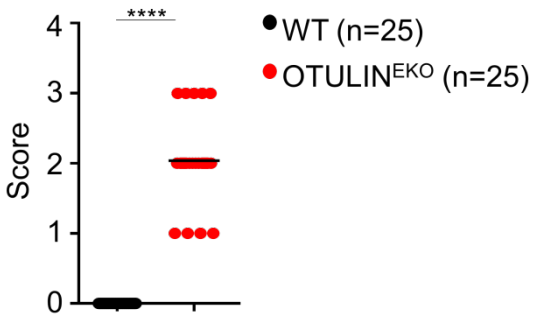

Figure 13: Macroscopic skin score in OTULIN$^{E\text{-}KO}$ mice.

Graph depicting macroscopic skin score of mice of the indicated genotypes. Each dot represents one mouse. Bars represent mean.

2.1.2 OTULIN$^{E\text{-}KO}$ mice display ongoing inflammation and cell death in the skin

Upon detailed histopathological analysis of 3-week old mice, inflammatory skin lesion areas in the tail and the back skin were marked with epidermal hyperplasia, increased cleaved caspase-3 (CC3) and cleaved caspase-8 (CC8) positive cells, indicative of ongoing apoptosis. Besides, increased Ki-67 positive cells revealed increased keratinocyte proliferation compared to WT littermate back and tail skin (Figure 14).

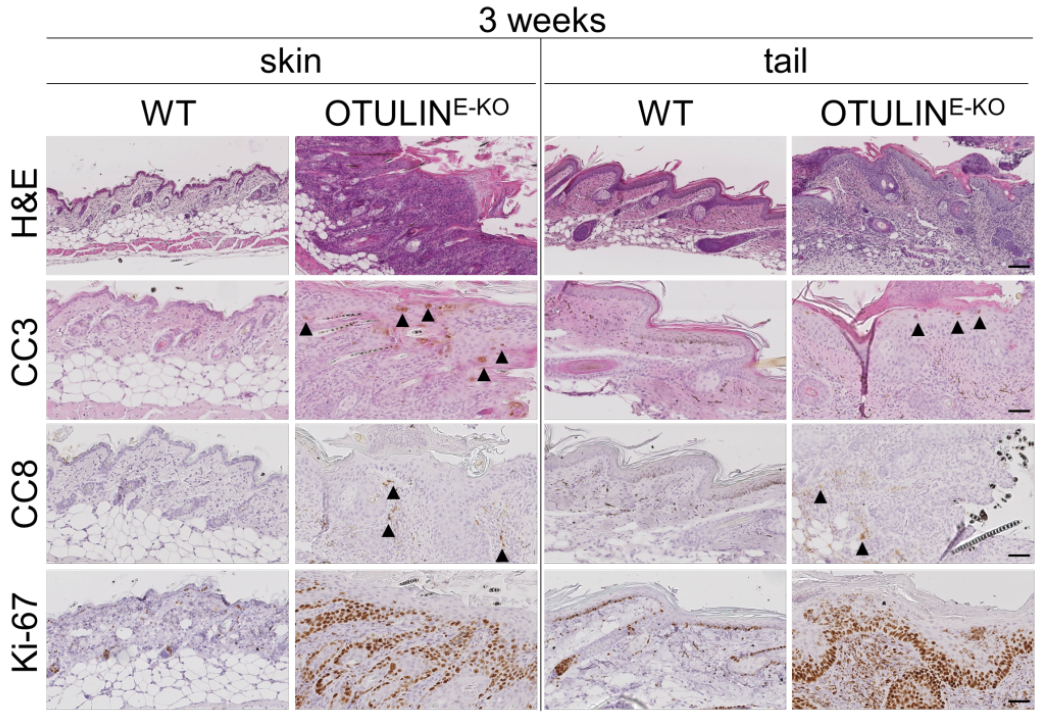

Figure 14: Hyperproliferation and cell death in OTULIN^{E-KO} mice.

Representative images from skin sections from 3-week old mice of the indicated genotypes stained with haematoxylin and eosin (H&E), or anti-cleaved caspase-3 (CC3), anti-cleaved caspase 8 (CC8) or anti-Ki67 antibodies. Arrowheads indicate position of $CC3^+$ and $CC8^+$ stained cells. Scale bar H&E = 100µm; CC3, CC8, Ki67 = 50µm.

OTULIN^{E-KO} mice that could be maintained up to 14 weeks did not only show maturation of the inflammatory skin foci revealed by H&E and Ki-67 staining, but also showed further increase in dying cells, marked by CC3 and CC8 staining in back and tail skin (Figure 15).

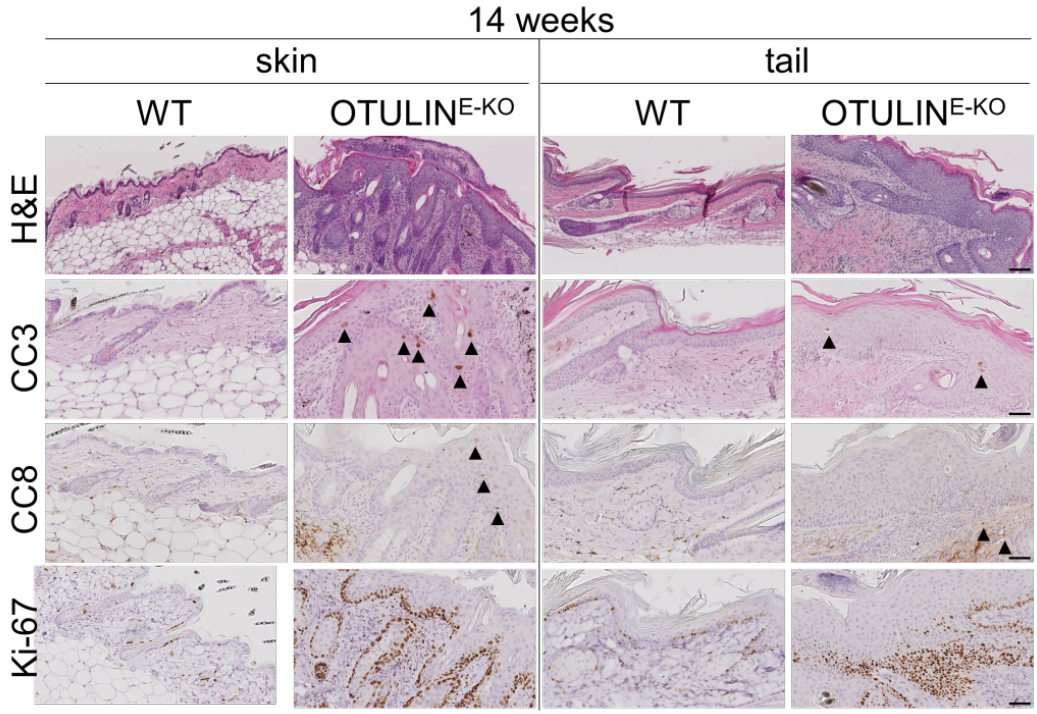

Figure 15: Hyperproliferation and cell death in adult OTULIN^{E-KO} mice.

Representative images from skin sections from 14-week old mice of the indicated genotypes, stained with H&E, or anti-CC3, anti-CC8 or anti-Ki67 antibodies. Arrowheads indicate position of $CC3^{+}$ and $CC8^{+}$ stained cells. Scale bar H&E = 100µm; CC3, CC8, Ki67 = 50µm.

Furthermore, OTULIN^{E-KO} skin revealed increased presence of keratin 6 (K6) positive cells as a marker for hyperplastic and inflamed epidermis. The epidermal differentiation markers keratin 10 (K10) showed strong expression, whereas the basal keratinocyte marker keratin 14 (K14) expression was reduced, therefore indicating hyperproliferation and loss of differentiation within the epidermal cell layers. Moreover, prominent staining for the macrophage marker F4/80 and the granulocyte marker Gr-1 revealed enhanced myeloid cell infiltration that was absent in WT skin sections at the age of 3 weeks (Figure 16).

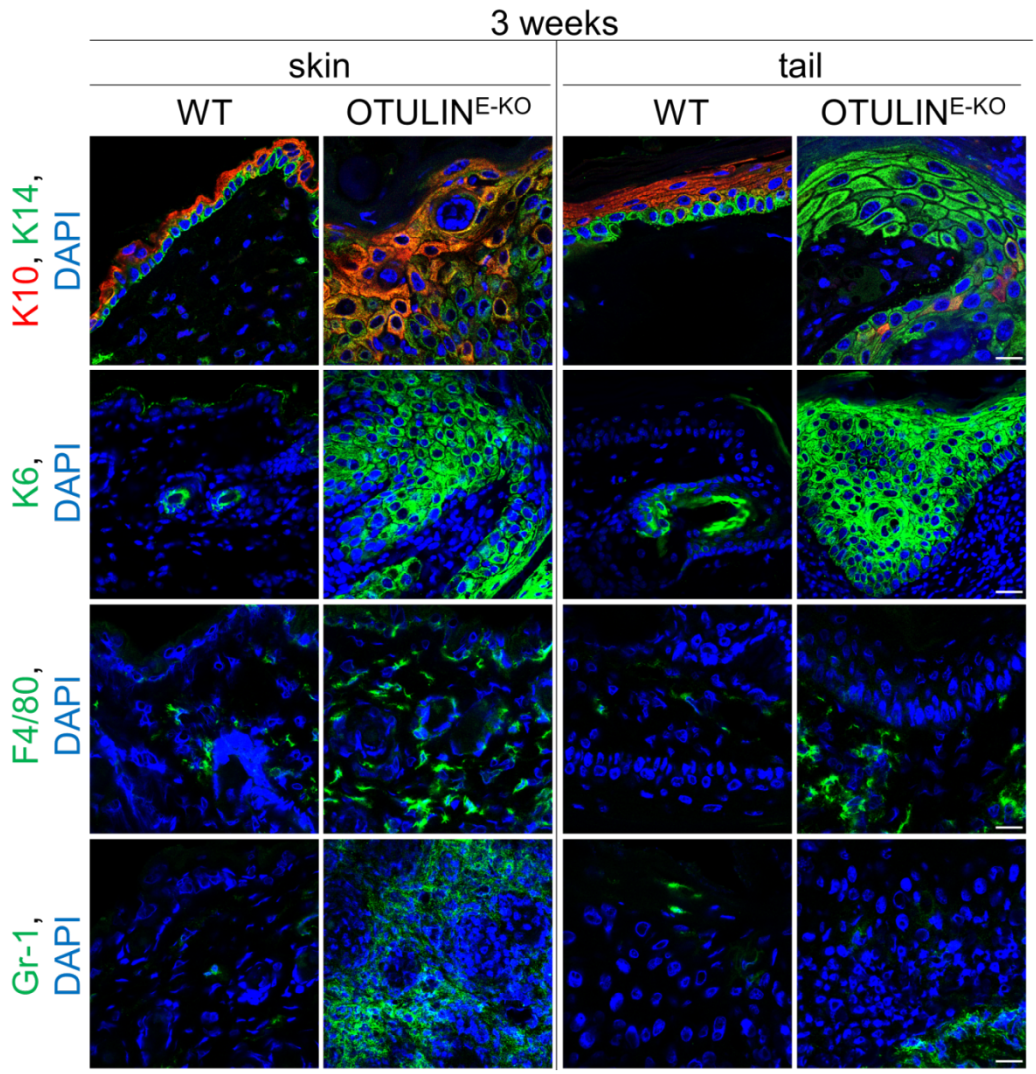

Figure 16: Loss of skin structure and increased myeloid immune cell infiltration in OTULIN$^{E\text{-}KO}$ mice.

Representative images from skin sections from 3-week old mice of the indicated genotypes, immunostained with anti-keratin 10 (K10), anti-keratin 14 (K14), anti-keratin 6 (K6), anti-F4/80, anti-Gr-1 and DAPI (DNA stain). Scale bar K10, K14, K6 = 20µm; F4/80, Gr-1 = 30µm.

In line with this, OTULIN$^{E\text{-}KO}$ mice at the age of 14 weeks were characterized by hyperproliferative epidermis, uncovered by increased K14 and K6 staining compared to WT skin. In addition, immune cell infiltration marked by F4/80 and Gr-1 staining was further enhanced in OTULIN$^{E\text{-}KO}$ tail and back skin (Figure 17).

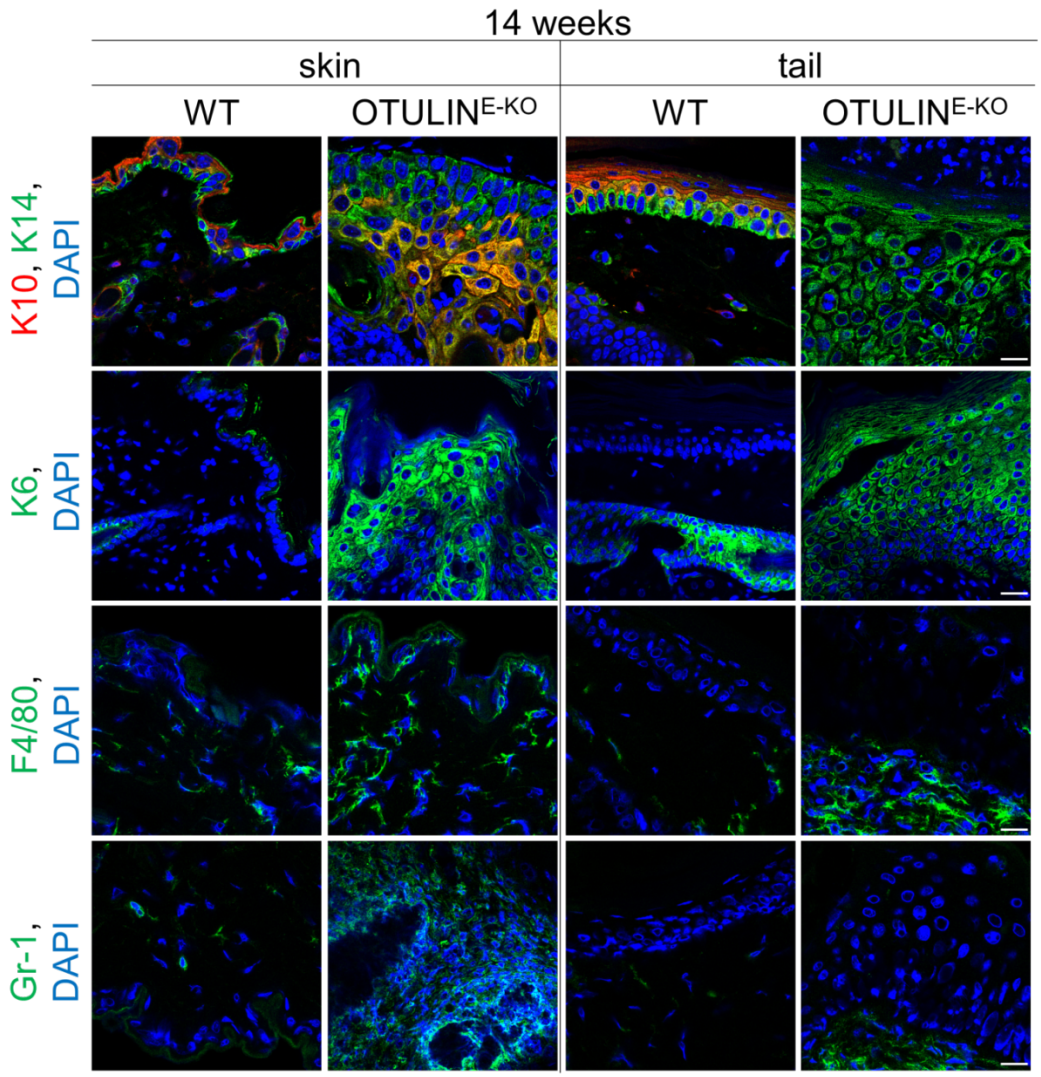

Figure 17: Loss of skin structure and increased myeloid immune cell infiltration in adult OTULIN^{E-KO} mice.

Representative images from skin sections from 14-week old mice of the indicated genotypes, immunostained with anti-K10, anti-K14, anti-K6, anti-F4/80, anti-Gr-1 and DAPI (DNA stain). Scale bar K10, K14, K6 = 20µm; F4/80, Gr-1 = 30µm.

Interestingly, non-lesional back skin from OTULIN^{E-KO} mice showed no signs of hyperplasia, inflammation, keratinocyte death or immune cell infiltration. Although the non-lesional areas were located close the lesional areas that formed papilloma-like structures, they appeared indistinguishable from WT skin samples (Figure 18). Nevertheless, the histopathological analysis suggested skin disease development due to increased inflammation and cell death in lesional back and tail skin areas of OTULIN^{E-KO} mice.

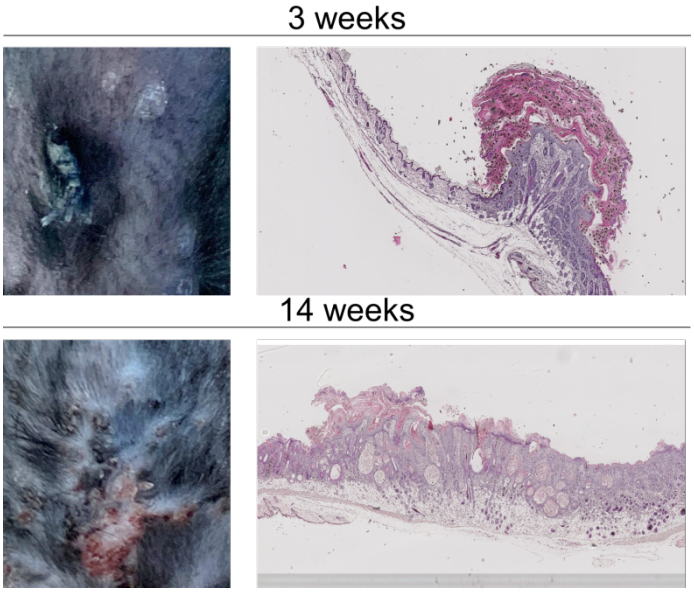

Figure 18: OTULIN$^{E\text{-}KO}$ mice develop papilloma-like structures.

Photographs of lesional skin from OTULIN$^{E\text{-}KO}$ mice at the age of 3 weeks and 14 weeks and representative images from skin sections from 3-week old or 14-week old mice from OTULIN$^{E\text{-}KO}$, stained with H&E. Images shown are representative of n > 25 OTULIN$^{E\text{-}KO}$ mice.

2.1.3 OTULIN$^{E\text{-}KO}$ mice show inflammatory gene expression signature in the skin

To test for differences in the gene expression profiles of lesional and non-lesional skin from OTULIN$^{E\text{-}KO}$ mice in comparison to WT skin, unbiased gene expression analysis of 3´mRNA Sequencing was performed. By comparing the lesional and non-lesional skin of OTULIN$^{E\text{-}KO}$ to WT skin tissue from 3-week old mice, expression of 549 genes revealed a significant up- or downregulation (Figure 19). Surprisingly, these significantly changed expression patterns appeared more alike between lesional and non-lesional skin then between non-lesional and WT skin, even though macroscopic and histological analysis suggested that WT and non-lesional skin are similar. Therefore, gene expression analysis did not only verify differences in skin tissue of WT and OTULIN$^{E\text{-}KO}$ mice, but also revealed similar gene expression between lesional and non-lesional skin of OTULIN$^{E\text{-}KO}$ skin, demonstrating that significant gene expression alterations occur before changes in the tissue architecture appear.

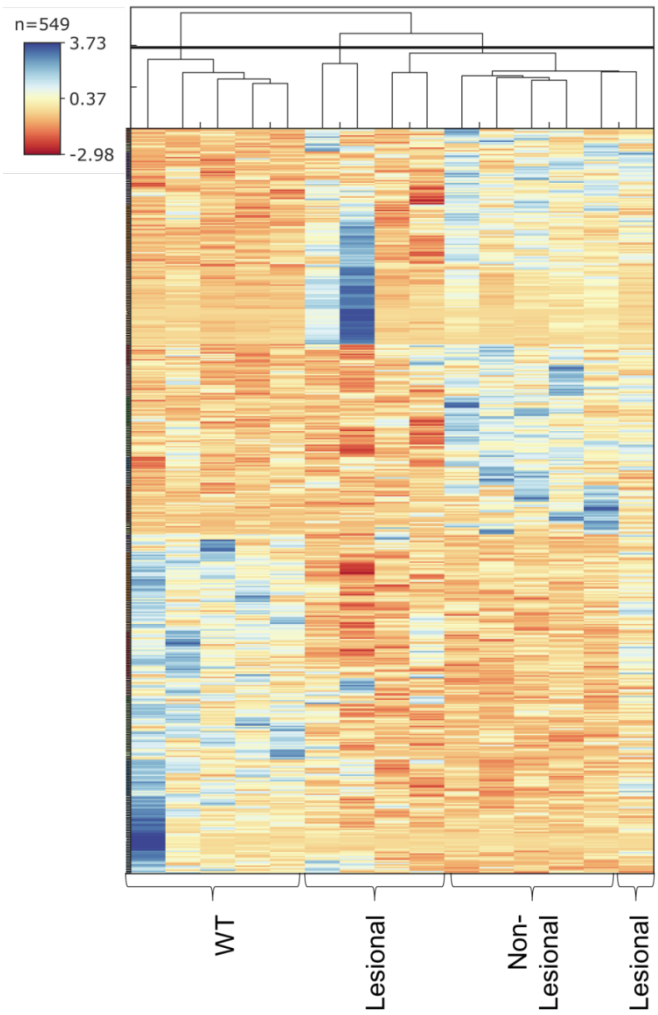

Figure 19: Gene expression analysis of skin sections from OTULIN$^{E\text{-}KO}$ mice.

Cluster heat map showing expression of genes that were significantly changed (logfold change R±1, $p < 0.05$) in OTULIN$^{E\text{-}KO}$ lesional or non-lesional skin tissue compared to skin from *Otulin*$^{FL/FL}$ control mice (WT). Z-Scores are shown. Each column represents one mouse at the age of 3 weeks (n=5).

The displayed gene expression changes revealed characteristics of pronounced upregulation of inflammatory signature genes in the lesional skin of OTULIN$^{E\text{-}KO}$ mice in comparison to WT skin tissue. Furthermore, gene ontology (GO) analysis revealed significant upregulation of Interferon-stimulated genes (ISGs) and genes associated with type I IFN signalling and anti-viral response signatures in non-lesional skin and even more significant in lesional skin of OTULIN$^{E\text{-}KO}$ mice (Figure 20a, b). Combined, lesional skin from OTULIN$^{E\text{-}KO}$ mice was characterized by induction of inflammatory genes, whereas upregulation of type I IFN responses was not only a prominent feature in lesional, but also in non-lesional skin from OTULIN$^{E\text{-}KO}$ mice.

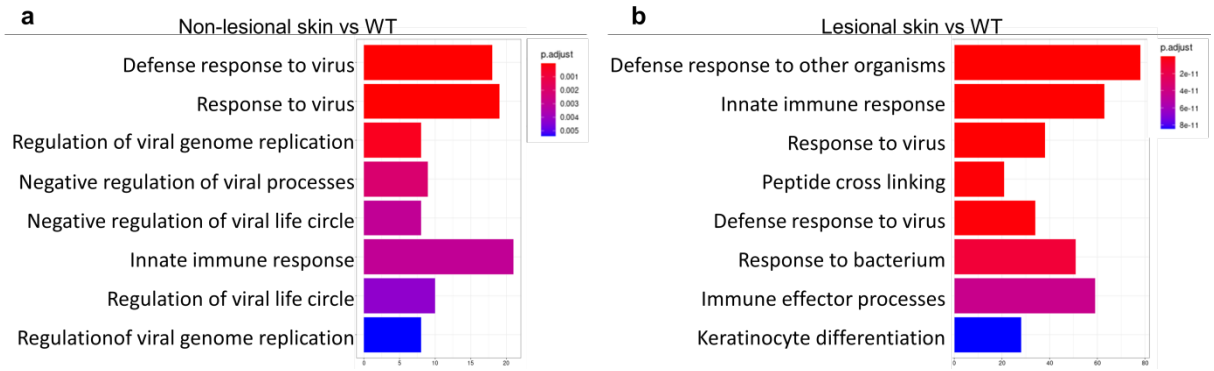

Figure 20: GO analysis of RNA sequencing data from the skin of OTULIN$^{E\text{-}KO}$ and WT mice.

(a) Functional annotation by gene ontology (GO) of significantly up-regulated genes in OTULIN$^{E\text{-}KO}$ non-lesional skin tissue compared to WT skin tissue. For over-representation (ORA) tests, the enrichGO function was used with standard parameters defined by cut-off on p-value and logFoldChange from gene expression data from 5 3-week old mice. 8 out of 61 enriched gene sets shown. (b) Functional annotation by GO of significantly up-regulated genes in OTULIN$^{E\text{-}KO}$ lesional skin tissue compared to WT skin tissue. For ORA tests, the enrichGO function was used with standard parameters defined by cut-off on p-value and logFoldChange from gene expression data from 5 3-week old mice. 8 out of 249 enriched gene sets shown.

2.1.4 Epidermis-specific OTULIN deficiency promotes linear ubiquitination in the skin

Since OTULIN is important for balancing the linear ubiquitination within TNFR1 signaling, the linear ubiquitination levels in skin samples were investigated. Interestingly, immunoblotting with antibodies against M1-linked Ubiquitin chains revealed the presence of increased amounts of linear Ubiquitin chains in lesional skin from 3-week or 14-week old OTULIN$^{E\text{-}KO}$ mice compared to WT mice. Moreover, enhanced M1-linked Ubiquitin chains could be detected in the tail skin samples from OTULIN$^{E\text{-}KO}$ mice, consistent with the loss of OTULIN DUB activity (Figure 21).

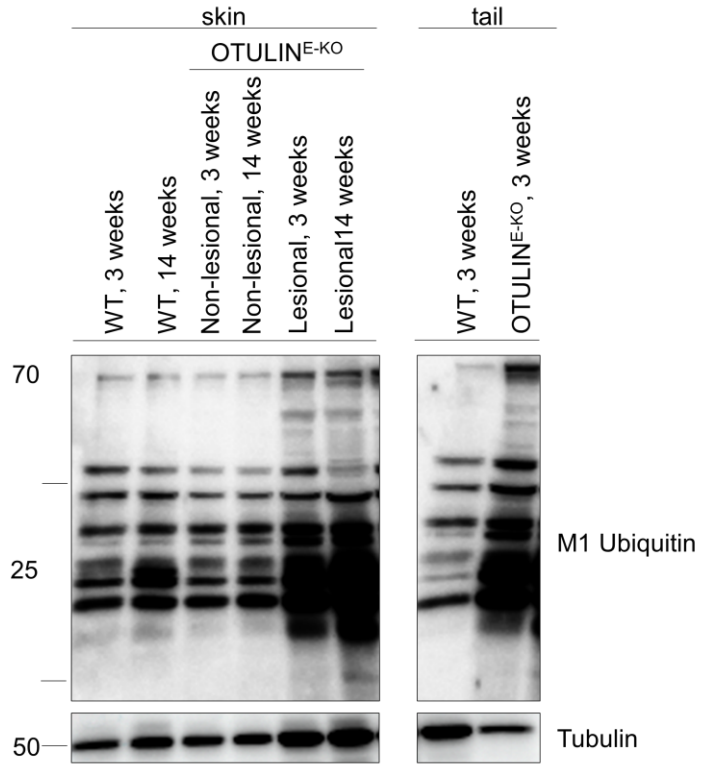

Figure 21: Increased linear ubiquitination in OTULIN^{E-KO} mice.

Immunoblot analysis of protein extracts from lesional and non-lesional skin or tail tissue from 3-week or 14-week old OTULIN^{E-KO} or WT mice with antibodies against linear (M1) Ubiquitin chains or Tubulin as loading control.

Considering linear ubiquitination being important for TNFR1-dependent inflammatory gene expression, its activation via NF-κB and MAPK signaling was further examined. Immunoblot analysis for the activation of essential proteins in those pathways did not show considerably differences on protein levels in OTULIN^{E-KO} mice skin and tail skin compared to WT skin and tail skin. Neither evident increase in p-IκBα and p-p65 levels, indicative for NF-κB pathway activation, nor strong p-JNK, p-p38 or p-ERK levels, indicative for MAPK pathway activation, could be observed in lesional from OTULIN^{E-KO} mice (Figure 22). These data suggested that keratinocyte specific deletion of OTULIN does not considerably affect the pro-inflammatory signaling events in the skin tissue and may not explain the observed phenotype.

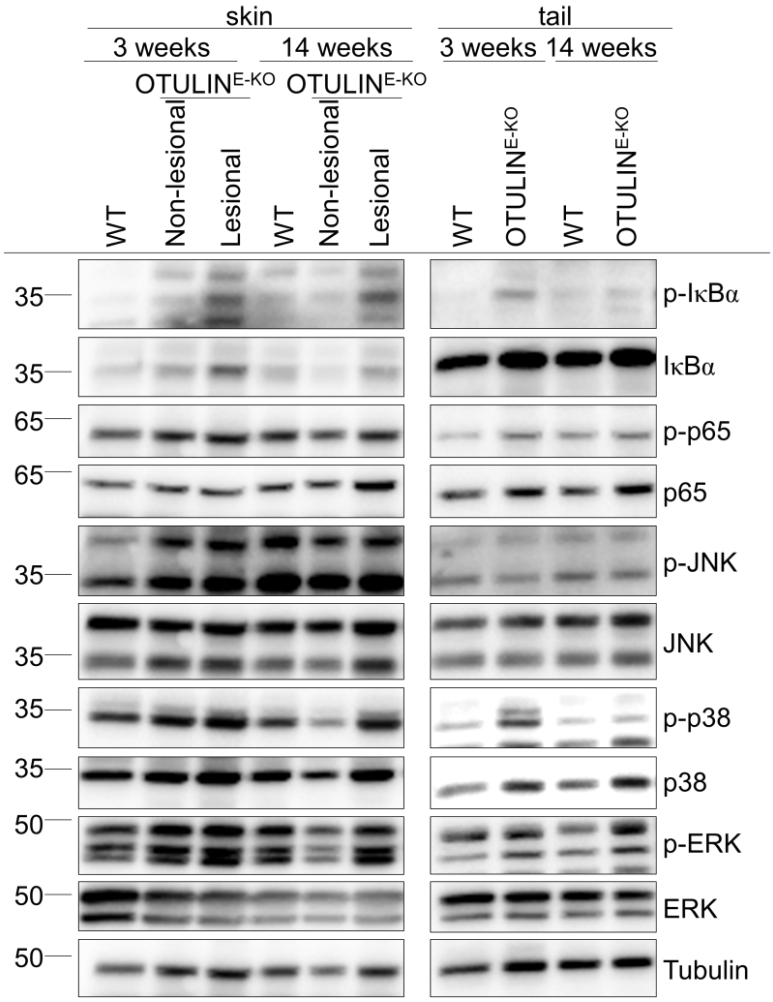

Figure 22: No difference in pro-survival signaling in OTULIN^{EKO} mice.

Immunoblot analysis with the indicated antibodies of protein extracts from 3-week or 14-week old lesional or non-lesional skin or tail skin tissue from OTULIN^{E-KO} mice or WT mice.

To exclude the possible compensatory effects and influence of other cells resident in the epidermis and expressing OTULIN, *in vitro* analysis of primary keratinocytes isolated from OTULIN^{E-KO} mice was performed. Surprisingly, OTULIN ablated keratinocytes did not show changes in NF-κB or MAPK signaling activation in response to TNF stimulation for different timepoints. TNF stimulation caused rapid phosphorylation and degradation of Iκbα after 15 min and robust phosphorylation of NF-κB subunit p65, comparably in keratinocytes isolated from both WT and OTULIN^{E-KO} mice. Consistently, MAPKs JNK, p38 and ERK were phosphorylated after 15 min of TNF treatment in OTULIN^{E-KO} and WT keratinocytes, respectively (Figure 23).

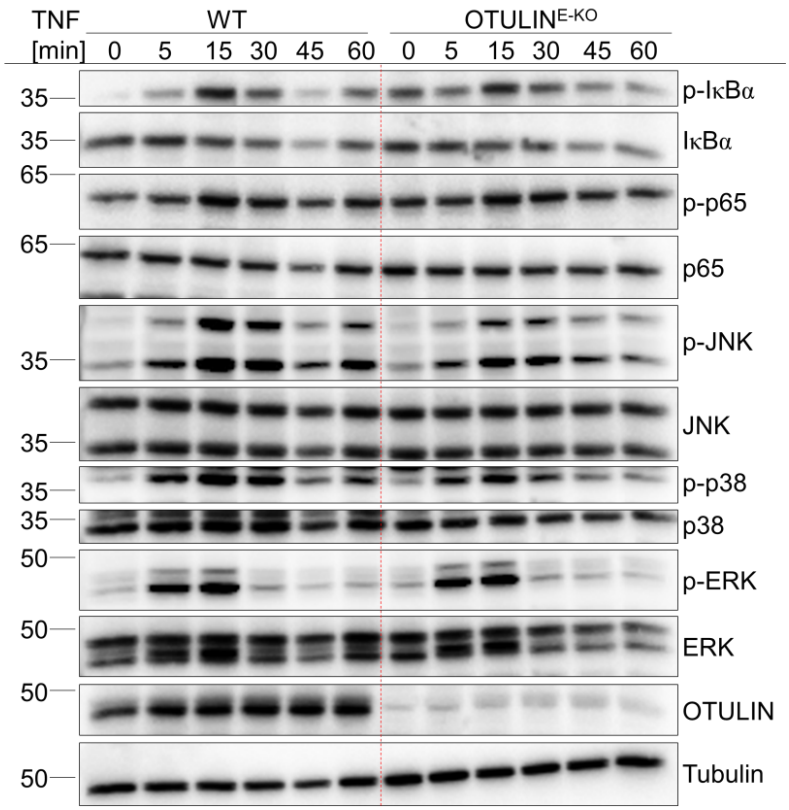

Figure 23: Primary keratinocytes derived from OTULIN^{E-KO} mice are not sensitized to TNF-induced pro-survival signaling.

Immunoblot analysis with the indicated antibodies of protein extracts of primary keratinocytes derived from OTULIN^{E-KO} mice or WT mice, which were left untreated (Medium) or stimulated with TNF for the indicated timepoints

Given the important function of LUBAC in preventing cell death [171, 221], keratinocytes derived from OTULIN^{E-KO} mice were analyzed for increased sensitivity to cell death using IncuCyte® real-time live cell imaging. Cells were stimulated for 24 h with TNF (T) alone or in combination with the pan-caspase inhibitor z-VAD-fmk (Z) and the SMAC mimetic (S) compound Birinapant, an inhibitor of cIAP1/2 resulting in destabilization of TNFR1-associated complex I. Furthermore, cells were stained with Draq7 to detect dying cells. Surprisingly, no differences in the kinetics and amount of Draq7 positive cells and thereby cell death could be observed between WT and OTULIN deficient keratinocytes (Figure 24a). However, the sensitizing effect of OTULIN deficiency to TNF-induced cell death might be masked by the increased amount of spontaneous death generally observed in primary keratinocyte cultures (Figure 24b). Taken together, the loss of OTULIN in keratinocytes is neither affecting NF-κB or MAPK signaling, nor sensitivity to cell death upon TNF stimulation

in vitro. Combined, the observed skin pathology in OTULIN$^{E\text{-}KO}$ mice demonstrates that OTULIN deficiency contributes to skin inflammation, however the cellular mechanisms remain unclear.

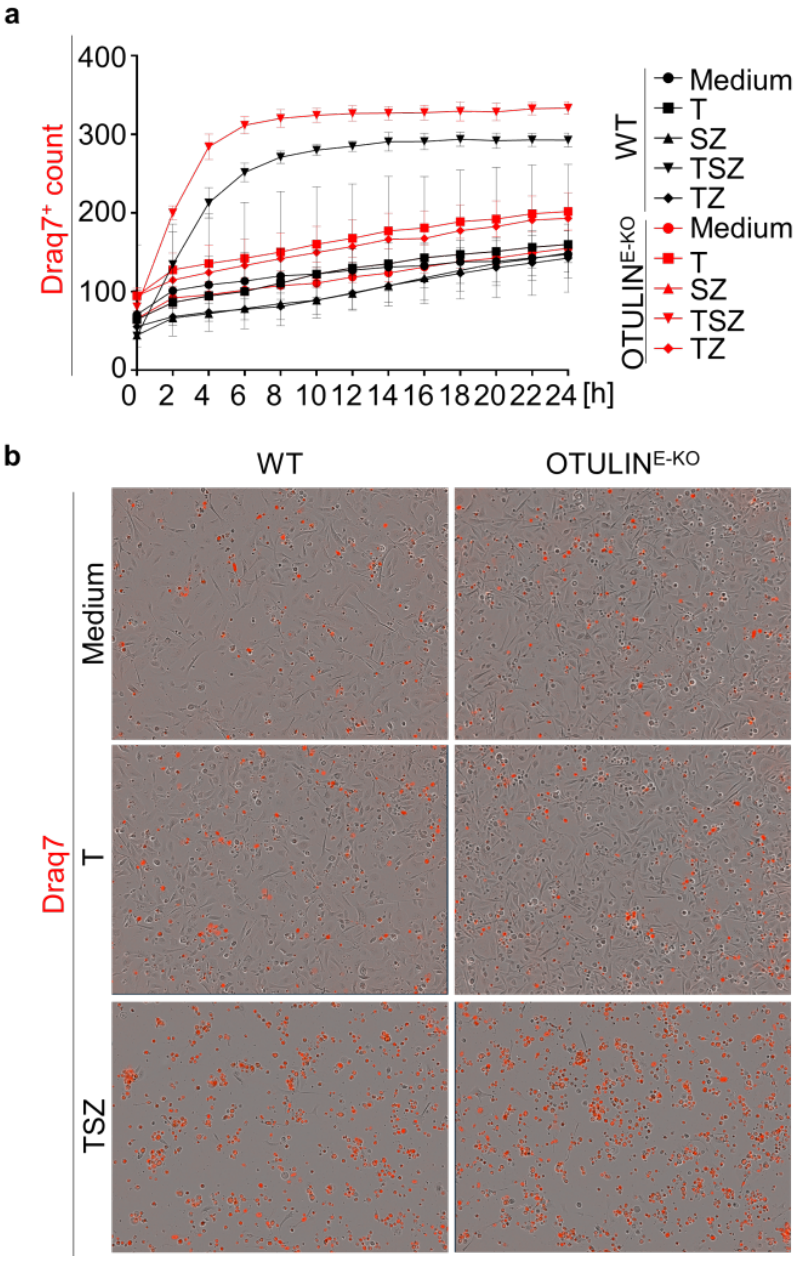

Figure 24: OTULIN$^{E\text{-}KO}$ keratinocytes are not sensitized to TNF cell death.

(a) Cell death measured by Draq7 uptake in primary keratinocytes of the indicated genotypes treated with combinations of TNF (T), SMAC mimetics (S) or Z-VAD-FMK (Z) for 24 h. Graph shows mean value from technical duplicates (n=2), from one representative out of three independent experiments. (b) Representative images from primary keratinocytes of the indicated genotypes treated with combinations of T, S or Z for 24 h. Dead cells are stained red from Draq7 uptake.

2.2 TNFR1 signaling mediates skin inflammation in OTULIN$^{E\text{-}KO}$ mice

2.2.1 Epidermis specific TNFR1 deficiency prevents skin pathology in OTULIN$^{E\text{-}KO}$ mice

Anti-TNF treatment was previously shown to prevent TNF-dependent systemic inflammation in humans and mice with inducible systemic OTULIN deficiency in ORAS patients [184-186]. To address the cell intrinsic role of TNFR1 signaling in inflammation and cell death in the skin of OTULIN$^{E\text{-}KO}$ mice, *Otulin*$^{fl/fl}$ *Tnfr1*$^{fl/fl}$ K14-Cre (hereafter referred to as OTULIN$^{E\text{-}KO}$; TNFR1$^{E\text{-}KO}$) mice were generated. OTULIN$^{E\text{-}KO}$; TNFR1$^{E\text{-}KO}$ mice were protected from developing spontaneous skin pathology during the first weeks of life and remained lesion-free up to 50 weeks (Figure 25a, b).

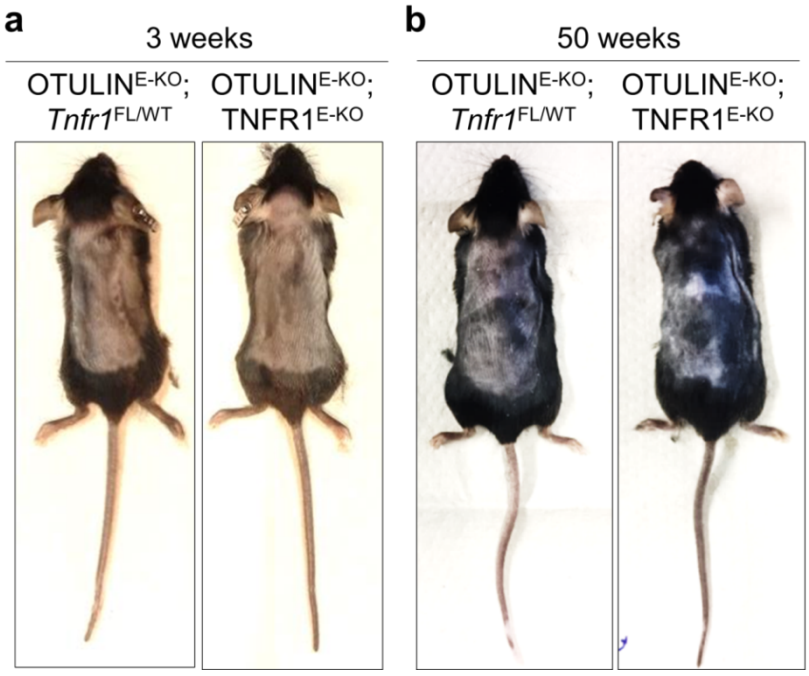

Figure 25: TNFR1 signaling promotes skin pathology in OTULIN$^{E\text{-}KO}$ mice.

Photographs of mice with the indicated genotypes at the age of 3 weeks. Images shown are representative of n > 25 OTULIN$^{E\text{-}KO}$; TNFR1$^{E\text{-}KO}$ mice. (b) Photographs of mice with the indicated genotypes at the age of 50 weeks. Images shown are representative of n > 25 OTULIN$^{E\text{-}KO}$; TNFR1$^{E\text{-}KO}$ mice.

Since the additional epidermis-specific deletion of TNFR1 protected OTULIN$^{E\text{-}KO}$ mice from skin disease, OTULIN$^{E\text{-}KO}$; TNFR1$^{E\text{-}KO}$ mice survived at least up to the age of one year, whereas OTULIN$^{E\text{-}KO}$ mice had to be culled around the age of 14 weeks (Figure 26).

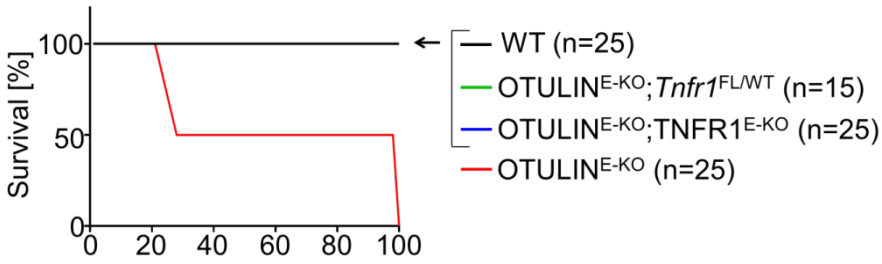

Figure 26: Ablation of TNFR1 signaling prevents lethality in OTULIN^{E-KO} mice.

Kaplan-Meier plot depicting survival of mice of the indicated genotypes.

All monitored OTULIN^{E-KO}; TNFR1^{E-KO} mice did not develop skin lesions and were indistinguishable from littermates. Furthermore, the keratinocyte-specific heterozygosity of TNFR1 strongly ameliorated the development of skin pathology in OTULIN^{E-KO} mice (Figure 27). Combined, these data demonstrate TNFR1 signaling to trigger the development of skin lesions in OTULIN^{E-KO} mice.

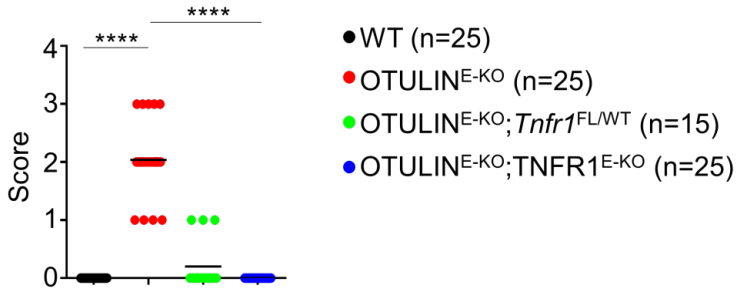

Figure 27: Macroscopic skin score.

Graph depicting macroscopic skin score of mice of the indicated genotypes. Each dot represents one mouse. Bars represent mean.

2.2.2 OTULIN^{E-KO}; TNFR1^{E-KO} mice display no inflammation and cell death in the skin

Consistent with absence of pathology, histological analysis of back skin and tail skin tissue revealed that keratinocyte specific ablation of TNFR1 fully prevented keratinocyte death reflected by CC3 and CC8 staining in 3-week old OTULIN^{E-KO} mice. Furthermore, epidermal hyperplasia presented by increased Ki-67 staining could not be observed in young OTULIN^{E-KO}; TNFR1^{E-KO} mice, further confirming that TNFR1 induces skin inflammation in OTULIN^{E-KO} mice (Figure 28).

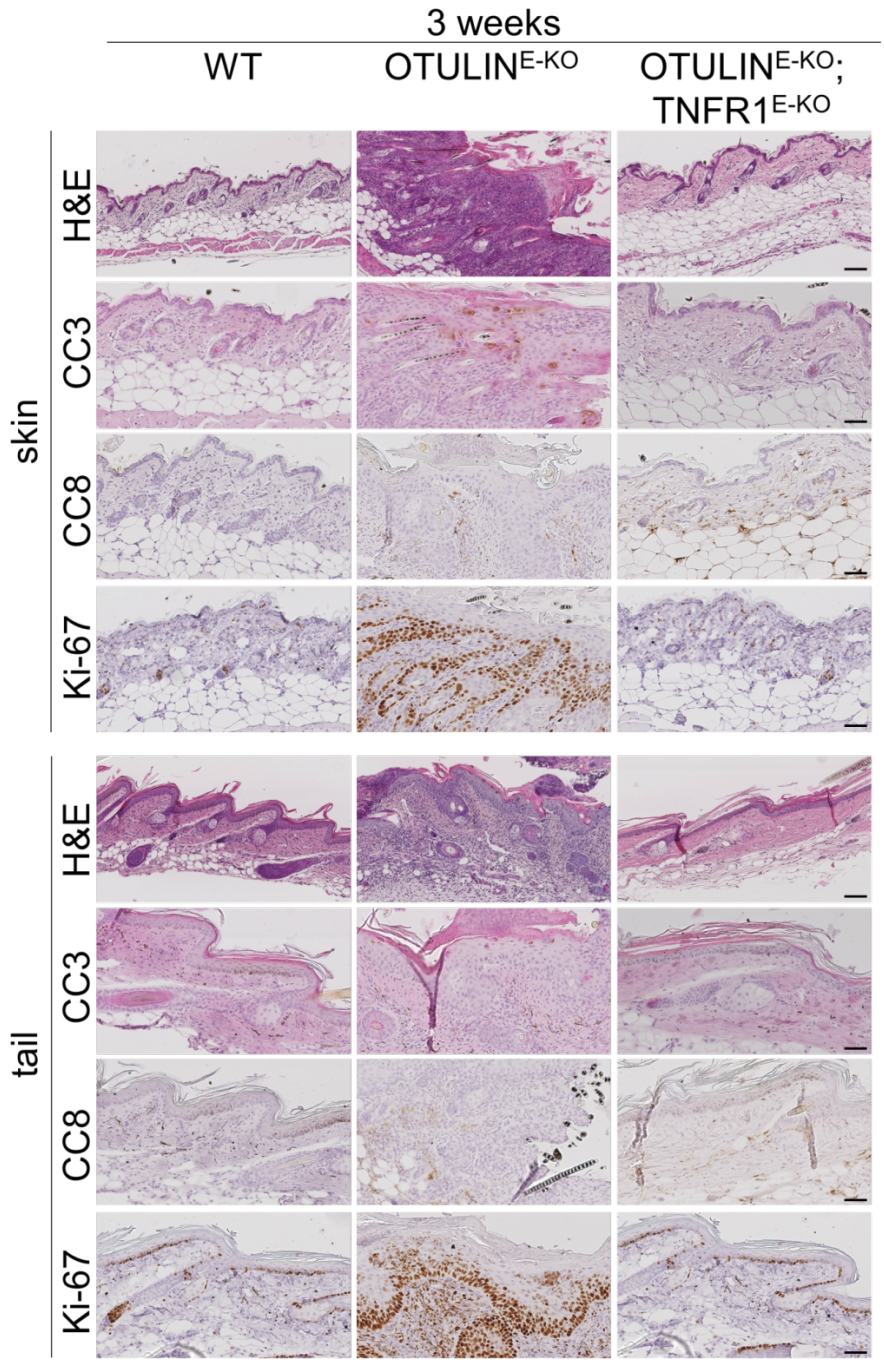

Figure 28: Ablation of TNFR1 prevents hyperproliferation and cell death in OTULIN^{E-KO} mice.

Representative images from skin sections from 3-week old mice of the indicated genotypes, stained with H&E, anti-CC3, anti-CC8 or anti-Ki67 antibodies. Scale bar H&E = 100µm; CC3, CC8, Ki67 = 50µm.

Cell death and hyperproliferation could not be observed in OTULIN$^{E\text{-}KO}$; TNFR1$^{E\text{-}KO}$ back and tail skin up to 50 weeks of age, demonstrating TNFR1 signaling to be the main driver of skin disease progression in OTULIN$^{E\text{-}KO}$ mice (Figure 29).

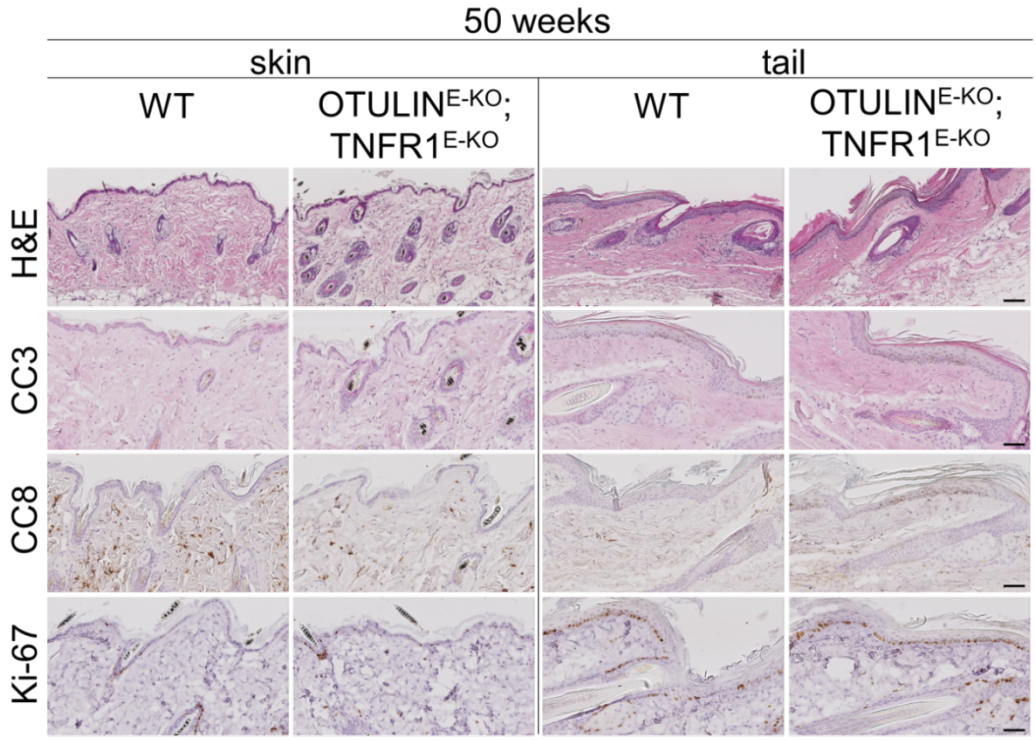

Figure 29: Ablation of TNFR1 prevents hyperproliferation and cell death in aged OTULIN$^{E\text{-}KO}$ mice.

Representative images from skin sections from 50-week old mice of the indicated genotypes, stained with H&E, anti-CC3, anti-CC8 or anti-Ki67 antibodies. Scale bar H&E = 100µm; CC3, CC8, Ki67 = 50µm.

In addition, staining for the epidermal differentiation marker K10 and K6 in skin samples from OTULIN$^{E\text{-}KO}$; TNFR1$^{E\text{-}KO}$ revealed no upregulated expression compared to OTULIN$^{E\text{-}KO}$ skin. Consistently, infiltrating immune cells were completely absent in OTULIN$^{E\text{-}KO}$; TNFR1$^{E\text{-}KO}$ back skin and tail skin, suggesting that myeloid cell infiltrates in OTULIN$^{E\text{-}KO}$ mice are a consequence of TNFR1 dependent induction of skin inflammation (Figure 30).

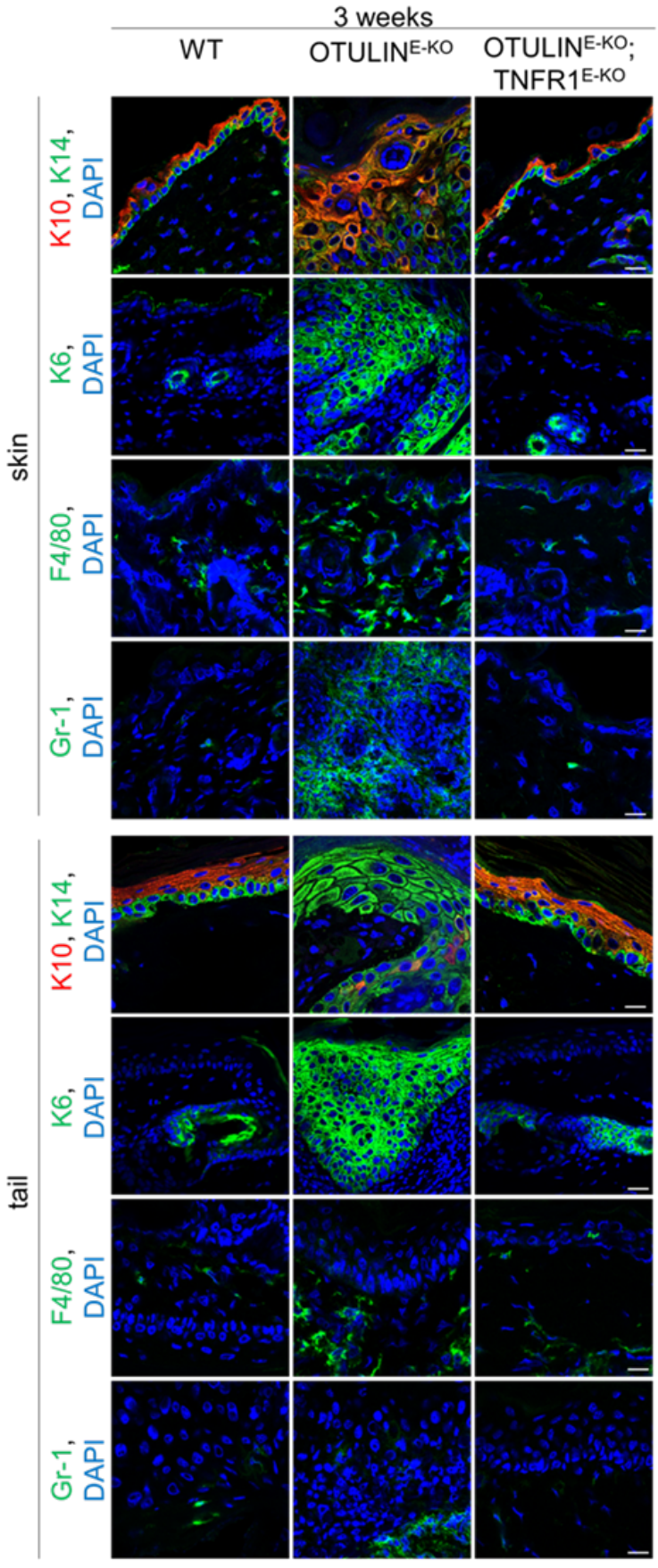

Figure 30: Restored skin structure and homeostasis in OTULIN$^{E\text{-}KO}$; TNFR1$^{E\text{-}KO}$ mice.

Representative images from skin sections from 3-week old mice of the indicated genotypes, immunostained with anti-K10, anti- K14, anti-K6, anti-F4/80, anti-Gr-1 and DAPI (DNA stain). Scale bar K10, K14, K6 = 20µm; F4/80, Gr-1 = 30µm.

Furthermore, the skin structure of OTULIN$^{E\text{-}KO}$; TNFR1$^{E\text{-}KO}$ mice appeared indistinguishable to WT skin up to the age of 50 weeks, without detecting immune cell infiltrates in the back and tail skin (Figure 31). In summary, keratinocyte-intrinsic TNFR1 signaling activation is crucial for the induction of skin inflammation in OTULIN$^{E\text{-}KO}$ mice.

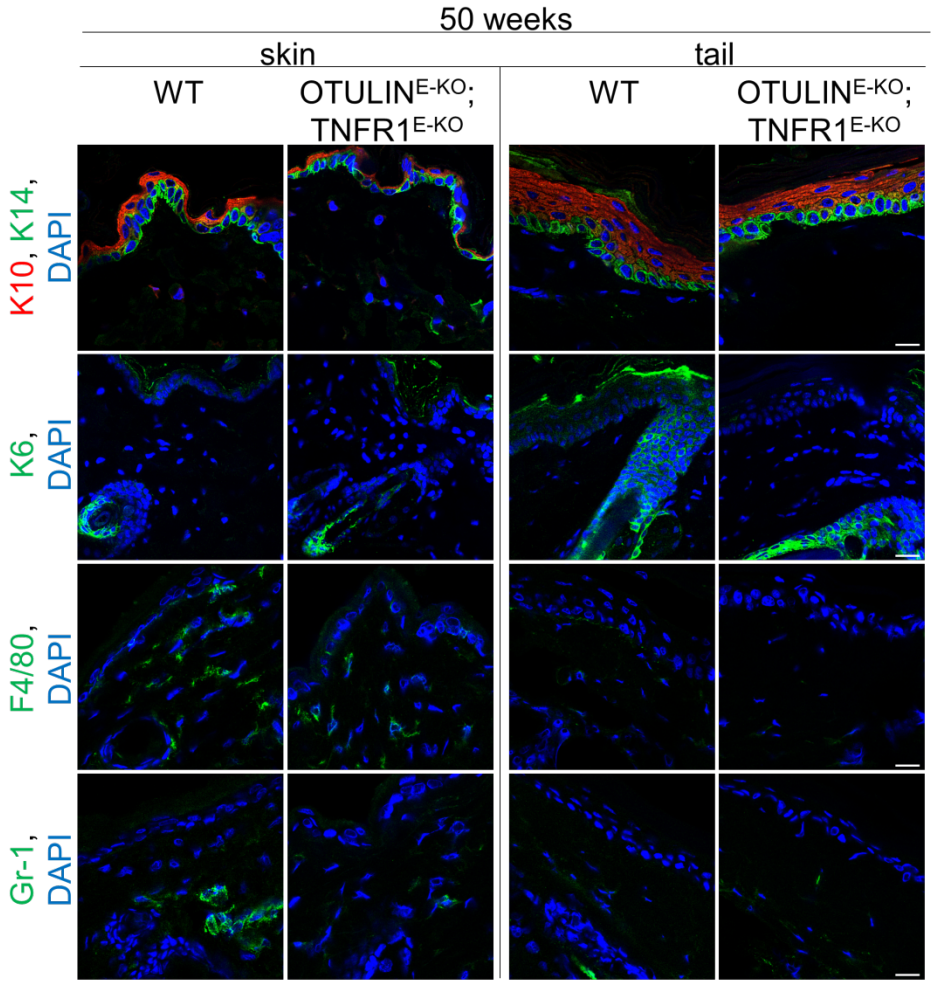

Figure 31: Restored skin structure and homeostasis in aged OTULIN$^{E\text{-}KO}$; TNFR1$^{E\text{-}KO}$ mice.

Representative images from skin sections from 50-week old mice of the indicated genotypes, immunostained with anti-K10, anti-K14, anti-K6, anti-F4/80, anti-Gr-1 and DAPI (DNA stain). Scale bar K10, K14, K6 = 20µm; F4/80, Gr-1 = 30µm.

2.2.3 OTULIN$^{E\text{-}KO}$; TNFR1$^{E\text{-}KO}$ mice display normalized expression of inflammatory genes

To further investigate the requirement of TNFR1 for skin inflammation we applied gene expression analysis of inflammatory cytokines chemokines. qRT-qPCR analysis revealed full restored and normalized gene expression of selected cytokines (*Il-6, Il-1β*) and chemokines

(*Ccl3, Cxcl3, Cxcl9, Cxcl10*) in skin lysates from OTULIN$^{E\text{-}KO}$; TNFR1$^{E\text{-}KO}$ mice further confirming that TNFR1 signaling is required for enhanced inflammatory gene expression in OTULIN$^{E\text{-}KO}$ mice (Figure 32). In summary, these results demonstrate that skin inflammation in OTULIN$^{E\text{-}KO}$ mice is fully dependent on keratinocyte specific TNFR1 signaling.

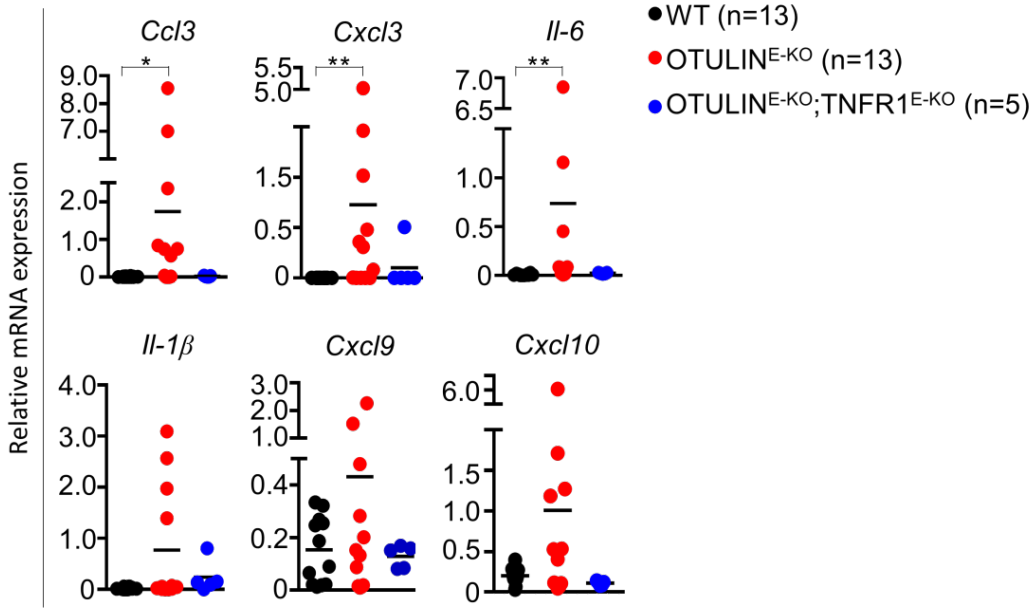

Figure 32: Deletion of TNFR1 prevents cytokine and chemokine upregulation in OTULIN$^{E\text{-}KO}$ skin.

Graphs depicting relative mRNA expression of the indicated genes in RNA from whole skin tissue of mice of the indicated genotypes at 3 weeks of age measured by qRT-PCR. Each dot represents one mouse. Bars represent mean.

2.3 RIPK1 kinase activity triggers cell death in OTULIN$^{E\text{-}KO}$ mice

2.3.1 RIPK1 kinase activity is required for the skin disease development in OTULIN$^{E\text{-}KO}$ mice

Although increased sensitivity to TNF-induced cell death could not be detected *in vitro* in OTULIN deficient keratinocytes, TNFR1 ablation fully protected OTULIN$^{E\text{-}KO}$ mice from skin lesion development. Moreover, dying keratinocytes could be observed in the epidermis of OTULIN$^{E\text{-}KO}$ mice, which sets off the question, whether TNFR1-triggered cell death is involved in driving skin pathology in OTULIN$^{E\text{-}KO}$ mice. If linear ubiquitination in TNFR1 signalling is dys-balanced, TNF will cause cell death by activating RIPK1-kinase mediated apoptosis and necroptosis [34, 151, 171]. Moreover, expression of a kinase inactive version of RIPK1 that harbors an exchange at amino acid 138 (D -> N at position 138) can block TNFR1 dependent

apoptosis and necroptosis *in vivo* [56, 216]. To elucidate the effect of RIPK1 kinase activity in provoking cell death in the epidermis of OTULIN$^{E\text{-}KO}$ mice, *Otulin*$^{fl/fl}$ *K14-Cre*$^{tg/wt}$ *Ripk1*$^{D138N/D138N}$ (hereafter referred to as OTULIN$^{E\text{-}KO}$; *Ripk1*$^{D138N/D138N}$) mice were generated and analyzed. OTULIN$^{E\text{-}KO}$; *Ripk1*$^{D138N/D138N}$ mice were indistinguishable from WT littermates and did not develop visible skin lesions up to 50 weeks of age. Additionally, the expression of one mutant allele of RIPK1 largely ameliorated the development of the skin disease observed in OTULIN$^{E\text{-}KO}$ mice, thereby allowing survival to adulthood (Figure 33a, b).

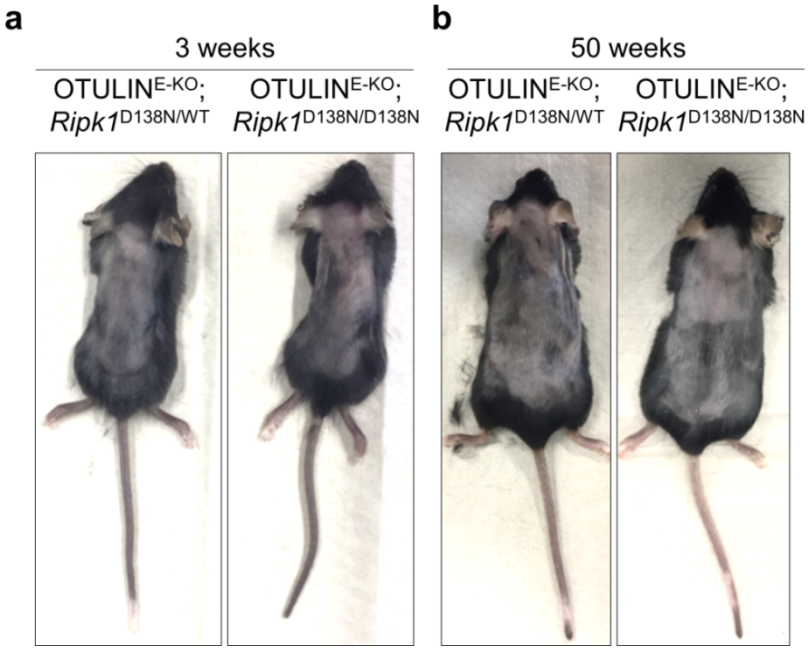

Figure 33: RIPK1 kinase activity drives skin pathology in OTULIN$^{E\text{-}KO}$ mice.

(a) Photographs of mice with the indicated genotypes at the age of 3 weeks. Images shown are representative of n > 25 OTULIN$^{E\text{-}KO}$; *Ripk1*$^{D138N/D138N}$ mice. (b) Photographs of mice with the indicated genotypes at the age of 50 weeks. Images shown are representative of n > 25 OTULIN$^{E\text{-}KO}$; *Ripk1*$^{D138N/D138N}$ mice.

Since OTULIN$^{E\text{-}KO}$; *Ripk1*$^{D138N/D138N}$ mice did not develop macroscopically visible skin lesions, they survived up to at least the age of one year and were protected from early lethality seen in OTULIN$^{E\text{-}KO}$ mice (Figure 34).

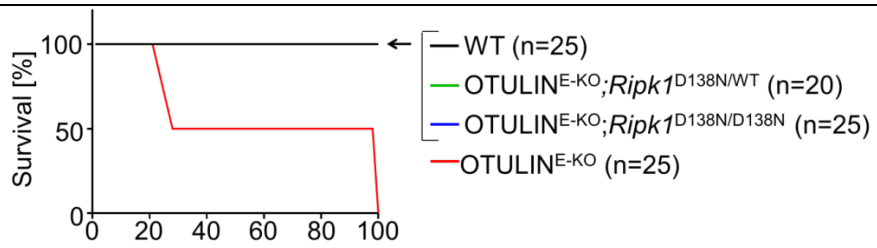

Figure 34: Loss of RIPK1 kinase activity prevents lethality in OTULIN$^{E\text{-}KO}$ mice

Kaplan-Meier plot depicting survival of mice of the indicated genotypes.

Correspondingly, all OTULIN$^{E\text{-}KO}$; *Ripk1*$^{D138N/D138N}$ mice were judged score 0 on a macroscopic skin check, demonstrating that RIPK1 kinase activity is important for the maturation of the skin disease in OTULIN$^{E\text{-}KO}$ mice (Figure 35).

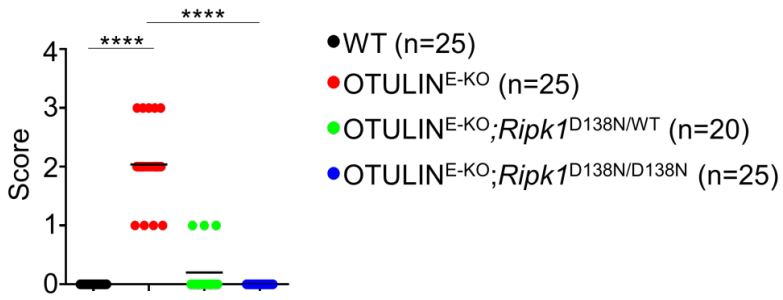

Figure 35: Macroscopic kin score.

Graph depicting macroscopic skin score of mice of the indicated genotypes. Each dot represents one mouse. Bars represent mean.

2.3.2 OTULIN$^{E\text{-}KO}$; *Ripk1*$^{D138N/D138N}$ mice are protected from cell death in the skin.

In line with a role for RIPK1 kinase activity in TNF induced cell death, immunohistological analysis against CC3 and CC8 on back skin and tail skin sections revealed protection from cell death in 3-week old OTULIN$^{E\text{-}KO}$; *Ripk1*$^{D138N/D138N}$ mice. Furthermore, Ki-67 positive cells displayed a similar pattern in OTULIN$^{E\text{-}KO}$; *Ripk1*$^{D138N/D138N}$ compared to WT skin, indicating inhibited hyperplasia compared to OTULIN$^{E\text{-}KO}$ mice (Figure 36).

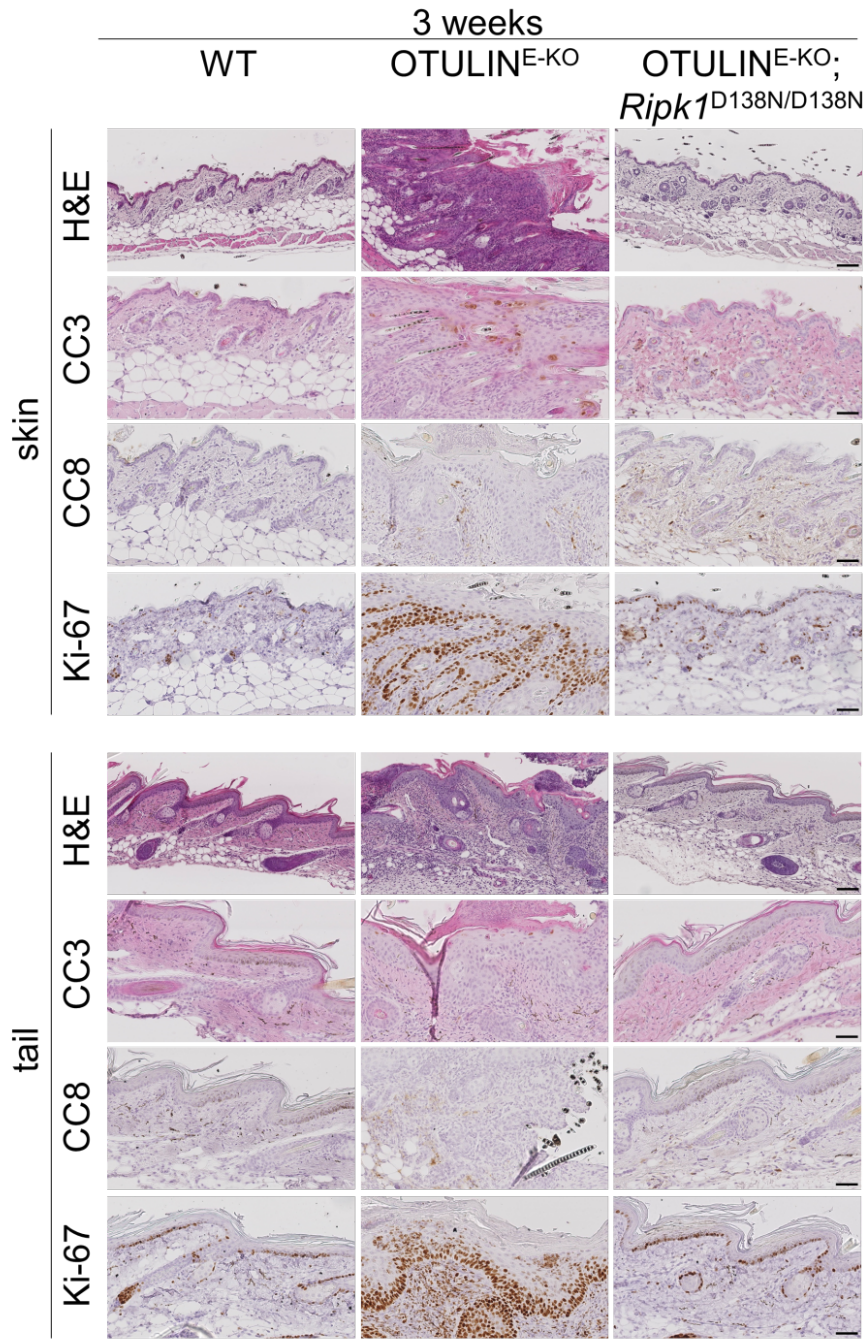

Figure 36: *Ripk1*^{D138N} mutation prevents hyperproliferation and cell death in OTULIN^{E-KO} mice.

Representative images from skin sections from 3-week old mice of the indicated genotypes, stained with H&E, anti-CC3, anti-CC8 or anti-Ki67 antibodies. Scale bar H&E = 100µm; CC3, CC8, Ki67 = 50µm.

However, few CC3 and CC8 positive stained cells in some skin areas could be detected in adult OTULIN^{E-KO}; *Ripk1*$^{D138N/D138N}$ mice, hinting to RIPK1 kinase-independent cell death in OTULIN^{E-KO} mice during aging. Moreover, slightly enhanced Ki-67 positive cells displayed mild epidermal hyperproliferation in OTULIN^{E-KO}; *Ripk1*$^{D138N/D138N}$ aged mice (Figure 37).

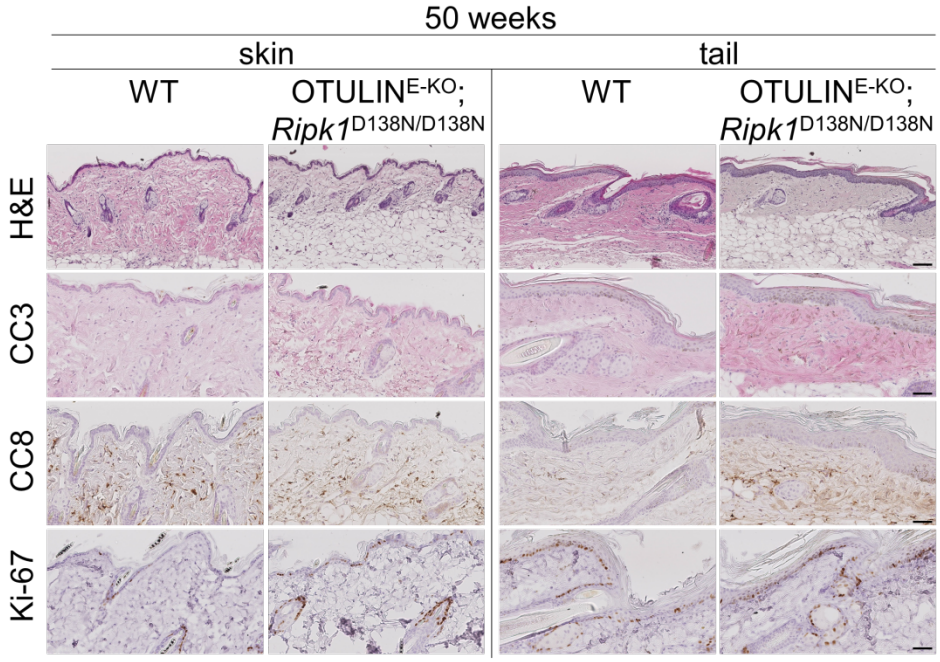

Figure 37: *Ripk1*^{D138N} mutation prevents hyperproliferation and cell death in aged OTULIN^{E-KO} mice.

Representative images from skin sections from 50-week old mice of the indicated genotypes, stained with H&E, anti-CC3, anti-CC8 or anti-Ki67 antibodies. Scale bar H&E = 100µm; CC3, CC8, Ki67 = 50µm.

The epidermal differentiation markers K10, K14 and K6 displayed similar expression in young OTULIN^{E-KO}; *Ripk1*$^{D138N/D138N}$ mice and WT mice. Furthermore, myeloid cell infiltrates were absent in the skin from 3 week-old OTULIN^{E-KO}; *Ripk1*$^{D138N/D138N}$ mice (Figure 38).

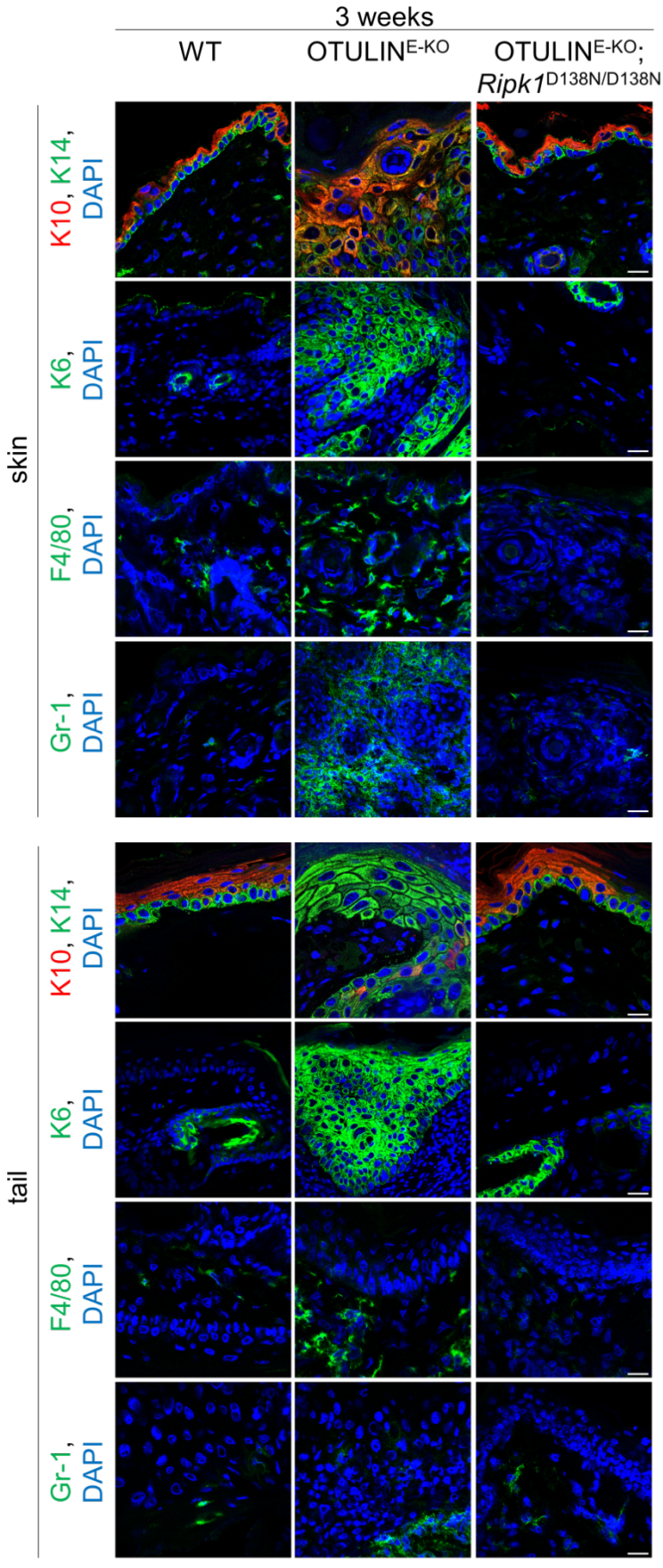

Figure 38: Restored skin structure in OTULIN$^{E\text{-}KO}$; *Ripk1*$^{D138N/D138N}$ mice.

Representative images from skin sections from 3-week old mice of the indicated genotypes, immunostained with anti-K10, anti- K14, anti-K6, anti-F4/80, anti-Gr-1 and DAPI (DNA stain). Scale bar K10, K14, K6 = 20µm; F4/80, Gr-1 = 30µm.

Detection of increased K14 and K6 positive cells in the tail epidermis from 50 week-old OTULIN$^{E\text{-}KO}$; *Ripk1*$^{D138N/D138N}$ mice revealed mild alterations in their expression compared to WT skin (Figure 39). However, increased myeloid cell infiltration in back and tail skin could not be detected in 50 week-old OTULIN$^{E\text{-}KO}$; *Ripk1*$^{D138N/D138N}$ mice (Figure 39). Therefore, RIPK1 kinase activity-dependent signaling triggers keratinocyte death and epidermal hyperplasia while RIPK1 kinase independent mechanisms mildly affect skin homeostasis during ageing.

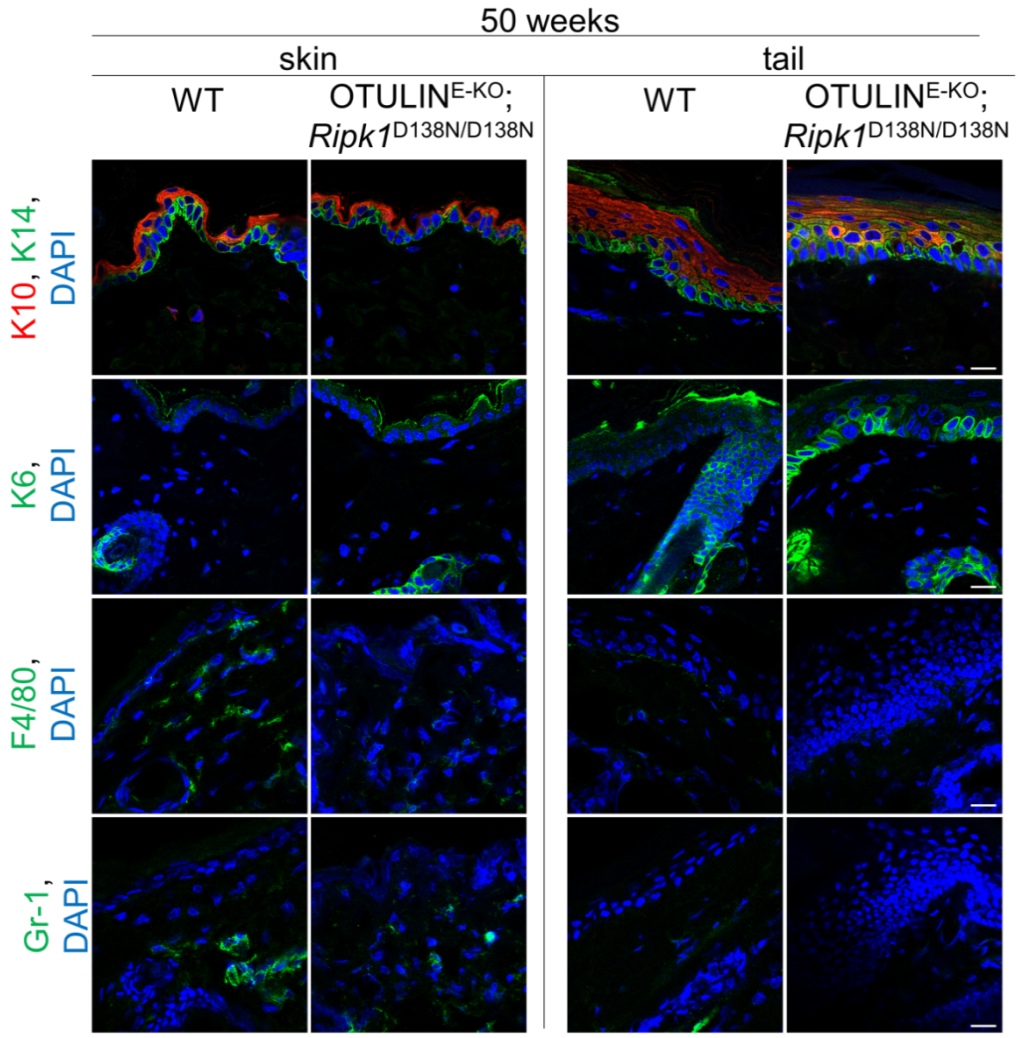

Figure 39: Mild changes in the skin structure in old OTULIN$^{E\text{-}KO}$; *Ripk1*$^{D138N/D138N}$ mice.

Representative images from skin sections from 50-week old mice of the indicated genotypes, immunostained with anti-K10, anti-K14, anti-K6, anti-F4/80, anti-Gr-1 and DAPI (DNA stain). Scale bar K10, K14, K6 = 20µm; F4/80, Gr-1 = 30µm.

2.3.3 OTULIN^{E-KO}; *Ripk1*$^{D138N/D138N}$ mice reveal no increased expression of inflammatory genes.

RT-qPCR analysis confirmed a restored and to WT level reduced normalized gene expression of selected cytokines and chemokines in skin lysates from OTULIN^{E-KO}; *Ripk1*$^{D138N/D138N}$ mice (Figure 40). Combined, the data uncover RIPK1 kinase activity as a critical factor to trigger skin inflammation in OTULIN^{E-KO} mice.

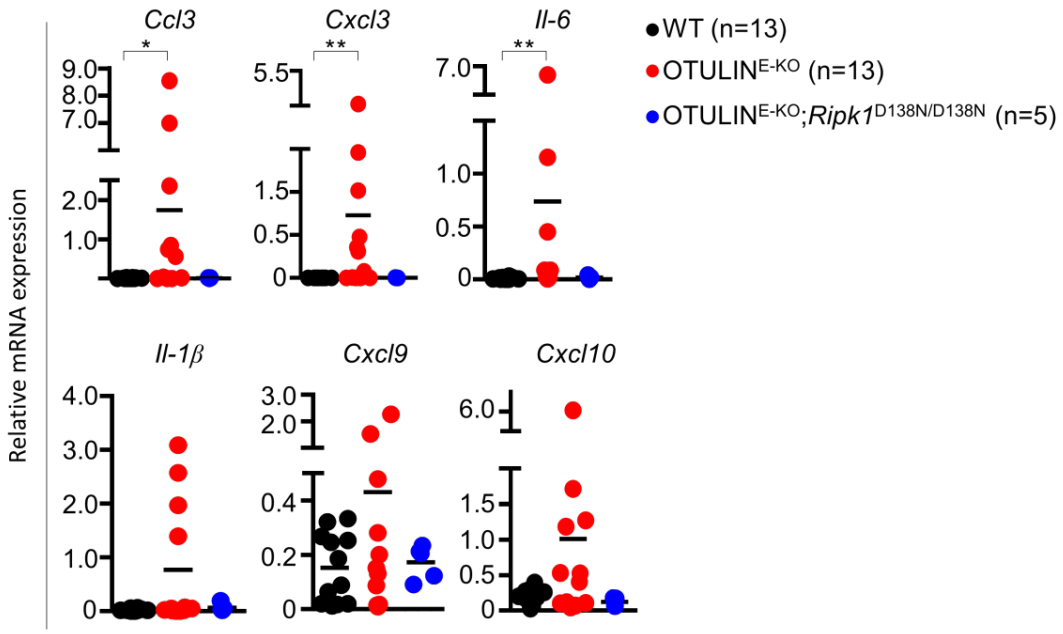

Figure 40: *Ripk1*^{D138N} mutation protects OTULIN^{E-KO} mice from cytokine and chemokine upregulation.

Graphs depicting relative mRNA expression of the indicated genes in RNA from whole skin tissue of mice of the indicated genotypes at 3 weeks of age, measured by qRT-PCR. Each dot represents one mouse. Bars represent mean.

2.4 Necroptotic cell death regulators implement skin disease in OTULIN^{E-KO} mice

2.4.1 RIPK3 and MLKL dependent necroptosis promotes skin pathology in OTULIN^{E-KO} mice

RIPK1 kinase activity has been identified to be important for FADD-caspase-8-dependent apoptosis and RIPK3-MLKL-dependent necroptosis [216]. Since necroptosis is considered to be a highly inflammatory type of cell death, RIPK1-dependent keratinocyte necroptosis could be causative for skin lesion development in OTULIN^{E-KO} mice [11, 228, 229]. To investigate the skin epithelial specific roles of RIPK3 and MLKL dependent necroptosis in OTULIN^{E-KO} mice,

OTULIN$^{E\text{-}KO}$; *Ripk3*$^{-/-}$ and OTULIN$^{E\text{-}KO}$; *Mlkl*$^{-/-}$ mice were generated by crossing OTULIN$^{E\text{-}KO}$ mice to *Ripk3*$^{-/-}$ and M*lkl*$^{-/-}$ mice. Both, ablation of RIPK3 and MLKL could strongly protect, however not fully prevent skin pathology in OTULIN$^{E\text{-}KO}$ mice. Despite the occurrence of small skin lesions, the tail skin was not affected in OTULIN$^{E\text{-}KO}$; *Ripk3*$^{-/-}$ and OTULIN$^{E\text{-}KO}$; *Mlkl*$^{-/-}$ mice (Figure 41a,b).

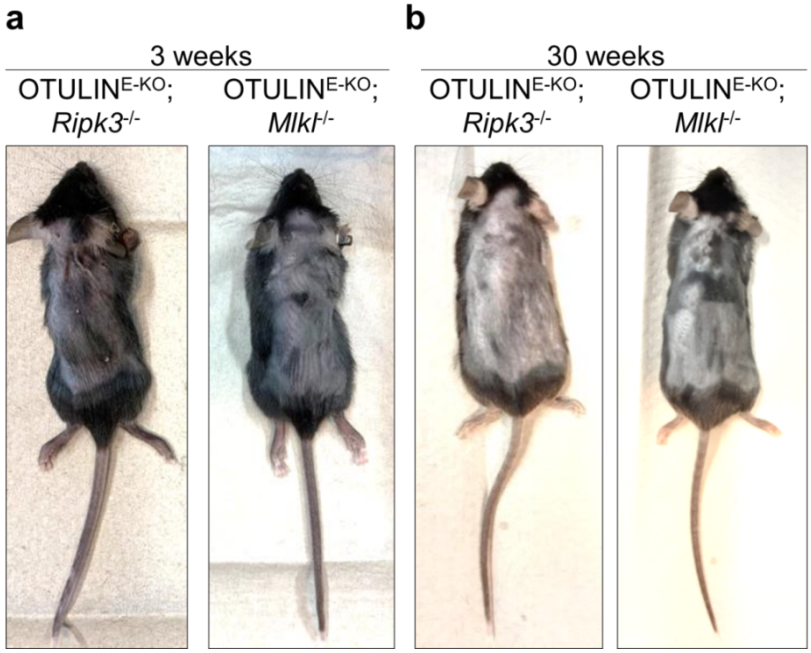

Figure 41: RIPK3 and MLKL deletion strongly ameliorate the skin disease in OTULIN$^{E\text{-}KO}$ mice.

Photographs of mice with the indicated genotypes at the age of 30 weeks. Images shown are representative of n > 10 mice with the indicated genotypes. (b) Photographs of mice with the indicated genotypes at the age of 30 weeks. Images shown are representative of n > 10 mice with the indicated genotypes.

Hence, OTULIN$^{E\text{-}KO}$; *Ripk3*$^{-/-}$ and OTULIN$^{E\text{-}KO}$; *Mlkl*$^{-/-}$ mice survived up to one year of age without developing skin lesions that required earlier sacrifice (Figure 42).

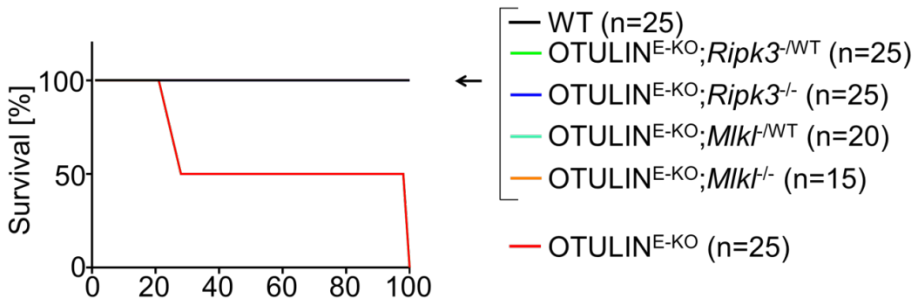

Figure 42: Loss of RIPK3 or MLKL prevents lethality in OTULIN$^{E\text{-}KO}$ mice.

Kaplan-Meier plot depicting survival of mice of the indicated genotypes.

Nonetheless, small spots with scaly skin could be observed on the back skin of OTULIN$^{E\text{-}KO}$; *Ripk3*$^{-/-}$ and OTULIN$^{E\text{-}KO}$; *Mlkl*$^{-/-}$ mice, reflected by a score of 1 on the skin score scale. Heterozygous deficiency of RIPK3 or MLKL also considerably ameliorated skin lesion development in OTULIN$^{E\text{-}KO}$ mice suggesting a gene dosage effect (Figure 43). Thus, RIPK3 and MLKL dependent necroptosis is critical in skin disease development in OTULIN$^{E\text{-}KO}$ mice.

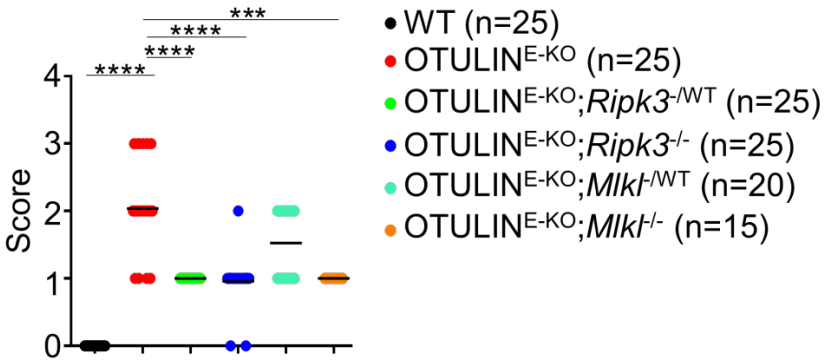

Figure 43: Macroscopic skin score.

Graph depicting macroscopic skin score of mice of the indicated genotypes. Each dot represents one mouse. Bars represent mean.

2.4.2 OTULIN$^{E\text{-}KO}$; *Ripk3*$^{-/-}$ and OTULIN$^{E\text{-}KO}$; *MLKL*$^{-/-}$ mice do not reveal inflammation and ongoing cell death in the skin

Histological skin tissue analysis confirmed the absence of severe skin lesions in 3-week old OTULIN$^{E\text{-}KO}$; *Ripk3*$^{-/-}$ and OTULIN$^{E\text{-}KO}$; *Mlkl*$^{-/-}$ mice, revealing only mild keratinocyte proliferation in the tail skin, detected by slightly increased Ki-67 staining. Moreover, cell death could not be observed by staining for CC3 and CC8 in back skin from OTULIN$^{E\text{-}KO}$; *Ripk3*$^{-/-}$ and OTULIN$^{E\text{-}KO}$; *Mlkl*$^{-/-}$ mice (Figure 44).

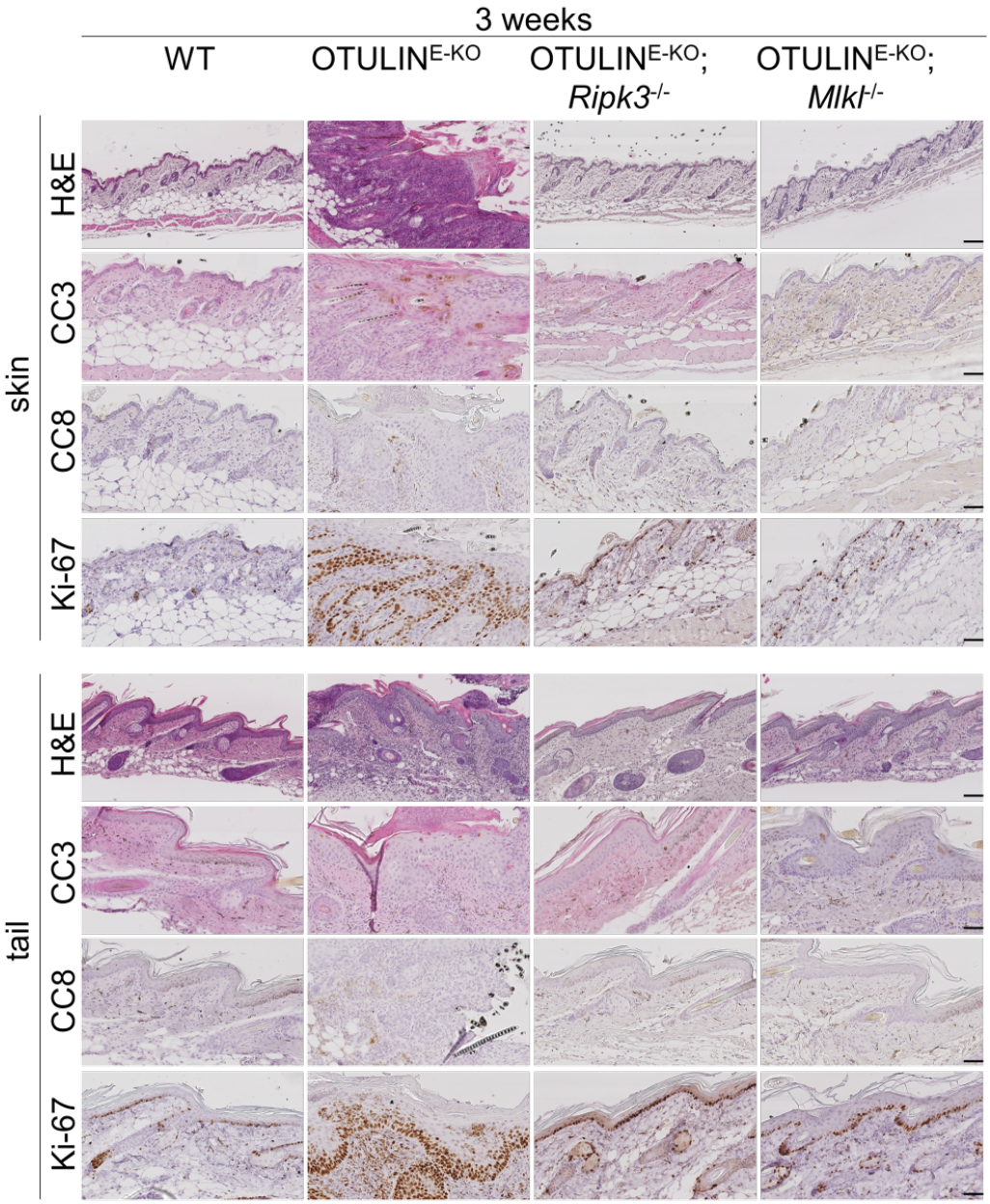

Figure 44: RIPK3 and MLKL promote inflammation and cell death in OTULIN^{E-KO} mice.

Representative images from skin sections from 3-week old mice of the indicated genotypes, stained with H&E, anti-CC3, anti-CC8 or anti-Ki67 antibodies. Scale bar H&E = 100µm; CC3, CC8, Ki67 = 50µm.

When followed up to 50 weeks, the skin lesions in OTULIN^{E-KO}; *Ripk3*$^{-/-}$ and OTULIN^{E-KO}; *Mlkl*$^{-/-}$ mice did not mature and displayed only mild epidermal hyperproliferation. Furthermore, only few CC3 and CC8 positive cells could be detected in the tail epidermis, while the back skin epidermis resembled WT skin (Figure 45).

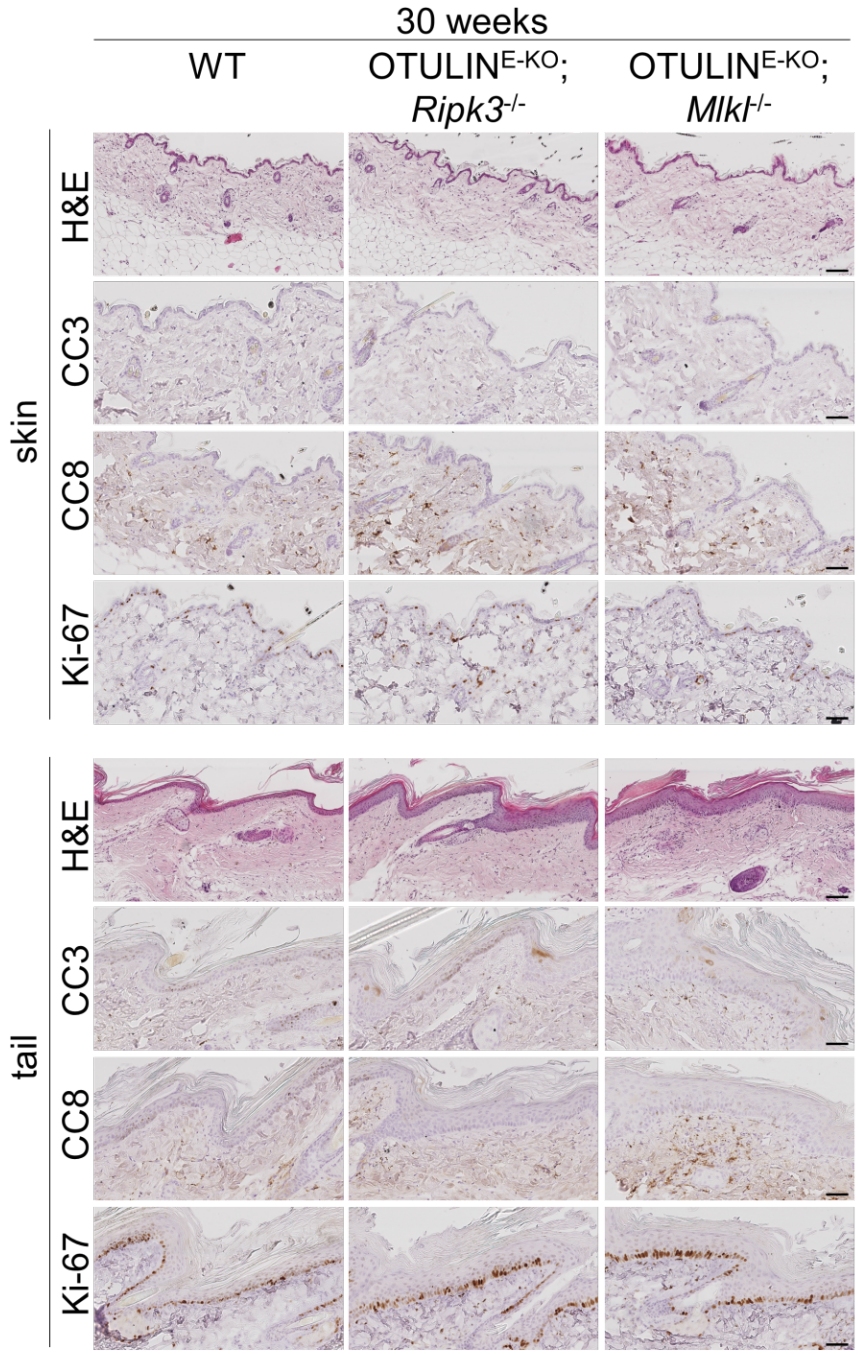

Figure 45: RIPK3 and MLKL drive inflammation and cell death in aged OTULIN^{E-KO} mice.

Representative images from skin sections from 30-week old mice of the indicated genotypes, stained with H&E, anti-CC3, anti-CC8 or anti-Ki67 antibodies. Scale bar H&E = 100µm; CC3, CC8, Ki67 = 50µm.

K10/14 and K6 staining revealed greatly restored skin architecture that appeared similar in young OTULIN^{E-KO}; *Ripk3*$^{-/-}$ and OTULIN^{E-KO}; *Mlkl*$^{-/-}$ mice compared to WT mice. Moreover, only few immune cell infiltrates could be detected in the back and tail skin of these animals (Figure 46).

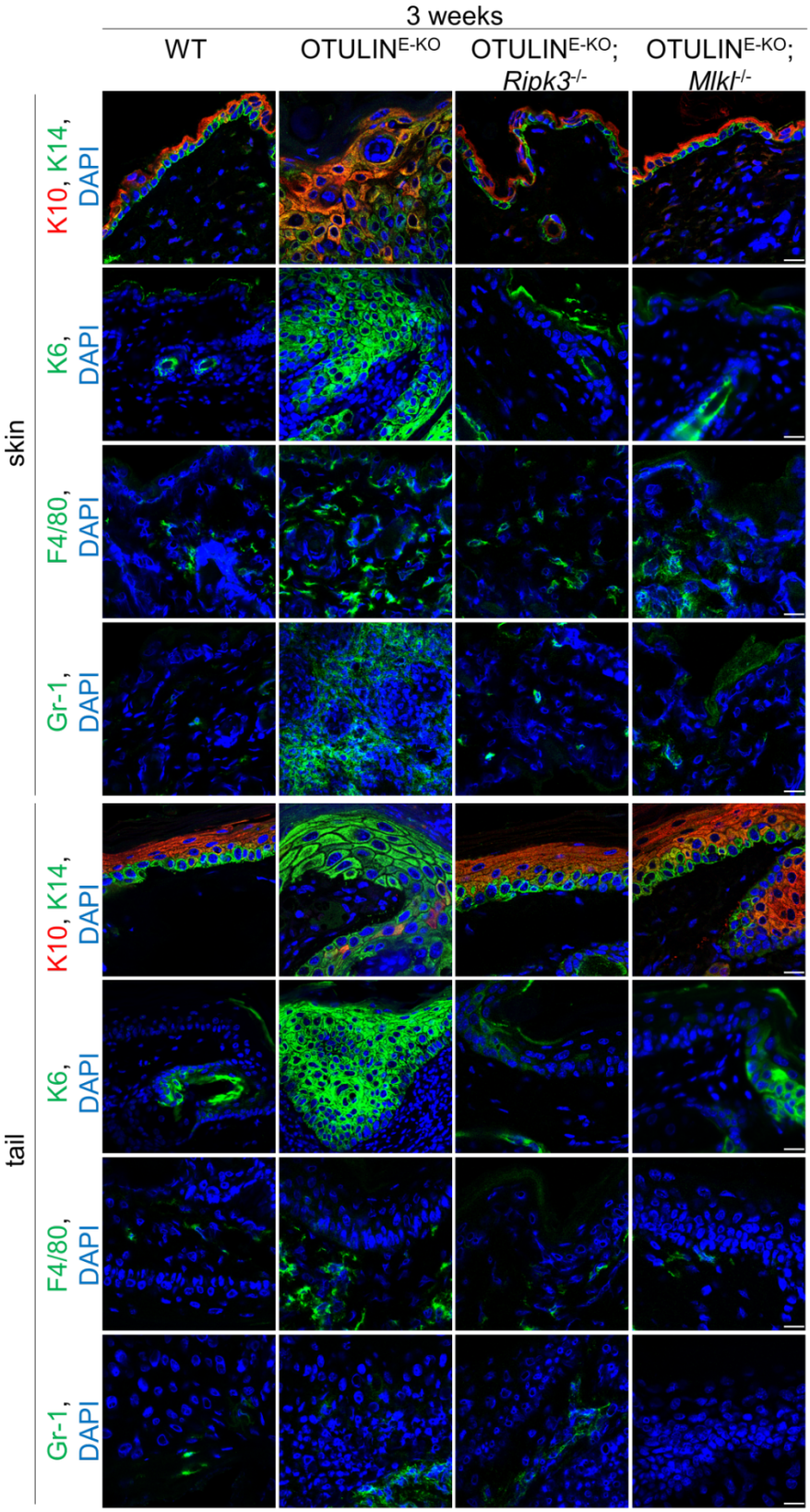

Figure 46: OTULIN^{E-KO}; *Ripk3*$^{-/-}$ and OTULIN^{E-KO}; *Mlkl*$^{-/-}$ mice are strongly protected from epidermal proliferation and immune cell infiltration.

Representative images from skin sections from 3-week old mice of the indicated genotypes, immunostained with anti-K10), anti- K14, anti-K6, anti-F4/80, anti-Gr-1 and DAPI (DNA stain). Scale bar K10, K14, K6 = 20µm; F4/80, Gr-1 = 30 µm.

Notably, myeloid cell infiltration was slightly elevated during aging of OTULIN$^{E\text{-}KO}$; *Ripk3*$^{-/-}$ and OTULIN$^{E\text{-}KO}$; *Mlkl*$^{-/-}$ mice. In addition, also slight tail skin structure changes appeared in 30-week old mice, shown by mildly enhanced K6 and K14 staining (Figure 47). Hence, these data suggest, that similar to the role of RIPK1 kinase activity, RIPK3 and MLKL-independent mechanisms are involved in the pathogenesis of skin lesions in OTULIN$^{E\text{-}KO}$ mice during ageing.

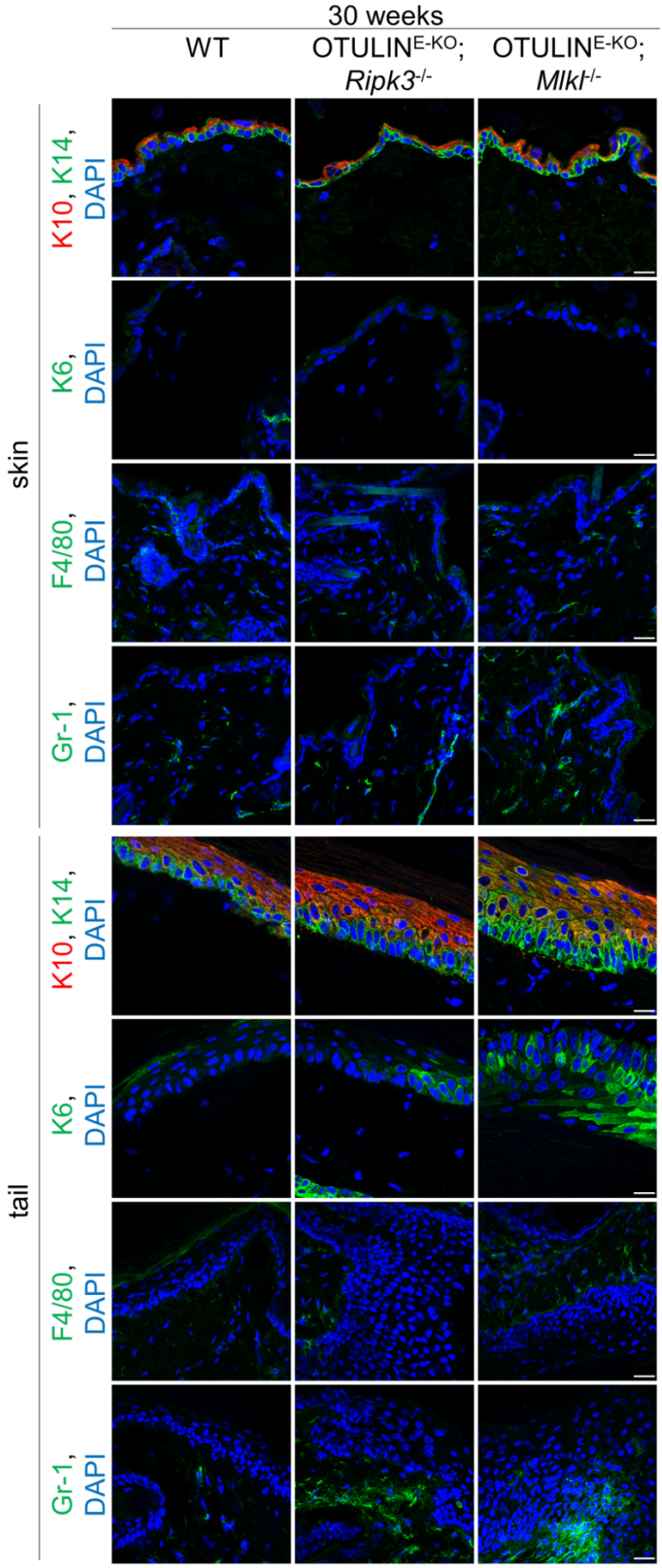

Figure 47: OTULIN$^{E\text{-}KO}$; *Ripk3*$^{-/-}$ and OTULIN$^{E\text{-}KO}$; *Mlkl*$^{-/-}$ mice are not fully protected from epidermal proliferation and immune cell infiltration during ageing.

Representative images from skin sections from 30-week old mice of the indicated genotypes, immunostained with anti-K10, anti-K14, anti-K6,, anti-F4/80, anti-Gr-1 and DAPI (DNA stain). Scale bar K10, K14, K6 = 20µm; F4/80, Gr-1 = 30µm.

2.4.3 OTULIN$^{E\text{-}KO}$; *Ripk3*$^{-/-}$ and OTULIN$^{E\text{-}KO}$; *Mlkl*$^{-/-}$ mice display slight upregulation of inflammatory genes

qRT-qPCR analysis revealed reduced expression of selected cytokines and chemokines in OTULIN$^{E\text{-}KO}$; *Ripk3*$^{-/-}$ and OTULIN$^{E\text{-}KO}$; *Mlkl*$^{-/-}$ skin, showing that absence of RIPK3 or MLKL in OTULIN$^{E\text{-}KO}$ mice decreased inflammatory gene expression (Figure 48). However, type I IFN genes were upregulated, indicating a necroptosis independent regulation. In summary, these results showed that RIPK3 and MLKL dependent necroptosis promotes skin inflammation in OTULIN$^{E\text{-}KO}$ mice.

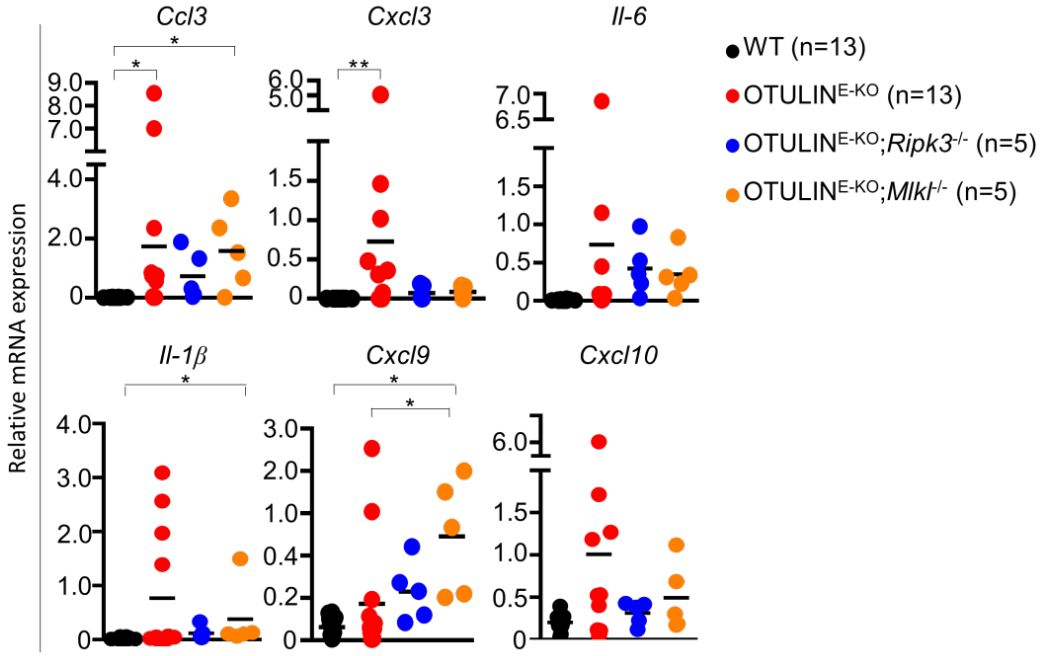

Figure 48: RIPK3 and MLKL deletion largely protects OTULIN$^{E\text{-}KO}$ mice from cytokine and chemokine upregulation.

Graphs depicting relative mRNA expression of the indicated genes in RNA from whole skin tissue of mice of the indicated genotypes at 3 weeks of age, measured by qRT-PCR. Each dot represents one mouse. Bars represent mean.

2.5 Combined ablation of FADD and RIPK3 fully protects OTULIN$^{E\text{-}KO}$ mice from skin lesion development

2.5.1 Epithelial FADD and RIPK3 promote skin disease in OTULIN$^{E\text{-}KO}$ mice

RIPK3 and MLKL deficiencies could strongly ameliorate, but not fully prevent the development of skin lesions in OTULIN$^{E\text{-}KO}$ mice. In line with this, previous studies showed that RIPK1 kinase activity can not only induce RIPK3-dependent necroptosis, but also FADD-

dependent apoptosis [216]. Moreover, detection of cleaved caspase-8 and cleaved caspase-3 positive stained keratinocytes in skin sections from OTULIN^{E-KO} mice implied that caspase-8-mediated apoptosis could also contribute to skin pathology (Figure 14). To assess the contribution of caspase-8-mediated cell death in skin lesion development in OTULIN^{E-KO} mice, *Otulin*$^{fl/fl}$ *Fadd*$^{fl/fl}$ K14-Cre *Ripk3*$^{-/-}$ (hereafter referred to as OTULIN^{E-KO}; FADD^{E-KO}; *Ripk3*$^{-/-}$) mice were generated. Keratinocyte specific ablation of FADD in combination with full body deletion of RIPK3 fully prevented skin disease development in OTULIN^{E-KO} mice up to 30 weeks of age (Figure 49a,b).

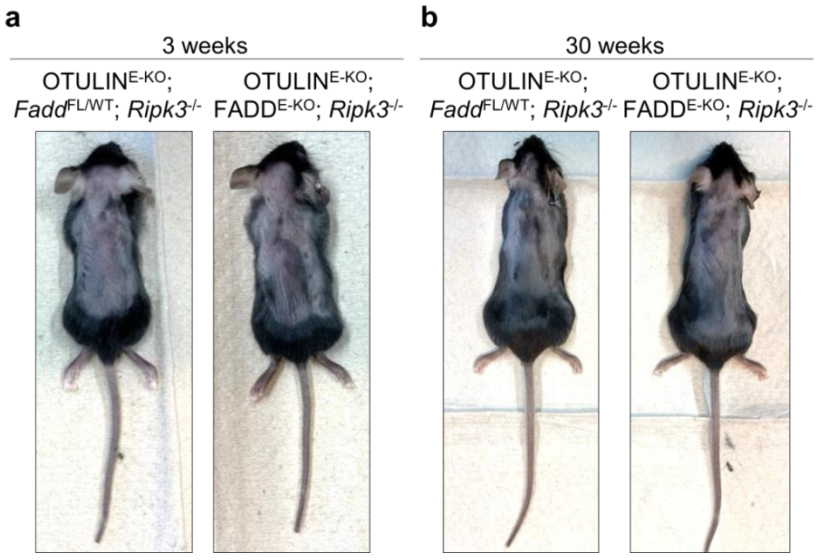

Figure 49: FADD and RIPK3 dependent cell death trigger skin pathology in OTULIN^{E-KO} mice.

(a)Photographs of mice with the indicated genotypes at the age of 3 weeks. Images shown are representative of n > 10 with the indicated genotypes. (b) Photographs of mice with the indicated genotypes at the age of 30 weeks. Images shown are representative of n > 10 with the indicated genotypes.

Thus, OTULIN^{E-KO}; FADD^{E-KO}; *Ripk3*$^{-/-}$ mice stayed alive up to one year of age without developing skin pathology and early required death (Figure 50).

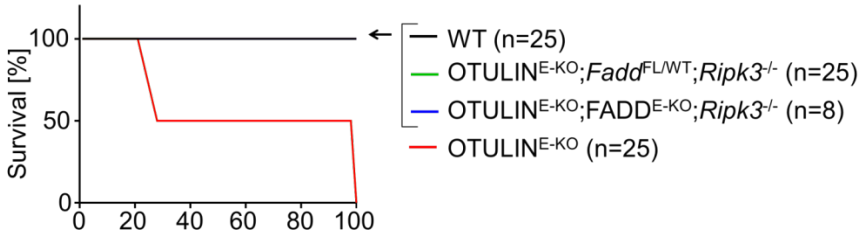

Figure 50: FADD and RIPK3 depletion prevent lethality of OTULIN^{E-KO} mice.

Kaplan-Meier plot depicting survival of mice of the indicated genotypes.

Accordingly, all OTULIN$^{E\text{-}KO}$; FADD$^{E\text{-}KO}$; Ripk3$^{-/-}$ mice were indistinguishable from WT littermates, therefore score 0 (

Figure **51**). Taken together, keratinocyte-specific FADD and full-body RIPK3 deficiency prevents skin lesion development in OTULINE-KO mice demonstrating that cell death is the key driver of the observed skin phenotype in the absence of OTULIN.

Figure 51: Macroscopic skin score.

Graph depicting macroscopic skin score of mice of the indicated genotypes. Each dot represents one mouse. Bars represent mean.

2.5.2 OTULIN$^{E\text{-}KO}$; FADD$^{E\text{-}KO}$; *Ripk3*$^{-/-}$ mice are rescued from developing skin pathology

RIPK3 and MLKL deficiency could ameliorate, however not prevent ongoing inflammation and cell death in the epidermis of older OTULIN$^{E\text{-}KO}$ mice (Figure 45). In comparison, combined inhibition of FADD in keratinocytes and full body RIPK3 ablation prevented OTULIN$^{E\text{-}KO}$ mice from epidermal hyperplasia and increased keratinocyte proliferation, presented by Ki-67 staining. Furthermore, dying cells could not be detected in the back and tail skin from OTULIN$^{E\text{-}KO}$; FADD$^{E\text{-}KO}$; *Ripk3*$^{-/-}$ mice (Figure 52).

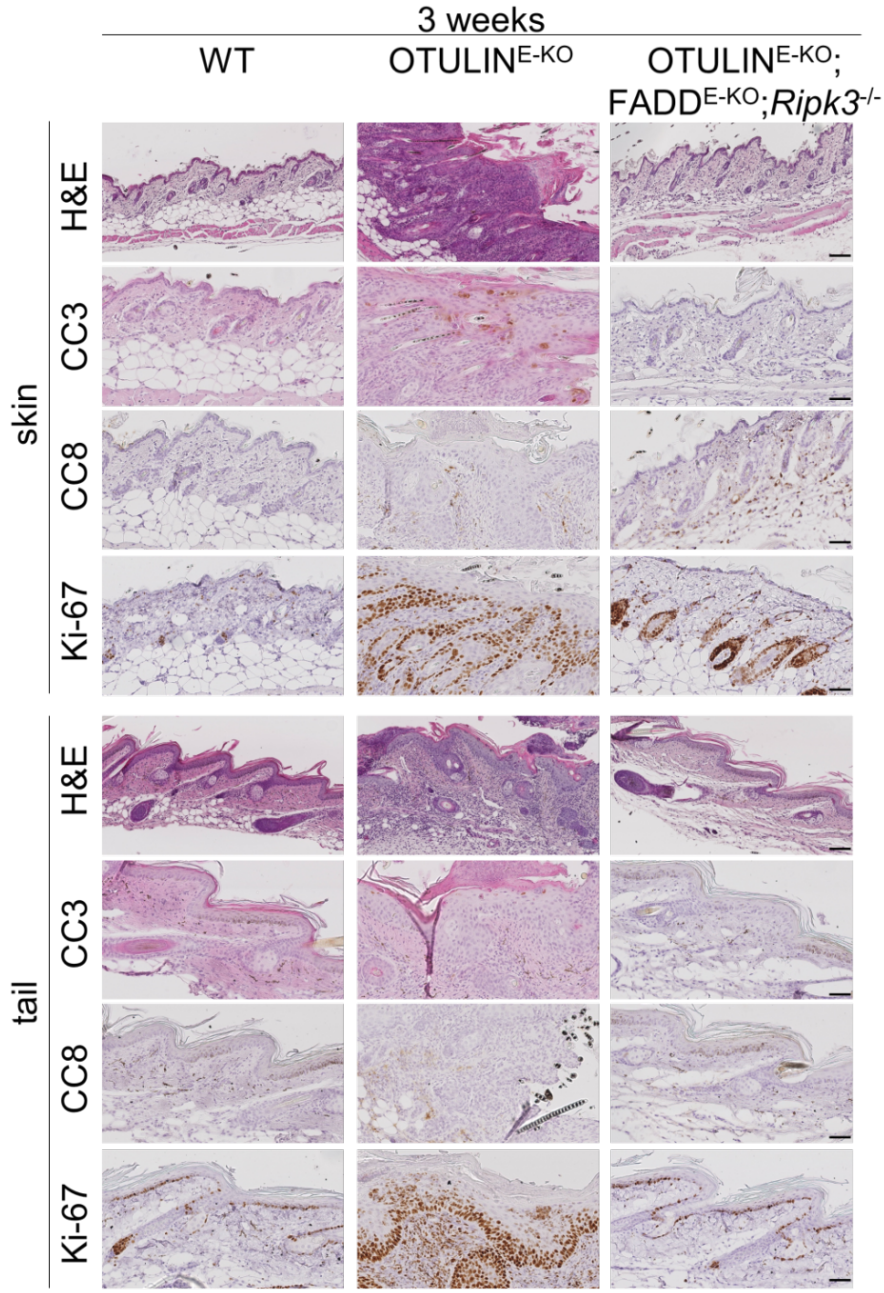

Figure 52: FADD and RIPK3 deletion prevents hyperproliferation and cell death in OTULIN^{E-KO} mice.

Representative images from skin sections from 3-week old mice of the indicated genotypes, stained with H&E, anti-CC3, anti-CC8 or anti-Ki67 antibodies. Scale bar H&E = 100µm; CC3, CC8, Ki67 = 50µ

Moreover, detection of CC3 and CC8 positive cells was completely absent in skin sections from OTULIN^{E-KO}; FADD^{E-KO}; *Ripk3*$^{-/-}$ mice up to 50 weeks of age. Additionally, Ki-67 expressing pattern in back and tail skin from OTULIN^{E-KO}; FADD^{E-KO}; *Ripk3*$^{-/-}$ mice appeared similar to WT skin (Figure 53).

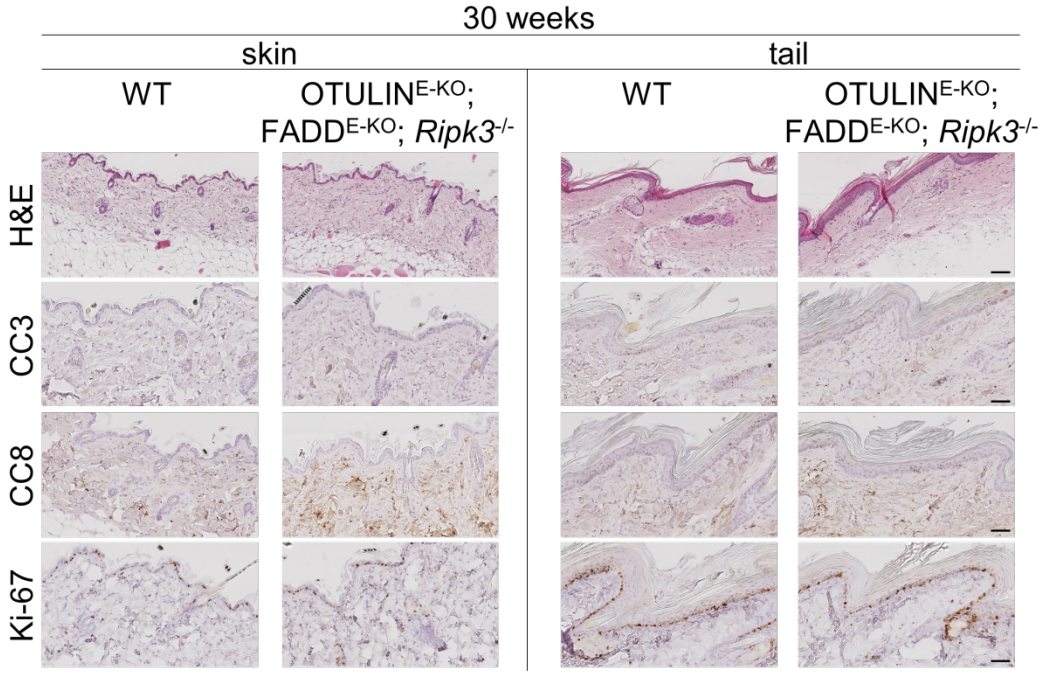

Figure 53: FADD and RIPK3 deletion fully protects skin inflammation and cell death in OTULIN^{E-KO} mice.

Representative images from skin sections from 30-week old mice of the indicated genotypes, stained with H&E, anti-CC3, anti-CC8 or anti-Ki67 antibodies. Scale bar H&E = 100µm; CC3, CC8, Ki67 = 50µm.

In line with these results, staining for the epidermal differentiation marker K10/14 on skin sections from OTULIN^{E-KO}; FADD^{E-KO}; *Ripk3*$^{-/-}$ mice was identical to WT skin in young mice and increased expression of K6 could not be detected. Furthermore, increased immune cell infiltrates could not be observed in the OTULIN^{E-KO}; FADD^{E-KO}; *Ripk3*$^{-/-}$ skin (Figure 54).

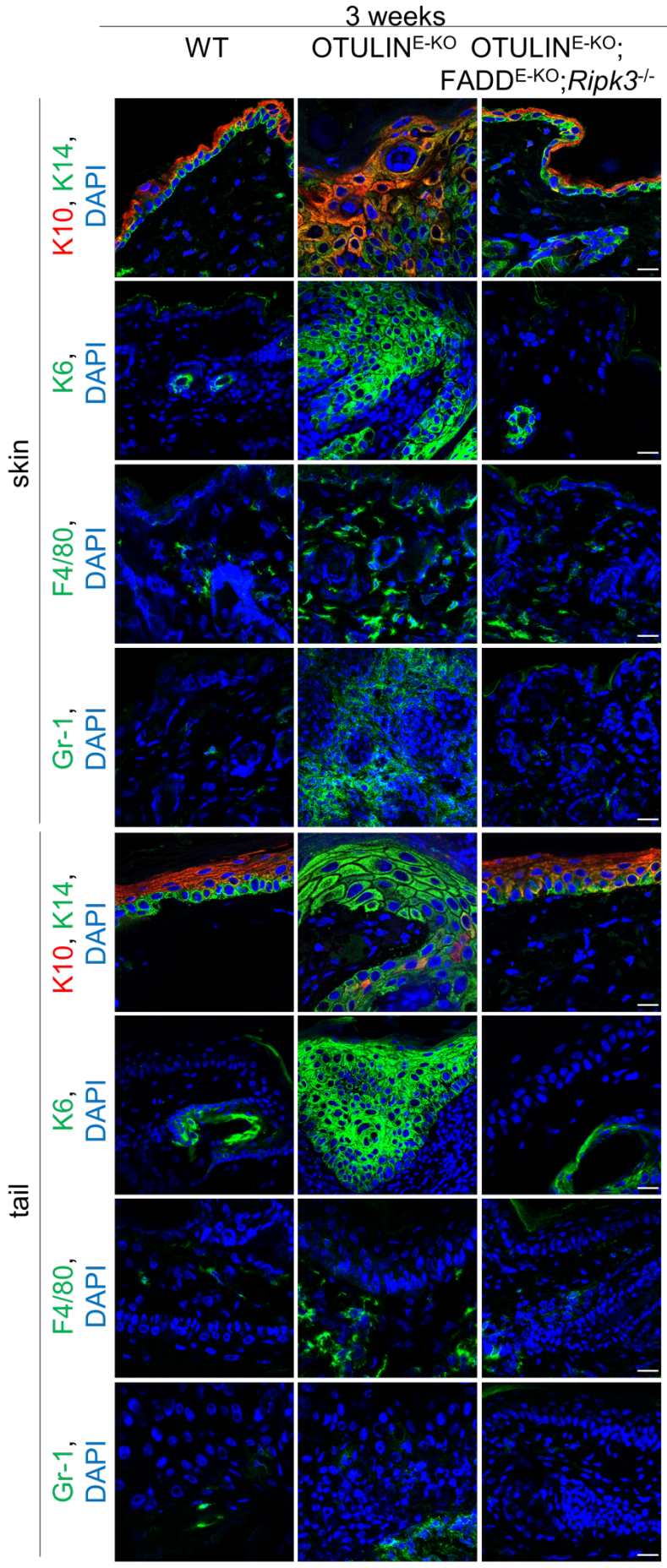

Figure 54: Restored skin architecture in OTULIN^{E-KO}; FADD^{E-KO}; *Ripk3*$^{-/-}$ mice.

Representative images from skin sections from 3-week old mice of the indicated genotypes, immunostained with anti-K10), anti- K14, anti-K6, anti-F4/80, anti-Gr-1 and DAPI (DNA stain). Scale bar K10, K14, K6 = 20µm; F4/80, Gr-1 = 30µm.

In skin samples from 30-week old OTULIN$^{E\text{-}KO}$; FADD$^{E\text{-}KO}$; *Ripk3*$^{-/-}$ mice neither increased expression of K6 and K14 nor increased immune cell infiltrates were present in 3, reflecting cell death being the trigger for immune cell recruitment in aged OTULIN$^{E\text{-}KO}$ mice (Figure 55). Thus, FADD-caspase-8-dependent apoptosis further promotes skin inflammation in OTULIN$^{E\text{-}KO}$ mice.

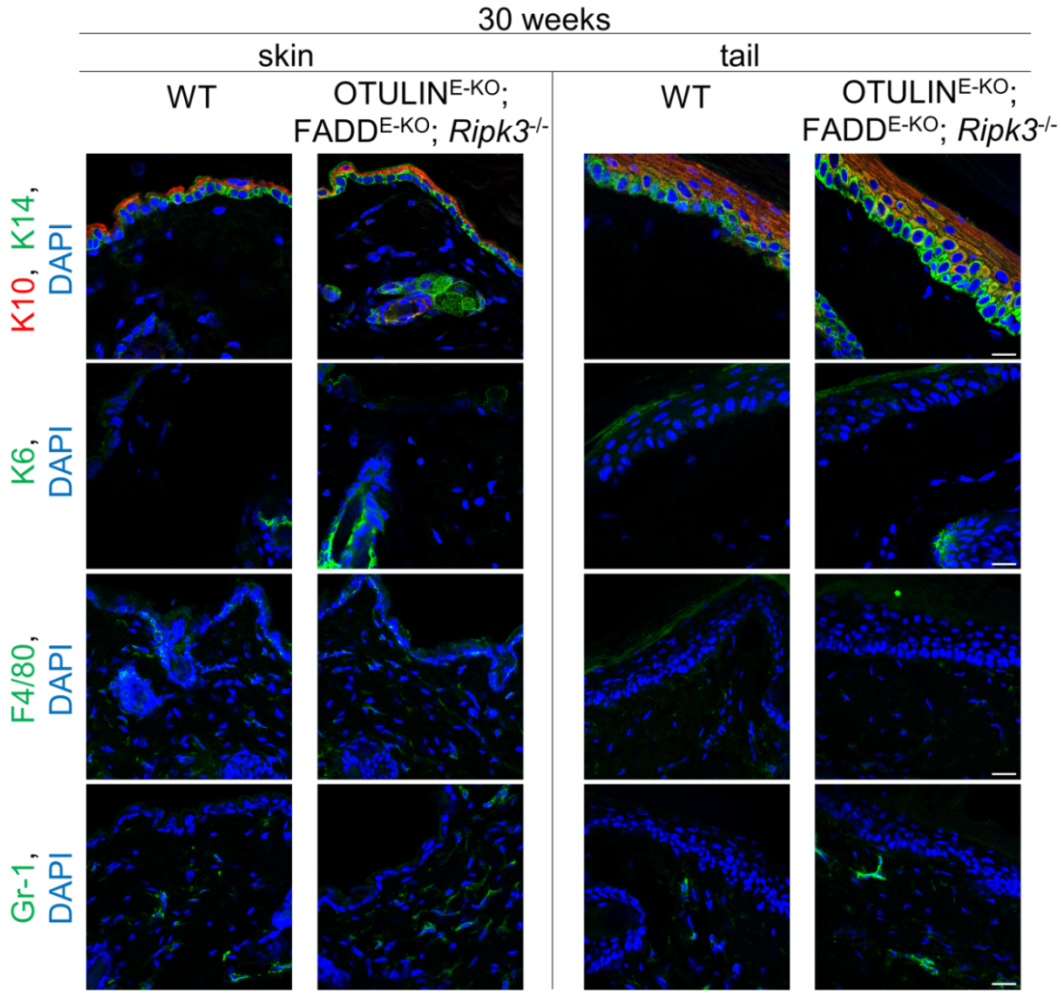

Figure 55: OTULIN$^{E\text{-}KO}$; FADD$^{E\text{-}KO}$; *Ripk3*$^{-/-}$ mice are fully protected from epidermal hyperproliferation and immune cell infiltration.

Representative images from skin sections from 30-week old mice of the indicated genotypes, immunostained with anti-K10, anti-K14, anti-K6, anti-F4/80, anti-Gr-1 and DAPI (DNA stain). Scale bar K10, K14, K6 = 20µm; F4/80, Gr-1 = 30µm.

2.5.3 OTULIN$^{E\text{-}KO}$; FADD$^{E\text{-}KO}$; *Ripk3*$^{-/-}$ mice are not prevented from ISG upregulation

qRT-PCR analysis of skin mRNA from 3-week-old OTULIN$^{E\text{-}KO}$; FADD$^{E\text{-}KO}$; *Ripk3*$^{-/-}$ mice revealed that the expression of Ccl3, Cxcl3 and Il-6 in OTULIN$^{E\text{-}KO}$ mice was normalized to the control WT levels. However, the expression of the type I IFN response genes Cxcl9 and Cxcl10 as well

as IL-1β were not suppressed in OTULIN^{E-KO}; FADD^{E-KO}; *Ripk3*$^{-/-}$ mice (Figure 56). In total, although RIPK3-MLKL-dependent necroptosis appears to be the main driver, the data obtained from analyzing OTULIN^{E-KO}; FADD^{E-KO}; *Ripk3*$^{-/-}$ mice demonstrate pivotal roles for both, apoptotic and necroptotic cell death in contributing to the development of the severe skin disease in OTULIN^{E-KO} mice.

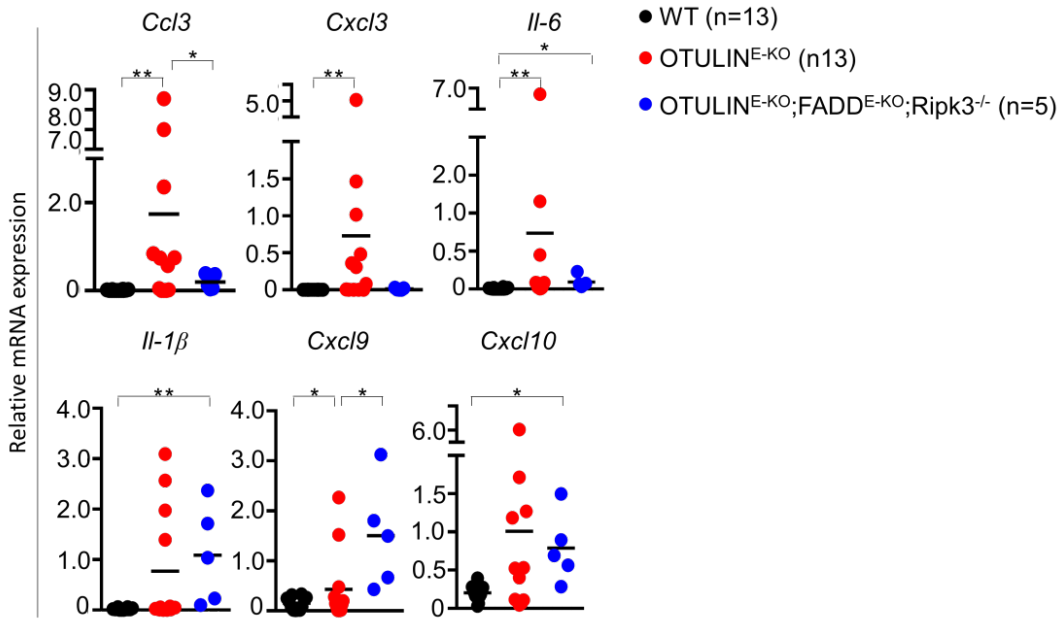

Figure 56: FADD and RIPK3 deletion partially protects OTULIN^{E-KO} mice from cytokine and chemokine upregulation.

Graphs depicting relative mRNA expression of the indicated genes in RNA from whole skin tissue of mice of the indicated genotypes at 3 weeks of age, measured by qRT-PCR. Each dot represents one mouse. Bars represent mean.

2.6 Skin disease in in OTULIN^{E-KO} mice is promoted by MyD88-dependent signaling

2.6.1 MyD88-dependent signalling contributes to the development of skin inflammation in OTULIN^{EKO} mice

OTULIN^{E-KO} mice start to develop skin pathology in the first week after birth with fast progression, suggesting a contribution of environmental factors in initiating skin disease development. Early after birth, the skin is colonized with commensal bacteria that are implicated in driving the expression of TNF and other inflammatory mediators via activating TLR signalling [230]. Interestingly, linear ubiquitination was associated with recognition of gram negative bacteria and PAMPs and further involved in activation of innate immunity via PRRs

[114, 146]. To investigate the role for TLR signaling in OTULIN$^{E\text{-}KO}$ mice, *Otulin*$^{fl/fl}$ *K14-Cre*$^{tg/wt}$ *MyD88*$^{-/-}$ (hereafter referred to as OTULIN$^{E\text{-}KO}$; *MyD88*$^{-/-}$) mice were generated. Deletion of the key TLR adaptor MyD88 strongly prevented the development of skin pathology in young OTULIN$^{E\text{-}KO}$ mice and old mice developed only mild skin lesions (Figure 57a,b).

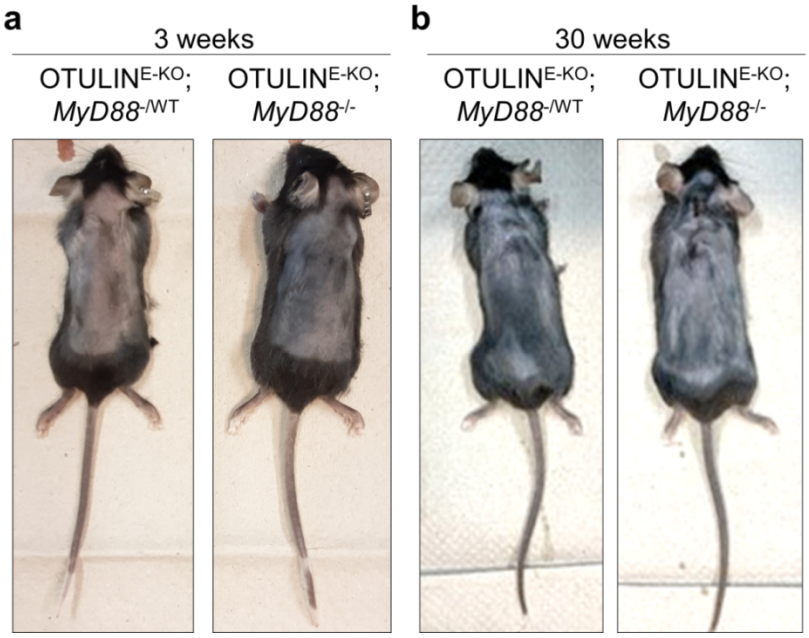

Figure 57: MyD88 dependent signalling contributes to the skin disease progression in OTULIN$^{E\text{-}KO}$ mice.

(a) Photographs of mice with the indicated genotypes at the age of 3 weeks. Images shown are representative of n > 15 with the indicated genotypes. (b) Photographs of mice with the indicated genotypes at the age of 30 weeks. Images shown are representative of n > 15 with the indicated genotypes.

OTULIN$^{E\text{-}KO}$; *MyD88*$^{-/-}$ mice survived up to 30 weeks of age without priming them to severe skin disease development and therefore to early death (Figure 58).

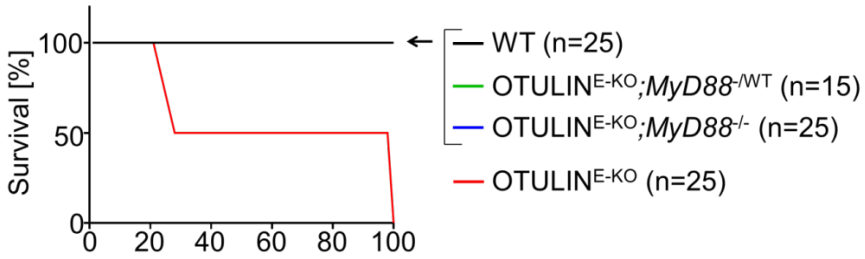

Figure 58: MyD88 ablation protects OTULIN$^{E\text{-}KO}$ mice from lethality.

Kaplan-Meier plot depicting survival of mice of the indicated genotypes.

Accordingly, 50% of the OTULIN$^{E\text{-}KO}$; *MyD88*$^{-/-}$ mice remained lesion-free up to 30 weeks and only few mice reached a maximum score of 1 (Figure 59). Combined, MyD88 deficiency prevents OTULIN$^{E\text{-}KO}$ mice from skin pathology.

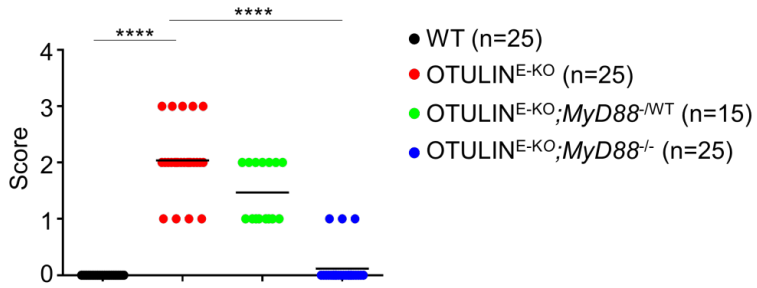

Figure 59: Macroscopic skin score.

Graph depicting macroscopic skin score of mice of the indicated genotypes. Each dot represents one mouse. Bars represent mean.

2.6.2 MyD88 deficiency ameliorates the skin pathology in OTULIN^{EKO} mice

Histological analysis of skin sections from 3-week old OTULIN$^{E\text{-}KO}$; *MyD88*$^{-/-}$ mice revealed mildly increased keratinocyte proliferation in the tail skin, represented by Ki-67 staining. Furthermore, less cell death could be detected in OTULIN$^{E\text{-}KO}$; *MyD88*$^{-/-}$ mice via CC3 and CC8 staining in comparison to OTULIN$^{E\text{-}KO}$ mice (Figure 60).

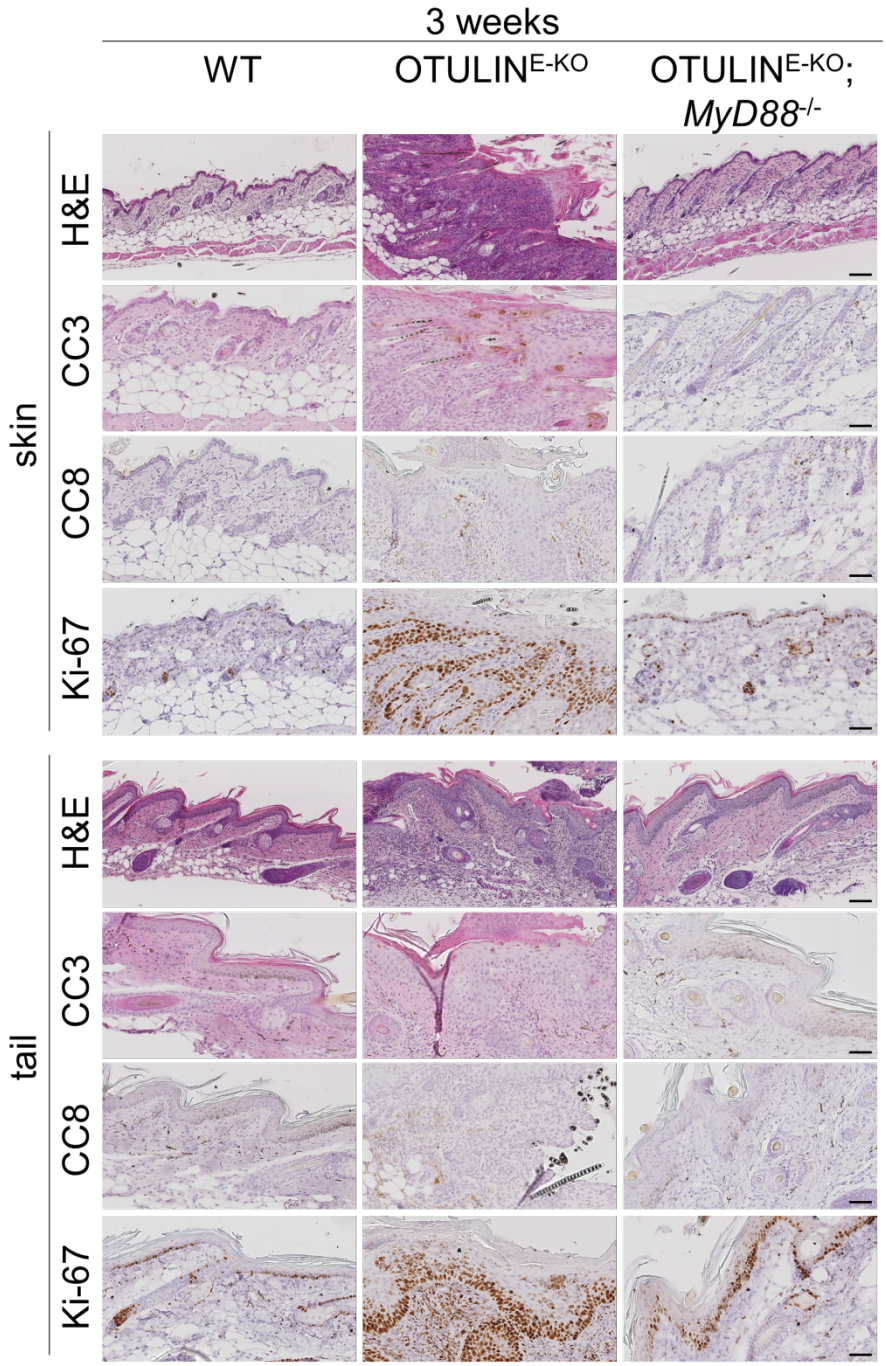

Figure 60: MyD88 ablation strongly prevents hyperproliferation and cell death in OTULIN^{E-KO} mice.

Representative images from skin sections from 3-week old mice of the indicated genotypes, stained with H&E, anti-CC3, anti-CC8 or anti-Ki67 antibodies. Scale bar H&E = 100µm; CC3, CC8, Ki67 = 50µm.

However, at the age of 30 weeks, more pronounced inflammation and ongoing cell death could be observed in OTULIN^{E-KO}; *MyD88*$^{-/-}$ mice indicated by epidermal hyperplasia and increased CC3, CC8 and Ki-67 positive cells in the skin (Figure 61).

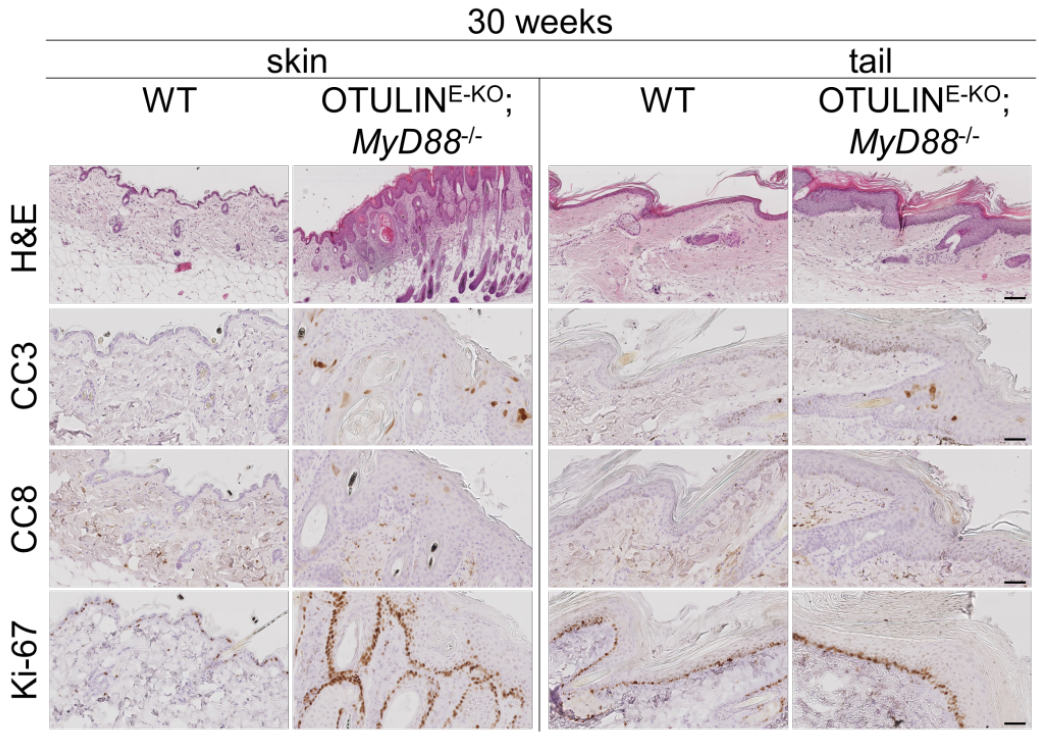

Figure 61: Aged OTULIN^{E-KO}; *MyD88*$^{-/-}$ mice show increased cell death and hyperproliferation in the skin.

Representative images from skin sections from 30-week old mice of the indicated genotypes, stained with H&E, anti-CC3, anti-CC8 or anti-Ki67 antibodies. Scale bar H&E = 100µm; CC3, CC8, Ki67 = 50µm.

In young OTULIN^{E-KO}; *MyD88*$^{-/-}$ mice and WT mice similar expression of K6 and K10/14 could be observed. Furthermore, immune cell infiltration indicated by increased F4/80^{+} and Gr1^{+} staining was prevented in OTULIN^{E-KO}; *MyD88*$^{-/-}$ mice compared to OTULIN^{E-KO} mice (Figure 62).

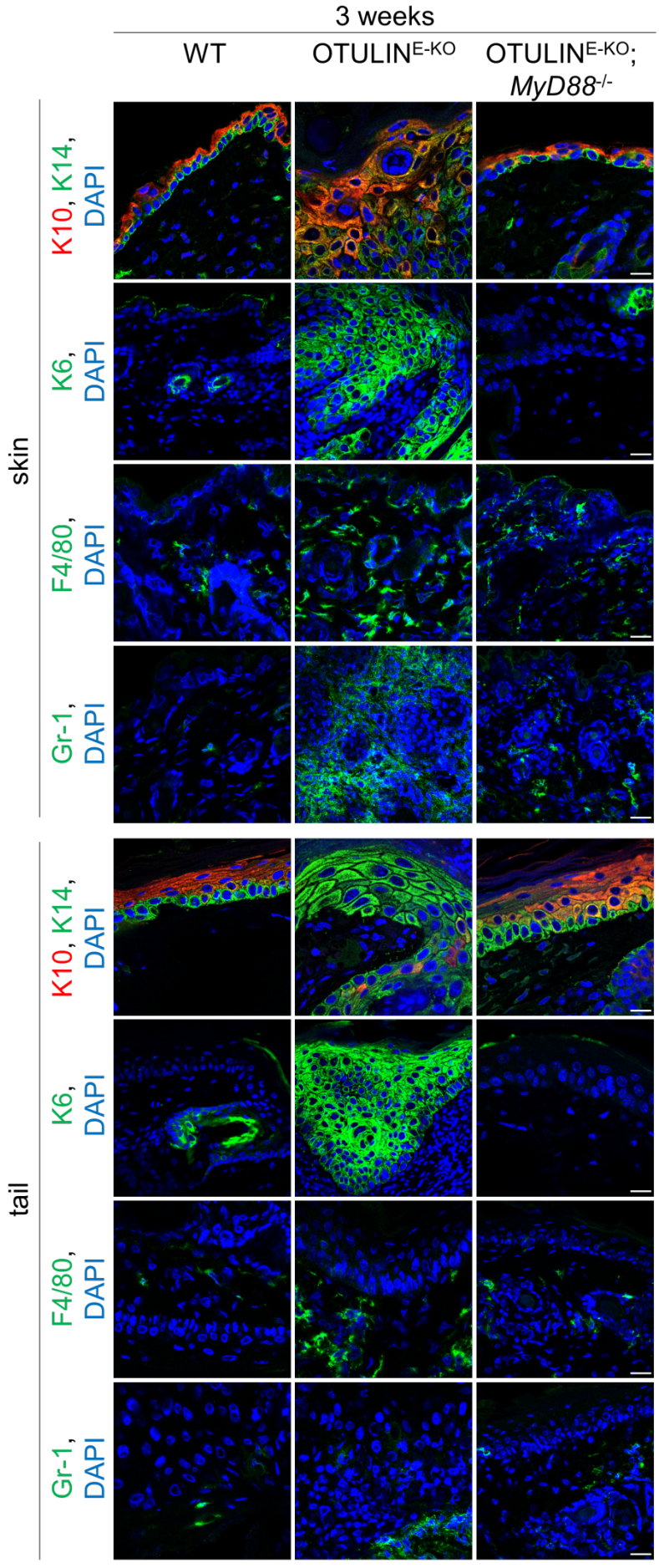

Figure 62: Normal skin structure and immune cell load in OTULIN$^{E\text{-}KO}$; *MyD88*$^{-/-}$ mice.

Representative images from skin sections from 3-week old mice of the indicated genotypes, immunostained with anti-K10, anti- K14, anti-K6, anti-F4/80, anti-Gr-1 and DAPI (DNA stain). Scale bar K10, K14, K6 = 20µm; F4/80, Gr-1 = 30µm

.

However, increased K10 and K6 expression could be detected in the epidermis of 30-week old OTULIN$^{E\text{-}KO}$; *MyD88*$^{-/-}$ mice, indicating a delayed disease onset in OTULIN$^{E\text{-}KO}$ mice. Moreover, infiltrates of F4/80^{+} and Gr-1^{+} cells appeared in the skin from adult OTULIN$^{E\text{-}KO}$; *MyD88*$^{-/-}$ mice compared to WT skin, pointing towards ongoing inflammation (Figure 63). In summary, these results open up that MyD88 signalling critically contributes to the development of inflammatory skin lesions in OTULIN$^{E\text{-}KO}$ mice.

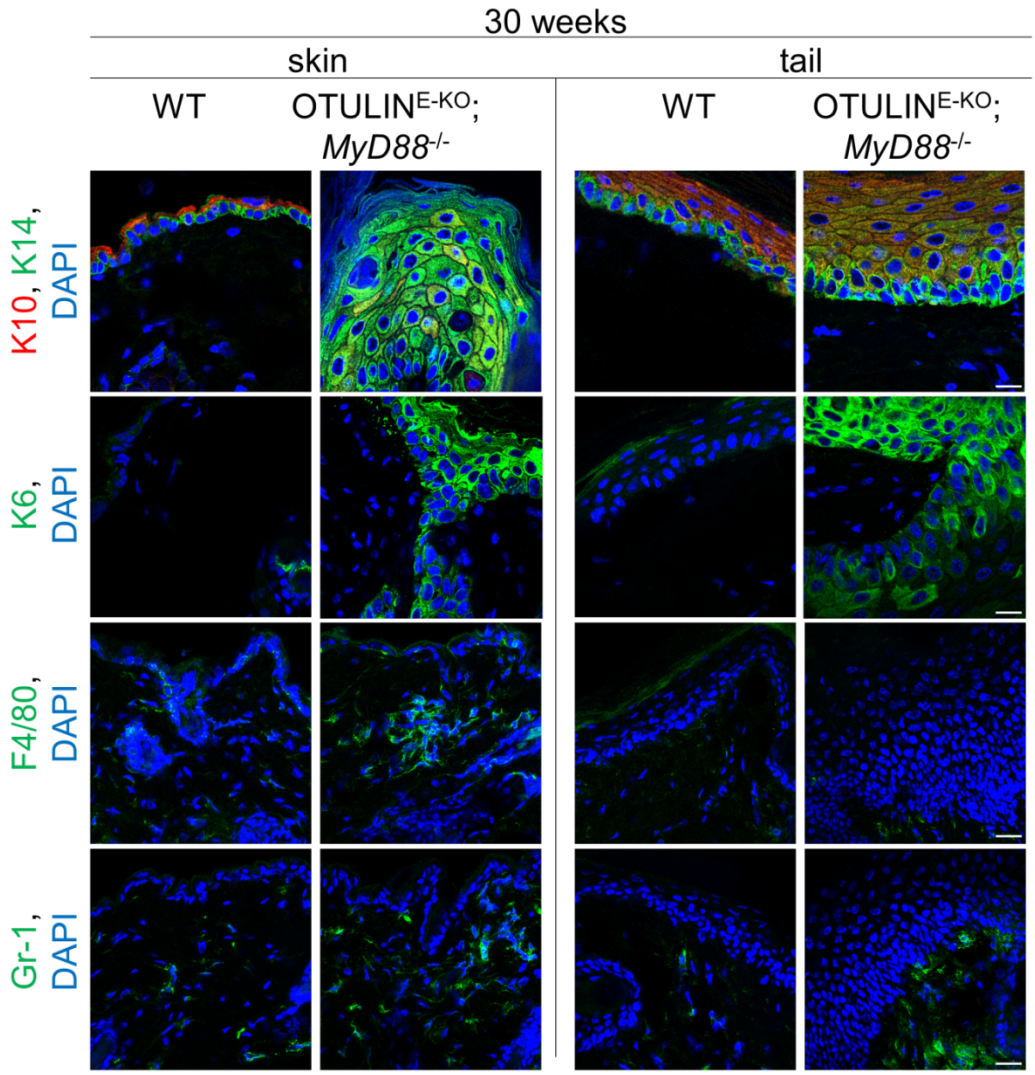

Figure 63: Changes in skin structure and increased immune cell load in aged OTULIN$^{E\text{-}KO}$; *MyD88*$^{-/-}$ mice.

Representative images from skin sections from 30-week old mice of the indicated genotypes, immunostained with anti-K10, anti-K14, anti-K6, anti-F4/80, anti-Gr-1 and DAPI (DNA stain). Scale bar K10, K14, K6 = 20µm; F4/80, Gr-1 = 30µm.

2.6.3 OTULIN$^{E\text{-}KO}$; *MyD88*$^{-/-}$ mice are protected from increased inflammatory gene expression.

Gene expression analysis revealed that deletion of MyD88 prevents increased expression of selected cytokines and chemokines in OTULIN$^{E\text{-}KO}$; *MyD88*$^{-/-}$ mice, thereby implying that MyD88 signaling plays a critical role in the upregulation of inflammatory genes (Figure 64). Collectively, these data reveal an important role for MyD88-dependent signaling in inducing inflammatory skin lesion development in OTULIN$^{E\text{-}KO}$ mice and announces a potential contribution of microbiota to the disease progression.

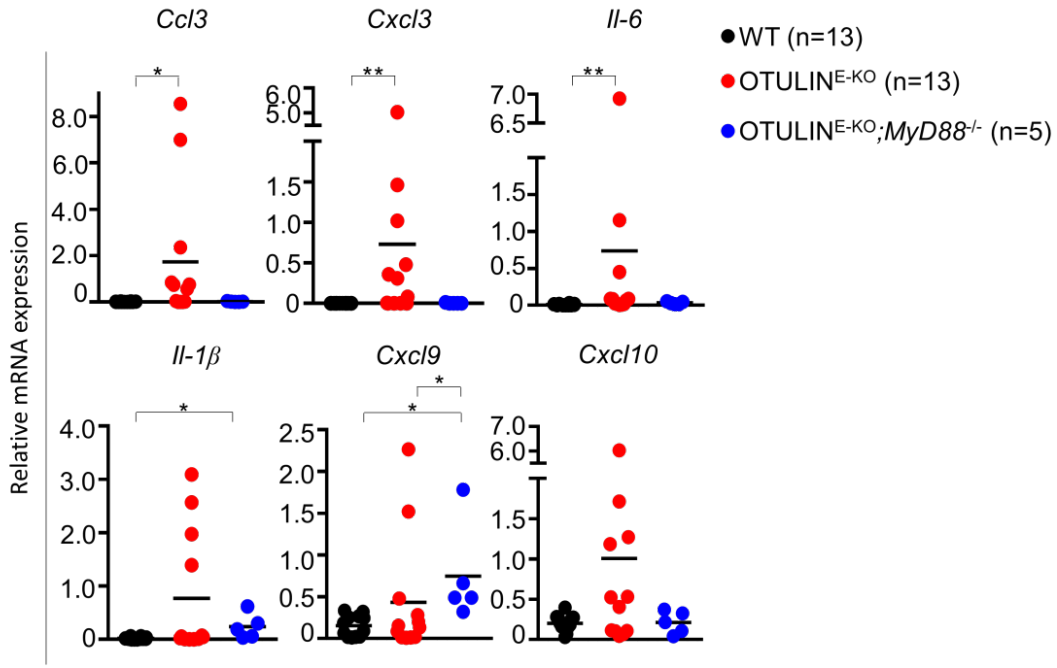

Figure 64: MyD88 deletion largely protects OTULIN$^{E\text{-}KO}$ mice from cytokine and chemokine upregulation.

Graphs depicting relative mRNA expression of the indicated genes in RNA from whole skin tissue of mice of the indicated genotypes at 3 weeks of age, measured by qRT-PCR. Each dot represents one mouse. Bars represent mean.

3. Discussion

3.1 OTULIN in the skin epithelium

3.1.1 OTULIN is crucial for skin homeostasis

Cell death and inflammation are crucial processes to preserve homeostasis and prevent pathology in individual organisms. OTULIN has been characterized as an important regulator during embryonic development, tissue homeostasis and in innate immune response signaling. In this thesis, the role of OTULIN in skin tissue was investigated by analyzing conditional OTULIN knockout mice lacking OTULIN specifically in epidermal keratinocytes. Under physiological conditions, OTULIN maintains LUBAC activity in TNFR1 signaling by hydrolyzing linear Ubiquitin chains directly on LUBAC, thereby preventing its auto-ubiquitination [34]. However, mice that are deficient in SHARPIN or with an epidermis specific deletion of SHARPIN, HOIP or HOIL-1L develop dermatitis and skin pathology that is different to the skin disease observed in OTULIN^{E-KO} mice [221, 222]. Our *in vivo* analysis revealed that OTULIN^{E-KO} mice develop inflamed skin loci that progress into papilloma like structures, allowing a maximum survival of 14 weeks of age. Surprisingly, the tail skin was also severely affected in OTULIN^{E-KO} mice, which was never observed in mice lacking LUBAC subunits in the skin [221, 222]. Furthermore, skin pathology in OTULIN^{E-KO} mice is presented with characteristics that start to appear at P6, whereas HOIP^{E-KO} and HOIL-1L^{E-KO} mice develop severe skin disease affecting the whole skin which results in the death between P4 and P6 [221]. However, histological analysis confirmed ongoing inflammation, cell death and increased immune cell appearance in the lesional skin and tail skin of 3 week old OTULIN^{E-KO} mice that is also observed in HOIP^{E-KO} and HOIL-1L^{E-KO} mice at P4 [221]. Even though HOIP^{E-KO}, HOIL-1L^{E-KO} and OTULIN^{E-KO} mice develop skin disease, these specific morphological and histological characteristics of the lesions suggest distinct mechanisms. While absence of LUBAC may differently affect cell signaling compared to miss-regulated LUBAC formation and activity in the absence of OUTLIN, OTULIN may also be involved in LUBAC independent signaling cascades. Although the underlying mechanisms remain unclear at present, the data presented in this thesis demonstrate an important function for OTULIN in maintaining skin homeostasis.

3.1.2 OTULIN is an important regulator of linear ubiquitination levels

Besides the differences in skin disease appearance in mice with epidermal ablation of OTULIN or LUBAC subunits, the results in this study confirm that OTULIN is important for regulating LUBAC auto-ubiquitination in cellular signaling processes. OTULIN$^{E\text{-}KO}$ mice exhibit increased linear Ubiquitin levels in the skin, indicating aberrant LUBAC activity, similar to OTULIN deficient hepatocytes and myeloid cells [185, 187]. Interestingly, keratinocytes isolated from OTULIN$^{E\text{-}KO}$ mice did neither reveal strong changes in TNF-induced NF-κB or MAPK signaling, nor in TNF induced cell death, where LUBAC deficiency was shown to play a critical role [221]. These data are in contrast to previous studies that demonstrated *in vitro* that both overexpression and knockdown of OTULIN sensitizes cells to TNF-induced cell death as a consequence of dys-balanced ubiquitination [32]. Furthermore, fibroblasts isolated from OTULIN deficient patients were found to be hypo-sensitive, whereas shOTULIN THP-1 cells were hypersensitive to TNF stimulation. Nevertheless, both cell types were sensitized to TNF induced cell death, showing that M1 Ubiquitin levels are crucial to protect cells from undergoing death [184]. Moreover, genetic deletion of LUBAC subunits causes reduced expression of NF-κB target genes and sensitization to TNF-induced cell death, indicating that LUBAC activity is critical for complex I stabilization [25, 26, 171] (Figure 65). The underlying cause for the discrepancy between our *in vivo*, *in vitro* and published data is currently unclear. One possibility is that spontaneous cell death observed in primary keratinocyte cultures masks increased sensitivity of OTULIN$^{E\text{-}KO}$ keratinocytes to TNF induced cell death. Another possibility is that OTULIN deficiency may affect differentiated keratinocytes or the differentiation processes itself that resemble the highly proliferating undifferentiated basal layer keratinocytes and are not recapitulated in our *in vitro* experiments. Nevertheless, OTULIN$^{E\text{-}KO}$ mice display increased linear M1 Ubiquitin chains in the skin indicating a regulatory function on LUBAC *in vivo* and thereby on ubiquitination levels and TNFR1 signaling in the skin. Therefore, it would be important to unravel the discrepancies between OTULIN function *in vitro* and *in vivo* and to consider the complex interplay of cellular signaling processes under physiological conditions.

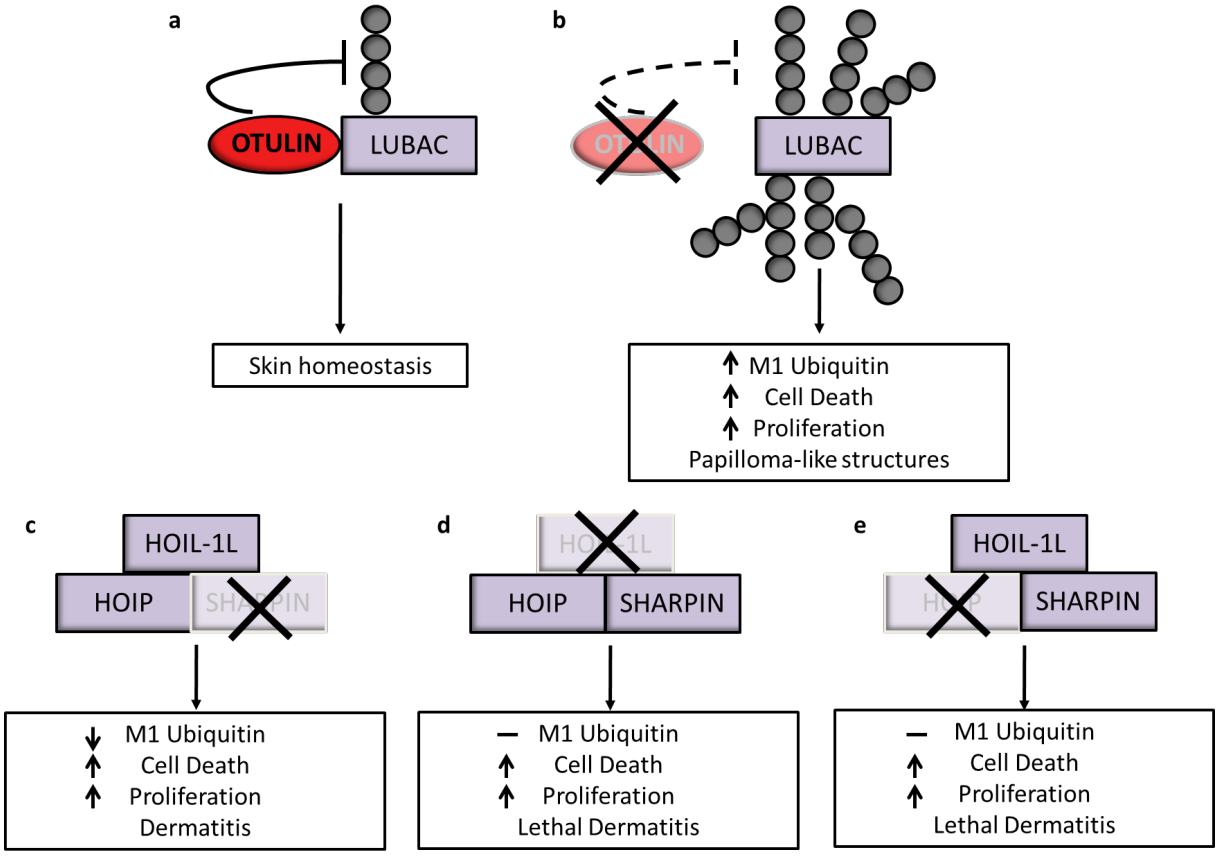

Figure 65: Model depicting the role of OTULIN and LUBAC in the skin.

(a) OTULIN prevents auto-ubiquitination of LUBAC. (b) Loss of OTULIN results in increased M1 ubiquitination, cell death and proliferation. (c) Loss of SHARPIN results in decreased M1 ubiquitination and increased cell death and proliferation. (d) Loss of HOIL-1L results in lack of ubiquitination and increased cell death and proliferation. (e) Loss of HOIP results in lack of ubiquitination and increased cell death and proliferation.

3.1.3 OTULIN is not the only DUB

OTULIN regulates M1 linear Ubiquitin linkages in TNFR1 signaling however, the DUBs CYLD, A20 are additional regulators that control this pathway [168]. While the data presented in this thesis demonstrate a key function for OTULIN in skin homeostasis, neither keratinocyte specific deletion of A20 nor expression of an inactive version of CYLD results in spontaneous skin inflammation [223, 226]. Given the important function of OTULIN in regulating LUBAC activity, absence of OTULIN and dys-balanced LUBAC function will severely affect complex I formation. In contrast, A20 and CYLD activity are likely to occur at later timepoints during TNF signaling to control the signaling process [35, 165]. Therefore, LUBAC function, and consequently an important role for OTULIN, are upstream of A20 and CYLD and may have a stronger impact on TNFR1 signaling. Among the DUBs, A20 has both, the ability to bind and to cleave Ubiquitin chains. However, A20 stabilizes, rather than hydrolyzes Ubiquitin chains leading to increased complex I stability. In the skin, A20 inhibits NF-κB signaling,

independent from its hydrolyzing activity, therefore, functioning more as a negative feedback regulator than as a DUB [223]. In contrast, CYLD hydrolyzes Ubiquitin chains on RIPK thereby sensitizing to necroptosis and regulates especially LUBAC activity in TNFR1 signaling by cleaving M1 linkages [35, 91, 231]. Interestingly, DMBA/TPA treatment revealed increased papilloma development due to missing inhibition of DNA damage-induced tumorigenesis in mice expressing catalytically inactive mutant CYLD and $CYLD^{E\text{-}KO}$ mice [225, 226, 232, 233]. This is in line with the development of papilloma-like structures in $OTULIN^{E\text{-}KO}$ mice, even though these occur spontaneously without chemical treatment. Similar to CYLD, overexpression of OTULIN was shown to downregulate NF-κB signaling, but also to hyperactivate NF-κB signaling, in a cell type and TNF dependent fashion [32, 35, 179]. However, changes in NF-κB pathway activation could not be observed on a molecular level in $OTULIN^{E\text{-}KO}$ skin, even though linear ubiquitination was increased. One possibility is that cytosolic LUBAC ubiquitination regulated by OTULIN does not affect downstream signaling of the TNFR1 pathway in the skin. However, another possibility is that CYLD compensates for OTULIN loss by regulating the OTULIN-controlled LUBAC pool via SPATA2 through its similar binding abilities. The distinct functions of all three DUBs in TNFR1 signaling may explain the phenotypical and molecular differences in epidermis-specific knockout mice. Therefore, it would be interesting to find out possible compensatory roles and further duties of OTULIN, particularly in a tissue dependent manner.

3.2 OTULIN mediates TNFR1 signaling in the skin

3.2.1 OTULIN is key for the TNFR1 pathway

The identification of patients with defects in TNFR1 signaling components highlight the importance of the tight regulatory processes in TNF driven pathways for the initiation and progression of inflammatory diseases [11, 234]. Normally, TNF induces NF-κB signalling to activate the expression of pro-inflammatory and pro-survival genes and thereby activates an immune response. However, inhibition of NF-κB sensitizes cells to TNF-induced cell death, either RIPK1 kinase activity-dependent or independent [12, 112]. On a molecular level, it was demonstrated that OTULIN is mainly important in regulating auto-ubiquitination of LUBAC in TNFR1 signaling, thereby preventing cell death [34]. Interestingly, full-body knockout mice deficient for LUBAC subunits HOIP and HOIL-1L are not greatly affected by the co-deletion of TNFR1 alone, implicating a role for LUBAC in other cellular pathways. These mice are

attributed with ongoing cell death and early lethality, similar to OTULIN deficient mice [32, 33, 151, 171]. Furthermore, keratinocyte-specific deletion of HOIP or HOIL-1L causes a lethal inflammatory skin disease, which is only partially dependent on TNFR1-induced cell death and can be redundantly triggered by TRAIL or CD95L [221]. The data in this thesis are in great contrast, since keratinocyte specific ablation of TNFR1 fully prevented OTULIN$^{E\text{-}KO}$ mice from developing skin pathology and early death. OTULIN deficiency might result in diminished LUBAC activity in the skin, similar to SHARPIN ablation in *cpdm* mice that is also fully driven by keratinocyte dependent TNFR1 signaling [169, 170]. However, if LUBAC is fully abolished only combined inhibition of TNFR1 and TRAIL/FAS signaling protects from skin disease in HOIP$^{E\text{-}KO}$ and HOIL-1L$^{E\text{-}KO}$ mice [221]. Thus, OTULIN controls LUBAC activity in TNFR1 signaling in the skin, however LUBAC might have additional essential functions in other pathways that do not rely on regulation by OTULIN. Furthermore, also OTULIN might have other cytosolic functions that are involved in TNFR1 signaling but do not rely on LUBAC interaction or linear ubiquitination. Lastly, OTULIN might have LUBAC-independent functions in LUBAC-independent cellular processes. Indeed, OTULIN has been implicated to have a scaffolding function in cellular trafficking events similar to the pseudo-DUB OTULINL (FAM105A) that is localized to the endoplasmic reticulum where it supposedly mediates protein interactions [235]. Nonetheless, the data in this thesis provide strong evidence that OTULIN plays a pivotal role in regulating TNFR1 signaling in the skin and to prevent cell death by balancing linear ubiquitination levels (Figure 66). Thus, it would be exciting to unravel new functions for OTULIN in TNFR1 signaling.

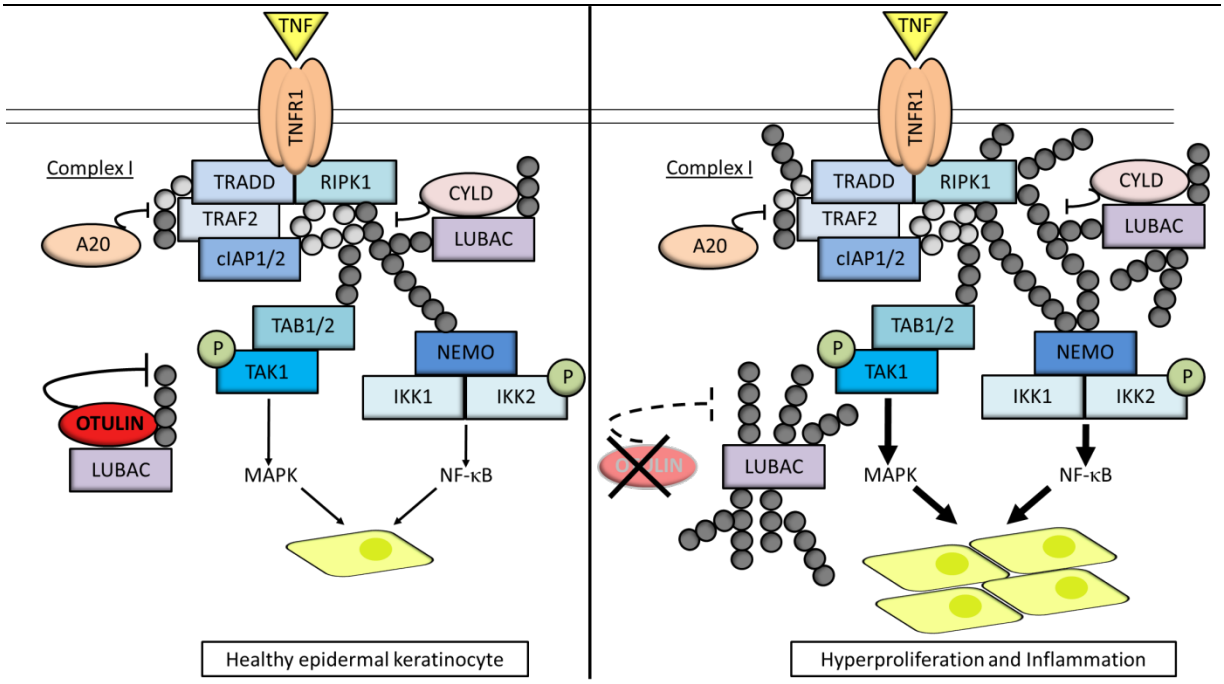

Figure 66: OTULIN regulates linear ubiquitination in TNFR1 signaling to prevent skin disease development.

TNFR1-dependent canonical NF-κB and MAPK signaling activation regulates cellular homeostasis in epidermal keratinocytes. OTULIN deficiency results in dys-balancing of linear ubiquitination, likely leading to hyper-activation of NF-κB and MAPK signaling activation and promotion of hyperproliferation and inflammation.

3.3 OTULIN prevents cell death in the skin

3.3.1 OTULIN inhibits RIPK1-kinase activity dependent cell death

The results obtained from genetic *in vivo* studies suggest that the regulation and balance of cell death and survival serve as important factors in inflammatory disease development [11, 234]. Especially the regulation of linear ubiquitination by OTULIN in the TNFR1 pathway was shown to protect from cell death [34]. Consistent with the role of OTULIN in maintaining LUBAC activity, also overexpression of OTULIN in epithelial cell lines abrogates the RIPK1-NEMO interaction thereby priming to cell death [32]. Interestingly, liver parenchymal cell-specific OTULIN deficiency caused liver inflammation and hepatocarcinogenesis, independent from TNFR1 signaling. However, liver pathology in these mice was driven by RIPK1-FADD-caspase8 dependent apoptosis, indicating TNFR1-independent cell death pathways to trigger the disease [187, 188]. Even though tissue inflammation and cell death in the skin of OTULIN$^{E\text{-}KO}$ mice was fully prevented by epithelial deletion of TNFR1, *in vitro* experiments could not confirm a sensitization of keratinocytes isolated from OTULIN$^{E\text{-}KO}$ mice to TNF-induced cell death. Similarly, also fibroblasts from ORAS patients are not

sensitized to TNF-induced cell death, even though they exhibit reduced LUBAC levels [184]. This is in contrast to LUBAC-deficient cells or cells expressing catalytically inactive OTULIN, which are thoroughly sensitized to cell death induced by TNF [24, 25, 34, 151, 171]. Nevertheless, increased dying cells were detected in skin sections from OTULIN^{E-KO} mice, indicating cell death to trigger skin inflammation *in vivo*. In addition, OTULIN^{E-KO} mice were fully protected from developing skin inflammation by inhibiting RIPK1 kinase activity. Thus, on the one hand, TNFR1 signaling is the key driver that results in inflammation and cell death that are causative for the development of severe skin pathology in the OTULIN^{E-KO} mice, which is in contrast to OTULIN deficiency in hepatocytes. On the other hand, similar to OTULIN deficiency in hepatocytes, OTULIN deficiency in keratinocytes causes pathology driven by RIPK1-kinase activity dependent cell death (Figure 67). Thus, it is crucial to untangle the role of OTULIN in different cell types to better understand cell death triggered disease development in different tissues.

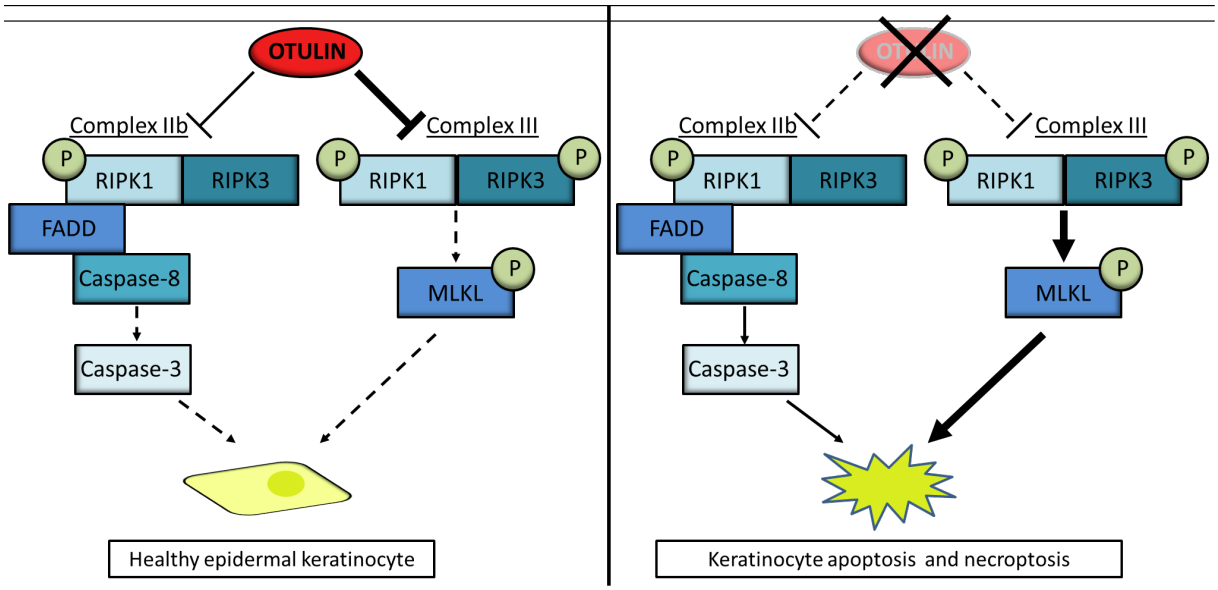

Figure 67: OTULIN suppresses RIPK1-kinase activity dependent cell death to prevent skin disease development.

OTULIN inhibits the formation of complex IIb and complex III in epidermal keratinocytes. Loss of OTULIN results RIPK1 kinase activity-dependent apoptotic and necroptotic cell death in the skin.

3.3.2 OTULIN inhibits FADD-dependent apoptosis

In TNFR1 signaling, destabilization of complex I by defective ubiquitination is causative for inactivation of cIAP1/2, TAK1, NEMO or IKK1/1 and results in defective RIPK1 phosphorylation and subsequent formation of cytosolic complex IIa or b [12, 204]. Especially, mice with ablation of the LUBAC subunits are more susceptible to TNF-induced cell death. In

detail, recent studies reported that SHARPIN-deficient MEFs are prone to TNF-induced apoptotic cell death in comparison to WT MEFs and that this is partially independent from NF-κB target gene activation. Interestingly, the inhibition of caspase activity via the pan-caspase inhibitor zVAD-fmk significantly suppressed TNF induced apoptosis *in vitro*, revealing a protective role for SHARPIN from apoptosis [24, 25]. By using genetic models, several studies demonstrated TNFR1 signaling being the main pathway that drives skin inflammation in SHARPIN deficient *cpdm* mice *in vivo* [169, 170]. Furthermore, these studies implicated the apoptosis regulator FADD and TRADD being involved in the disease, by using epidermis specific FADD or TRADD ablated mice that rescued skin inflammation in *cpdm* mice [169, 170]. However, keratinocytes isolated from OTULIN$^{E\text{-}KO}$ mice revealed no sensitization to chemically induced apoptosis or necroptosis. In contrast, previous studies showed that loss of OTULIN or expression of catalytically inactive OTULIN in cells could render them hypersensitive towards TNF/CHX-induced apoptosis. Furthermore, these cells were sensitized to TNF/CHX/zVAD-fmk-induced necroptosis demonstrating a role for OTULIN in both, apoptosis and necroptosis [180, 184]. Interestingly, knock-in mice expressing catalytically inactive OTULIN were also not rescued by RIPK3 deficiency. However, additional deletion of caspase-8 prevents embryonic death, demonstrating that apoptosis is mediating the lethality in these mice [34]. In this thesis, combined deletion of RIPK3 and keratinocyte-specific ablation of FADD fully protect OTULIN$^{E\text{-}KO}$ mice from skin pathology, indicating that apoptosis contributes to the disease development. These experiments show, that OTULIN has varying effects on both, TNFR1 induced apoptosis and necroptosis. Therefore, it will be critical to investigate the role of OTULIN in controlling the switch to cell death, dependent on the cell type and tissue.

3.3.3 OTULIN inhibits RIPK3/MLKL-dependent necroptosis

In this thesis we demonstrate that epidermis-specific OTULIN deficiency is largely triggered by necroptosis, while in mice with skin-specific impaired LUBAC function caspase-8-dependent keratinocyte apoptosis drives skin inflammation. Epidermis specific deletion of HOIP and HOIL-1L results in postnatal lethal dermatitis due to caspase-8-dependent apoptosis that is prevented to adulthood by deletion of TNFR1. The late skin disease development can be further prevented by combined ablation of TNFR1, TRAIL and CD95L that induces RIPK1-kinase-dependent apoptosis and necroptosis [221]. In contrast, the sole

deletion of RIPK3 or MLKL strongly protects OTULIN^{E-KO} mice from developing the inflammatory skin disease, demonstrating necroptosis to be the major driver of inflammation. However, inflammation and cell death were not fully prevented in aged mice, indicating other mechanisms to drive the skin pathology during ageing. Since deficiency of FADD and RIPK3 in combination fully protected pathology in OTULIN^{E-KO} mice, it might be apoptosis triggering skin disease development in adult mice. Nonetheless, these data unquestionably show that skin pathology in OTULIN^{E-KO} mice is mainly driven by RIPK3 and MLKL dependent necroptosis and therefore in great contrast to HOIP^{E-KO} , HOIL-1L^{E-KO} and *cpdm* mice, where RIPK3 and MLKL deletion have no protective effect [169, 221]. Thus, skin-specific ablation of OTULIN leads to cell death induction that is different to LUBAC deficiency indicating two possible scenarios: either OTULIN prevents necroptosis independent from LUBAC, or cell fate in keratinocytes depends on whether LUBAC subunits are absent or present but dys-regulated. Previous studies demonstrated that OTULIN ablation results in different effects on LUBAC either leading to subunit degradation due to hyper-ubiquitination or increased activity depending on the cell type [34, 185]. However, RIPK3 deficiency is not rescuing knock-in mice expressing catalytically inactive OTULIN, whereas RIPK3 ablation largely prevents disease development in OTULIN^{E-KO} mice [34]. These data indicate a possible scaffolding function for OTULIN independent from its catalytic activity, to regulate LUBAC and prevent necroptosis. Compared to LUBAC ablation in the skin, hampering OTULIN in the epidermis and thereby its regulatory activity on LUBAC is not only resulting in a different pathology development but also in different cellular mechanism to drive skin inflammation. Thus, solving cell type and tissue specific dependence of OTULIN and its regulation on LUBAC is critical in the future.

3.4 OTULIN is crucial for immune response mechanisms in the skin

3.4.1 OTULIN is important for the regulation of type I IFN signaling

During the past years, LUBAC has been found to be important for the regulation of several immune receptor signalling pathways besides TNFR1 signaling. Among those, type I IFN signaling was shown to play an important role in mice with impaired LUBAC and a liver specific OTULIN deficiency [34, 171, 188, 236]. Since type I IFN signature genes were enriched in lesional skin in OTULIN^{E-KO} mice, type I IFN signaling appears to be also critical in skin disease development. Therefore, another possible explanation for the observed skin phenotype

specific to OTULIN$^{E\text{-}KO}$ mice could be uncontrolled type I IFN signaling that promotes TNFR1-dependent skin inflammation. Moreover, HOIP$^{E\text{-}KO}$ and HOIL-1L$^{E\text{-}KO}$ mice display enhanced type I IFN signaling which is in line with increased type I IFN signature observed in OTULIN$^{E\text{-}KO}$ mice [221]. OTULIN was shown to suppress type I IFNs via IFNAR signaling when LUBAC or OTULIN are impaired [34, 171]. Furthermore, increased expression of type I IFN genes in OTULIN$^{LPC\text{-}KO}$ mice and reduced liver pathology in OTULIN$^{LPC\text{-}KO}$; IFNAR1^{KO} mice revealed a critical role for type I IFN production in driving pathology [188]. In addition, *Otulin*$^{C129A/C129A}$*Ripk3*$^{-/-}$*Casp8*$^{-/-}$ BMDMs exhibit spontaneous activation of IKKε and TBK1, suggesting that OTULIN suppresses type I IFN production pathways [34]. Interestingly, recent studies demonstrated IFN signaling to be crucial for the initiation of necroptosis suggesting constitutive IFN signaling to sensitize cells to MLKL- or ZBP1-dependent necroptosis [237, 238]. Since disease development in OTULIN$^{E\text{-}KO}$ mice is largely driven by MLKL-dependent necroptosis, type I IFN signaling might be important for the induction and amplification of cell death and inflammation in the skin. Surprisingly, also non-lesional skin exhibit significantly upregulated expression of type I IFN genes and inflammatory genes, thereby implying possible priming to necroptosis in these skin areas. Therefore, the requirement to activate these innate immune response processes before skin lesion appearance might be associated with a threshold of IFN gene expression to determine inflammation and cell death induction. Taken together, the data in this thesis indicate that besides TNFR1-dependent cell death signaling also type I IFN signaling strongly contributes to the disease onset and progression. Hence, future studies should unravel the function of OTULIN in type I IFN signaling in a cell type and tissue dependent manner.

3.4.2 OTULIN plays a critical role in MyD88-signaling

As first line of defense, the skin is attributed with different receptor types that activate a rapid and specific immune response as it is constantly exposed to environmental stimuli [230]. MyD88 signaling, activated via the LPS triggered TLR4 and IL-1 receptors, was reported to be highly regulated by linear ubiquitination to mediate immune responses [24, 25, 149, 213] (Figure 68). In detail, M1 Ubiquitin chains are attached to K63 Ubiquitin chains during TLR and IL-1 signaling, thereby generating hybrid chains [149]. These data imply that LUBAC binds via the NZF domain in HOIP to K63 Ubiquitin chains that are created at the Myddosome and conjugates linear chains to target proteins [114]. However, it is still unknown how LUBAC is

recruited and whether it is regulated in these signaling complexes. Nevertheless, downstream signaling processes were shown to be clearly dependent on balanced linear ubiquitination levels, since MEFs expressing a catalytically inactive HOIP C879S mutant reveal abolished M1 ubiquitination and diminished IKK complex formation upon IL-1 stimulation [149]. Interestingly, skin inflammation in *cpdm* mice is fully prevented by additional deletion of MyD88 [174]. In our study, fully body deletion of MyD88 in OTULIN$^{E\text{-}KO}$ mice prevented the development of skin inflammation up to 30 weeks of age. However, during adulthood skin lesions occurred in some mice, although, without progressing into severe skin disease. Even though the ongoing inflammation and cell death appeared mildly compared to OTULIN$^{E\text{-}KO}$ mice, the data showed that other mechanisms drive skin pathology during ageing. One possibility is that the skin requires MyD88 signaling and the resulting immune response in young age. Since colonization of the skin with commensal bacteria happens during the early postnatal period, skin disease in OTULIN$^{E\text{-}KO}$ mice starts to develop one week after birth and is delayed by MyD88 deficiency, demonstrating that MyD88 signaling to play a critical role in disease onset [230]. Another possibility is that, since MyD88 signaling plays a central role in promoting inflammation and ongoing cell death in OTULIN$^{E\text{-}KO}$ mice, MyD88 could signal in a feedback loop upon DAMPs released from dying cells. Currently, it is believed that TLR and IL-1 signaling play an essential role in host defense by activating innate and adaptive immunity via the production of cytokines, chemokine and antimicrobial factors [122]. IL-1 signaling promotes inflammation in response to the alarmins IL1α and Il1β that are both released by dying or damaged cells [145]. Thus, it is of major interest to decipher the roles of PAMPs and DAMPs in driving OTULIN-related diseases. In summary, the data in this study support the importance of different immune response mechanism being involved in skin disease onset and progression in OTULIN$^{E\text{-}KO}$ mice.

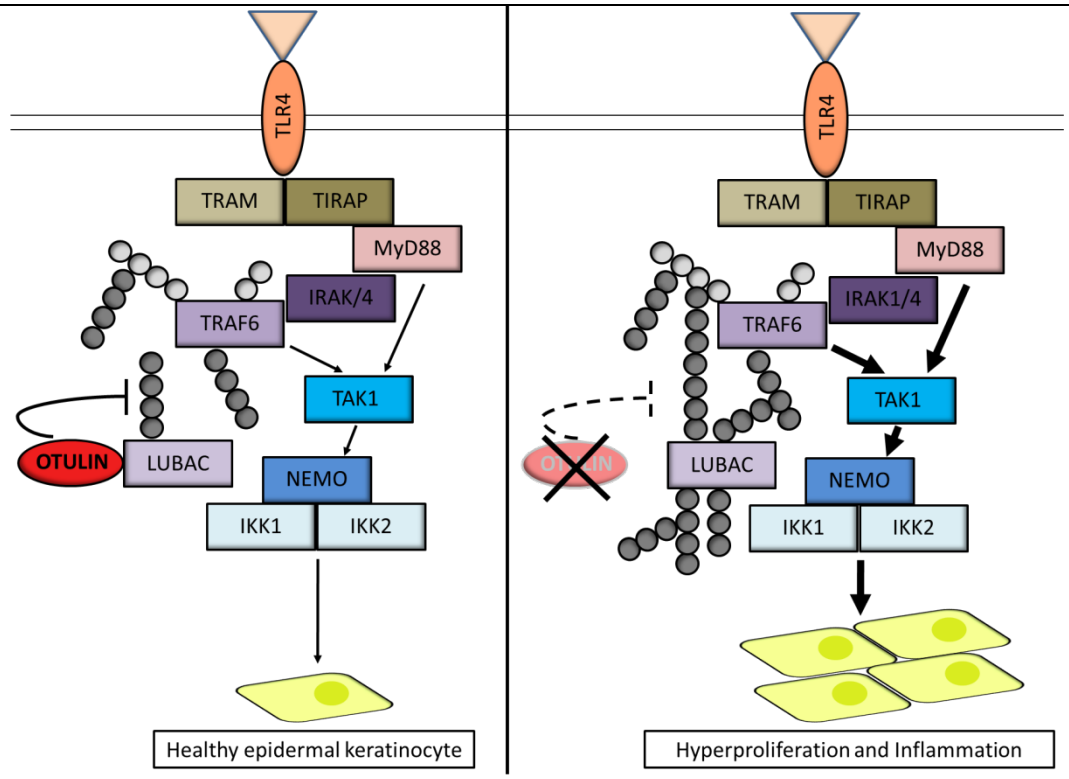

Figure 68: OTULIN regulates linear ubiquitination in MyD88 signaling to prevent skin disease development.

TLR4-dependent MyD88 signaling activation regulates cellular homeostasis in epidermal keratinocytes. Dys-balancing of linear ubiquitination results in MyD88-signaling dependent hyper-proliferation and inflammation.

3.5 Concluding remarks

In conclusion, the results presented in this thesis demonstrate that OTULIN is a critical regulator in skin homeostasis by protecting epidermal keratinocytes from undergoing TNFR1 driven and RIPK1 kinase-dependent cell death and inflammation. OTULIN is identified to play a pivotal role in protecting the skin epithelium mainly from necroptosis which drives inflammation with contribution of apoptotic keratinocyte death promoting skin disease development. It remains unclear if the function of OTULIN is restricted to the regulation of LUBAC activity or if OTULIN has additional linear Ubiquitin-dependent and -independent roles also in other immune signaling pathways. However, this work is in agreement with recent studies that present OTULIN as a key mediator of cell death, inflammation and cancer development in liver tissue. In contrast to the data in this thesis, the regulatory effects of OTULIN appear to be independent of TNFR1 signaling in the liver epithelium, thereby unraveling cell type specific processes [187, 188]. In line with possible compensatory functions of A20 and DUB in TNFR1 signaling, deubiquitination events by other DUBs might function in a redundant manner and need to be further investigated. Furthermore, our findings provide

important insights into the role of OTULIN in MyD88 signaling and type I IFN signaling, thereby demonstrating different signaling pathways to contribute to disease development. Altogether, these findings provide novel insights in how uniquely OTULIN controls immune receptor signaling in a cell- and context-dependent fashion and highlight the importance of finding targeting therapeutic strategies for ORAS patients. Therefore, it is indispensable to unravel the molecular mechanism of OTULIN function and regulation in different tissues and cell types in the future.

4. Material and Methods

4.1 Materials and chemical reagents

Kits and chemicals used in this work were purchased from the described companies. All solutions were prepared with double-distilled water (ddH2O) (Table 1, Table 3).

Table 1: Reagents and Chemicals used in this study

Reagents/ Chemicals	Supplier	Catalog number
Acrylamid/Bis solution	Serva	10688.01
Ammonium persulphate (APS)	Sigma	A3678-100G
β-mercaptoethanol	Sigma	M7522
4-2-hydroxyethyl-1-piperazineethanesulfonicacid (HEPES)	Invitrogen	15630-056
Agarose ultra-pure	Biozym	840004
Albumine bovine fraction (BSA)	Biorad	500-0006
Birinapant	BioVision	2597
Bromophenol blue	Merck	B0126
Complete (Protease EDTA-free Inhibitor Cocktail Tablets	Roche	11836145001
DMEM (Ca2+ DMEM/Ham's F12)	Biochrom	F 9092-0.46
diMethyl sulfoxide (DMSO)	AppliChem	A3672,0050
Dispase II	Sigma	D4693
Draq7	Cell Signaling	4084L
ECL Detection Reagents	GE Healthcare	RPN2132
ECL Detection Reagents (femto)	Thermo Scientific	34095
Entellan	Merck	107960
Ethylenediaminetetraacetic acid (EDTA)	JT-Baker	8993-01
Ethanol absolute	AnalR Normapur	20821-321
Fetal calf serum (FCS)	PAA	A15-101
Fluoromount-G	Southern Biotech	0100-01
100x L-Glutamine (200mM)	Invitrogen	25030123
Glycerol	VWR	24386-298
Hydrochloride acid (HCl) 37%	AppliChem	A2427-2500
Isopropanol (2-Propanol)	AppliChem	A3928
Methanol	Sigma	494437
Nitrogen (liquid)	Sigma	N4638
Paraformaldehyde (PFA)	AppliCHem	A3813
PBS (without Ca^{2+} and Mg^{2+})	Gibco	14190-094
100x Penicillin (10000U/ml)/Streptomycin (10000ug/ml)	Invitrogen	15140163
Phosphatase inhibitor cocktail tablets, PhosSTOP	Roche	04906837 001
Phosphate buffered saline (PBS)	Gibco	14190-094
Pierce™ 660 nm Protein Assay	ThermoScientific	22660
Poncaeu	Sigma	09276
Proteinase K	Roche	3115852
Proteinmarker PeqGold	Peqlab	27-2210
Recombinant mouse TNF	VIB Gent	1
Sodium dodecyl sulfate (SDS)	Millipore	817034.1000
100x Sodium pyruvate (100mM)	Gibco	11360-039
Stripping buffer	ThermoScientific	21059
TaqMan Gene Expression Master Mix	ThermoScientific	4369542
N,N,N',N' Tetra Methylenediamine (TEMED)	Serva	35925
Tissue-Tek O.C.Tä Compound	Sakura	4583

Tris HCL/Base	VWR	443864E
Triton X-100	AppliChem	A4975-0500
Trizol reagent	Invitrogen	15596-018
Trypsin EDTA (TrypLE)	Gibco	12603-010
Tween-20	Sigma	P1379-500

Table 2: Kits used in this study

Kits	Supplier	Catalog number
ABC Kit Vectastain Elite	Vector	PK 6100
Avidin/Biotin Blocking Kit	Vector	SP-2001
Liquid DAB Substrate Chromogen System	DakoCytomation	K3466
RNA extraction RNeasy mini Kit	Qiagen	74106
RNase-free DNase set	Qiagen	79254
SuperScriptIII cDNA synthesis Kit	Invitrogen	18080-044
TaqMan® Gene expression Master Mix	Applied Biosystems	4369542

Table 3: Buffers and solutions used in this study

Buffers and solutions	Composition
Western blot blocking buffer	PBS Non-fat dry milk 5%
Tail lysis buffer	Tris/HCl 100 mM EDTA 5 mM SDS 0.2% NaCl 200 mM
Cell lysis buffer	Tris/HCl 0.2 M pH 8 KCl 0.1 M $(NH_4)2SO_4$ 0.1 M $MgSO_4$ (20 mM) Triton X-100 1% (v/v)
5x Laemmli loading buffer	Tris-HCL (pH 6.8) 250 mM SDS 10% (w/v) Glycerol 50% (v/v) Bromphenolblue 0.01% (w/v) β-Mercaptoethanol 10% (v/v)
IHC blocking buffer	PBS Bovine serum albumin 1% (w/v) NGS 10% cold fish skin gelatin 0.2% (v/v) Triton X-100 0.3% (v/v)
PBS (1x), pH 7.3	NaCl 137 mM KCl 2.7 mM $Na^2HPO^4 – 7H_2O$ 4.3 mM KH_2PO^4 1.4 mM
Primary and secondary antibody dilution buffer for immunoblots	PBS Tween 0.1% Sodium azide
Peroxidase blocking buffer	NaCitrate 0.04 M Na_2HPO_4 0.121 M NaN_3, 3% H_2O_2 0.03M
Retrieval buffer	NaCitrate 10mM Tween-20, pH6 0.05% Tri-sodium citrate 2,94 g

TAE Buffer (25x) for 10l	Tris-Base 1210 g 0.5 M EDTA (pH 8.0) 500 ml Acetic acid 285.5 ml
TE Buffer	Tris-HCl (pH 8.0) 10 mM EDTA (pH 8.0) 1 mM
SDS polyacrylamid gel	<u>10% resolving gel (for 20 ml)</u> H_2O 7.9 ml 30% Acrylamide mix 6.7 ml 1.5 M Tris (pH 8.8) 5.0 ml 10% (w/v) SDS 0.2 ml 10% (w/v) APS 0.2 ml TEMED 0.008 ml <u>5% stacking gel (for 10 ml)</u> H_2O 6,8 ml 30% Acrylamide mix 1.7 ml 1 M Tris (pH 6.8) 1.25 ml 10% (w/v) SDS 0.1 ml 10% (w/v) APS 0.1 ml TEMED 0.01 ml
Western blot Running Buffer	Tris25 mM Glycine 92 mM SDS 0.1%
Western blot Transfer Buffer	Tris-Base 25 mM Glycine 192 mM Methanol 20%

4.2 Animal handling and mouse experiments

4.2.1 Animal care

All animal procedures and experiments were performed in compliance with protocols and licenses approved by local government authorities (Bezirksregierung Köln) and were performed in accordance with European, national and institutional guidelines. All protocols were approved by local government authorities (Landesamt für Natur, Umwelt und Verbraucherschutz Nordrhein-Westfalen, Germany). Mice were maintained in a conventional animal facility in individually ventilated cages (IVC) in a specific pathogen free (SPF) mouse facility in the CECAD Research Center, University of Cologne. Mice were housed with 3-4 animals per cage at 22-24°C, under a 12 hours (h) light/dark cycle, given acidified water and a regular chow diet (Teklad Global Rodent 2018, Harlan) *ad libitum*. For breeding, male and female mice were placed together at an age of 8 weeks minimum. Litters were marked with ear tags at minimum age of 2 weeks, tail biopsies were taken for genotyping at that time and litters were weaned at the age of 3 weeks.

4.2.2 Causes recombination (Cre)/LoxP conditional gene targeting

The Cre/LoxP mediated recombination of conditional genes was used to generate cell type-specific deletion during development of genes of interest to enable cell type-specific analysis of gene functions. Two LoxP sites need to be inserted in the same orientation to flank the gene locus or exon of interest, thereby generating a conditional knockout allele [239, 240]. The LoxP sites with a specific 34 bp DNA sequence consist of an 8 bp spacer, that contributes to the orientation of the LoxP sites and is flanked by two 13 bp inverted palindromes. LoxP sites that are inverted induce the inversion of the exon of interest, while LoxP sites that are orientated in the same direction lead to excision of the gene/exon of interest. For deletion of your gene/exon of interest, mice carrying an allele with LoxP sites (floxed (FL) mice) are crossed to mice expressing a bacteriophage P1-derived Cre recombinase under the control on a tissue-specific promotor (Cre mice). This ensures that only in Cre-expressing cells LoxP sites are recognized, recombined by Cre recombinase, resulting in excision of the floxed gene fragment and inactivation of the gene/exon of interest.

4.2.3 Generation of conditional and full body knockout mice

To generate mice with a deletion of OTULIN specifically in the epidermal skin, female *Otulin*$^{FL/FL}$ were crossed with male K14-Cre transgenic mice [227]. OTULIN^{E-KO} mice were crossed to *Ripk1*$^{D138N/D138N}$ mice [56]. *Tnfr1*$^{FL/FL}$ mice [241], *Ripk3*$^{-/-}$ mice [242], *Mlkl*$^{-/-}$ mice [211], *Fadd*$^{FL/FL}$ mice [243], *Ripk3*$^{-/-}$ mice [244] and MyD88$^{-/-}$ mice [245] to generate double or triple deficient mice. All mice were analyzed at 3 weeks, 14 weeks 30 weeks or 50 weeks unless indicated otherwise and littermates not carrying the K14-Cre transgene were used as control mice.

4.2.4 Preparation of tissue biopsies

Mice were euthanized by cervical dislocation and under the age of 3 weeks by decapitation.

4.2.5 Scoring

Mice were assessed for the presence and the stage of the phenotype development according to Table 4. The mice were scored at the age of 3 weeks or 14 weeks. In the corresponding graphs, each dot represents one mouse per genotype in which the indicated Score was identified accordingly (Table 4).

Table 4: Skin scoring system

Score	Phenotype
0	No lesion
1	Skin lesion
2	Skin lesion, tail skin lesion
3	Papilloma-like structures, tail skin lesion

4.2.6 Tissue preparation

After euthanasia, the back skin was shaved and cut into pieces. The fat was removed and small pieces of about 0.25 cm length were collected for RNA extraction. For histological examination, pieces of about 0.5 cm length were collected, stretched to paper and fixed in 4% paraformaldehyde (PFA) in histological cassettes or in TissueTek in cryomolds at -80°C.

4.2.7 Isolation of keratinocytes

Primary keratinocytes were isolated from skin of mice that were euthanized latest 2 days after birth. The mice were washed in ice-cold PBS and 70% (v/v) EtOH. After washing again in PBS the skin was removed from the body incubated in 10% Dispase II in PBS at 4°C for 16 h, to break cellular connection between dermis and epidermis. To isolate keratinocytes from the epidermis, dermis and epidermis were separated and the epidermis was digested in 500µl TrypLE for 20 minutes (min) at room temperature (rt). Afterwards, the isolated keratinocytes were centrifuged at 1000 rpm for 5 min in keratinocyte medium and plated on collagen-coated plates.

4.3 Molecular biology

4.3.1 Isolation of genomic DNA

To determine the genotype of a mouse, mouse tail biopsies were digested in tail lysis buffer (s. table 3) with 10 mg/ml Proteinase K overnight at 56°C. For genomic DNA precipitation, 1 volume of isopropanol was added. After centrifugation for 2 min at 13000 rpm, the DNA pellet was washed with 70% ethanol (v/v) and centrifuged for 2 min at 13000 rpm. The pellet was dried at room temperature for 20 min and subsequently resuspended in TE buffer.

4.3.2 PCR for genotyping

PCR was performed to genotype mice by using specific primers (Table 5). 3 µM of the specific primer mix was mixed with 2 µl genomic DNA with 12.5 µl ready-to-use Mastermix (VWR) and 10.5 µl H_2O. The DNA template was amplified by using thermal cycler and specific

PCR programs, including initialization (95-98°C, 4 min), denaturation (95-98°C, 20-30 s), annealing (50-65°C, 20-40 s) and finally extension and elongation (72-80°C, 4 min). The denaturation, annealing and extension/elongation steps are repeated 35 times to ensure amplification of the DNA template.

Table 5: Primer-sequences for genotyping PCRs and PCR-amplified fragment sizes.

WT: wildtype; Tg: transgene; FL: floxed; KO: knockout; DEL: deleted; Exp: expected

Typing	Primer Sequence (5'-3')	Band size (bp)	Temperature	Time	Cycles
FADD^{FL}	TCACCGTTGCTCTTTGTCTACGTA ATCTCTGTAGGGAGCCCT AAGGCATCAGCAAGAGCAGT	WT: 200 FL: 280 DEL : 380	94 °C	3 min	35x
			94 °C 60 °C 72 °C	30 s 45 s 30 s	
			72 °C	3 min	
K14 Cre	AGCACCTTCTCTTCACTCAGC CGCATAACCAGTGAAACAGCAT	Exp: 400-450	94 °C	3 min	30x
			94 °C 58 °C 72 °C	20 s 20 s 20 s	
			72 °C	2 min	
MLKL^{Del}	CATCAAGTTAGGCCAGCTCA TCTGCTGGTTAGCCTCCTTC	WT: 204 DEL: 173	94 °C	3 min	35x
			94 °C 58 °C 72 °C	30 s 30 s 60 s	
			72 °C	3 min	
MyD88^{KO}	GGAGGAAGGCTCAGAGAAGC GTCTGCAGGCAGCTACAGTG CGCTACAGACGTTGTTTGTC	WT: 250 KO: 505 FL: 290	94 °C	4 min	40x
			94 °C 60 °C 72 °C	30 s 30 s 40 s	
			72 °C	3 min	
OTULIN^{FL}	TCAAACCGTCTGTCCTGAGCTAC GTATCAT GCAGAGCCCACAGGGCGTACTG CAGTTCCA	WT: 500 FL: 600	98 °C	2 min	35x
			98 °C 68 °C	20 s 45 s	
			72 °C	3 min	
RIPK1^{D138N}	TACCTTCTAACAAAGCTTTCC AATGGAACCACAGCATTGGC CCCTCGAAGAGGTTCACTAG	WT: 220 Exp: 180	94 °C	2 min	40x
			94 °C 60 °C 72 °C	30 s 30 s 30 s	
			72 °C	5 min	
RIPK3^{DEL}	CTACCGGACAAGAACCTTTC CAAGCTGTGTAGGTAGCACAT	WT: 500 KO: 410	94 °C	3 min	35x
			94 °C 60 °C 72 °C	30 s 30 s 30 s	
			72 °C	10 min	
RIPK3^{KO}	CGCTTTAGAAGCCTTCAGGTTGA C GCCTGCCCATCAGCAACTC CCAGAGGCCACTTGTGTAGCG	WT: 320 KO: 485	94 °C	4 min	30x
			94 °C 60 °C 72 °C	1 min 30 s 1 min	
			72 °C	10 min	

TNFR1^{FL}	CAAGTGCTTGGGGTTCAGGG CGTCCTGGAGAAAGGGAAAG	WT: 134 Exp: 195	94 °C	3 min	
			94 °C 60 °C 72 °C	30 s 1 min 2 min	29x
			72 °C	5 min	

4.3.3 Agarose gel electrophoresis

Agarose gel electrophoresis is used to separate the DNA fragments according to their sizes. For this, 10 µl of the PCR products were analyzed using 2% (w/v) agarose gels, containing 0.5 mg/ml ethidium bromide. Gels were run in 1x TAE buffer, 120 V for 30 min. The DNA bands were visualized using a Gel Doc Systems (Thermo Fisher Scientific) and compared to a standard DNA marker (Peqlab).

4.3.4 RNA Isolation

For RNA isolation from whole skin tissues or keratinocytes, the samples were homogenized in 1 ml Trizol reagent (Invitrogen) and centrifuged for 10 min at 13000 rpm. The supernatant was transferred into a new tube and 200 µl chloroform were added and mixed vigorously to extract nucleic acids. After 5 min incubation, the samples were centrifuged for 15 min at 13000 rpm to separate the organic and the aqueous phase. The aqueous phase was transferred into a new tube and an equal volume of 70% /v/v) ethanol was added and mixed. Afterwards, the samples were further processed using the Quiagen RNeasy Kit following manufacturer's guidelines. To allow binding of nucleic acids to the filter, samples were loaded on the columns and centrifuged for 1 min at 9000 rpm. Afterwards, RNase-free DNase diluted in RDD buffer was added to the filter of the column for 20 min to digest genomic DNA. To wash the RNA, bound to filters, the columns were washed twice with 500 µl washing buffer and subsequently centrifuged at 9000 rpm for 30 s. To elute the RNA, 100 µl nuclease free water were added to the columns, followed by centrifugation for 1 min at 13000 rpm. Finally the RNA was tested for possible genomic DNA contamination, by using β-Actin PCR and the concentration and purity of the extracted RNA were measured using a NanoDrop.

4.3.5 QuantSeq 3'mRNA Sequencing

RNA quality was evaluated based on RNA integrity number (RIN) and OD260/280 and OD260/230 ratios. RIN value was determined using TapeStation4200 and RNA Screen Tapes (Agilent Technologies). Gene expression was determined using QuantSeq 3' mRNA-Seq

Library Prep Kit FWD for Illumina (Lexogen). Sample exclusion criteria were OD260/280<1.8, OD260/230<1.5 and RIN<4. Five skin tissues samples from wildtype mice (WT), five affected (lesional) skin tissue samples and five non-affected (non-lesional) tissue samples from OTULINEKO mice with a RIN below 4 were included for the analysis. Illumina adapters were clipped off the raw reads using cutadapt with standard parameters and a minimum read length of 35 after trimming (shorter reads were discarded). QuantSeq specific features were subsequently removed from the trimmed reads following the workflow described in https://rstudio-pubsstatic.s3.amazonaws.com/171024.html. Trimmed and cleaned reads were mapped to a concatenation of the mouse genome Mus_musculus.GRCm38.dna. chromosome.*.fa.gz (ftp://ftp.ensembl.org/pub/release-100/fasta/mus_musculus/dna/) and theERCC92 Spike In sequences (https://assets.thermofisher.com/TFS-Assets/LSG/manuals/ERCC92.zip), using subread-align version v2.0.1 with parameters -t 0 -d 50 -D 600 --multiMapping -B 5. For counting, only high-quality uniquely mapping matches was retained, using samtools view -hb -q 30 -F 256. These matches were then combined into a count table using featureCounts with parameters -F "GTF" -t "exon" -g "gene_id" --minOverlap 20 -M --primary -O -J -T 4. Differential Gene Expression Analysis was done in R-4.0.0, using package DESeq2 (https://bioconductor.org/packages/release/bioc/html/DESeq2.html). Before heatmap visualization, gene counts were converted to Counts Per Million (CPM) and the CPM values were scaled by log10 (adding a pseudocount of 0.1). Heatmaps were drawn using Instant Clue [246]. The individual heatmaps show genes that were significant in DESeq2 at a given p-value cutoff and had a logFoldChange of 1 or larger. For over-representation (ORA) tests, which compare a pre-defined subset of genes to the universe of all genes, the enrichGO function was used with standard parameters. The query gene subset for ORA analysis was defined by cutoffs on p-value and logFoldChange.

4.3.6 cDNA synthesis

In order to synthesize cDNA from extracted RNA, the Superscript III kit (Invitrogen) was used, according manufacturer's instructions. For 10 µl final reaction volume, 1 µg RNA was added to 1 µl of 50 ng/µl random hexamer primers and 1 µl of 10 mM dNTPs. The reaction mix was incubated at 65°C for 5 min, to allow primer annealing and subsequently cooled down on ice for 1 min. Meanwhile, 10 µl cDNA reaction mix containing 2 µl 10x RT-reaction buffer, 4 µl 25 mM $MgCl_2$, 2 µl 0.1 M DTT, 1 µl RNase OUT (40 U/µl) and 1 µl of SuperScript III polymerase

(200 U/µL) were prepared and added to the samples. Reverse transcription was performed for 10 min at 25°C, followed by cDNA synthesis for 50 min at 50°C and heat-inactivation was performed for 5 min at 85°C in a PCR cycler. To digest the remaining RNA 1 µl RNaseH was added to the reaction mix and the samples were incubated for 20 min at 37°C. Finally, the cDNA reaction mix was diluted 10-fold in nuclease-free water and 2 µl of cDNA was used for β-Actin-PCR, to check successful cDNA synthesis, and for quantitative real time-PCR (qRTPCR).

4.3.7 qRT-PCR

Probe-based Taqman qRT-PCR was performed to quantify gene expression. The final volume of 10 µl consisting of 2 µl cDNA, 5 µl Mastermix (Applied Biosystems), 5 µl primer-probe mix (Applied Biosystems) and 2.5 µl nuclease-free water (Table 6). The samples were run in two technical replicates with TATA-box-binding protein (*Tbp*) as reference gene. All reactions were carried out in 384-well plates and the PCR was performed by using a Quant Studio Real-Time PCR System (Thermo Fisher Scientific). The Polymerase was activated at 95°C for 10 min, followed by 40 amplification cycles, each with 95°C for 10 s and 60°C for 1 min. The relative expression of gene transcripts was analyzed by using the $2^{-\Delta Ct}$ Method.

Table 6: Taqman probes used for qRT-PCR

Gene	Taqman probe
Ccl3	Mm00441258_M1
Cxcl3	Mm01701838_M1
Cxcl9	Mm00434946_M1
Cxcl10	Mm00445235_M1
Il-1β	Mm00434228_M1
Il-6	Mm00446190_M1
Tbp	Mm00446973_M1

4.4 Cellular biology

4.4.1 Preparation skin tissue for histological analysis

For histological examination skin samples were dehydrated for 2 h in 30% (v/v), 50% (v/v), 70% (v/v), 96% (v/v) and 100% (v/v) EtOH and incubated in Xylol for 2 h. Afterwards, samples were embedded in liquid paraffin in paraffin block and sectioned into 7 µM-thick skin sections on glass slides.

4.4.2 Haematoxylin and Eosin (H&E) staining of skin tissue sections

The skin sections were deparaffinized by incubating in Xylol for 20 min, re-hydrated in decreasing EtOH-concentrated solutions and afterwards incubated in Heamatoxylin for 10 s. Afterwards, samples were differentiated in tap water for 15 min and were incubated in Eosin for 1 min. Finally, sections were dehydrated increasing EtOH solutions, fixated in Xylol for 2 min each and subsequently mounted with Entellan.

4.4.3 Immunohistochemistry

The tissue sections were deparaffinized as described in section 4.4.2. and antigen retrieval was performed in citrate, TRIS buffer, pH6 for 30 min in a waterbath at 100°C. Afterwards, endogenous peroxidase activity as blocked by incubation with peroxidase blocking buffer for 20 min at rt. After washing three times for 5 min with water, the samples were incubated with IHC blocking buffer supplemented with Avidin for 1 h at rt to block unspecific background. Subsequently, primary antibodies were diluted in IHC blocking buffer supplemented with Biotin and incubated at 4 °C over night in a wet chamber (Table 7). Next day, the samples were washed three times in PBS with 0.5 % (v/v) Tween-20, followed by the incubation of the biotinylated secondary antibodies, diluted in IHC blocking buffer for 1 h at rt (Table 8). Thereafter, sections were washed three times in 0.5% PBS-T and applied with Avidin-Biotin-HRP (ABC Kit Vectastain Elite (Vector Laboratories) for 45 min at rt. To visualize the stainings, DAB substrate (DAKO and Vector Laboratories) was exposed to the sections and followed under the microscope. As soon as sufficient signal intensity was reached, the reaction was stopped with tab water and samples were counterstained with Hematoxylin for 10 s and subsequently dehydrated as described in 4.4.2.

Table 7: Primary antibodies used for immunohistochemistry

Antibody	Company	ID	Host	Dilution
α-cleaved Caspase-3	Cell Signaling	9661	Rabbit	1:1000
α -cleaved Caspase-8	Cell Signaling	8592	Rabbit	1:8000
α -Ki-67	Dako	M724901	Rat	1:1000

Table 8: Secondary antibodies used for immunohistochemistry

Antibody	Company	ID	Host	Dilution
Biotinylated α -rabbit IgG	Perkin Elmer	NEF813	Goat	1:1000
Biotinylated α -rat IgG	DAKO	E0468	Rabbit	1:1000

4.4.4 Fluorescent Staining

The tissue sections were deparaffinisized as described in section 4.4.2 and antigen retrieval was performed In citrate, TRIS buffer, pH6 (Table 3) for 30 min in a waterbath at 100°C. Afterwards, blocking was performed using PBS with 10 % (v/v) natural goat serum for 1h at room temperature. The primary antibodies were diluted in PBS + 10 % NGS and applied to the sections for 20 h at 4 °C (Table 9). Thereafter, the sections were washed three times in PBS with 0.5 % (v/v) Tween-20, followed by the incubation of the fluorescent secondary antibodies, diluted in PBS + 10 % NGS for 1.5 h at room temperature (Table 10). Sections where washed three times 5 min with 0.5 % PBS-T and 5 min with distilled water. Finally, the sections were mounted with Fluoromount G. (Southern Biotech) and stored at 4 °C.

Table 9: Primary antibodies used for fluorescent staining

Antibody	Company	ID	Host	Dilution
α -Keratin 14	LabVision	Clone LL002	Mouse	1:400
α -Keratin 10	Covance	PRB-159P	Rabbit	1:300
α -Loricrin	Covance	PRB-145P	Rabbit	1:600
α –F4/80	homemade	homemade	Rat	1:1000
α –Gr-1	Serotec	MCA2387GA	Rat	1:1000

Table 10: Secondary antibodies used for fluorescent staining

Antibody	Company	ID	Host	Dilution
α -mouse alexa 488	Molecular Probes Inc.	A-11001	Goat	1.800
α -rabbit alexa 594	Molecular Probes Inc.	A-11012	Goat	1:800
α -rat Alexa 488	Molecular Probes Inc.	A21210	Rabbit	1:800

4.4.5 Assessment of cell death

Cell death assay was performed and analyzed using the IncuCyte® bioimaging platform (Essen). The cells were plated in 96-well plate (Corning, BioCoat, 354407) ($1x10^2$ cells/well) for 24 h at 37°C with 5% (v/v) CO_2 atmosphere. The cells were pre-treated for 30 minutes with Z-VAD-fmk (Enzo, ALX-260-020-M005, 20µM) and Birinapant (BioVision, 2597) and stimulated with human recombinant Tnf (20 ng/ml) for 24 h at 37°C with 5% (v/v) CO_2 atmosphere in cell culture medium hours in the presence of the dead stain Draq7 (Invitrogen, D15106, 0.3µM). Two to four images per well were captured, analyzed and averaged. Cell death was measured by the incorporation of Draq7.

4.5 Biochemical Analysis

4.5.1 Preparation of protein extracts from skin tissue

For total protein extraction from whole skin, skin samples were collected and homogenized using Precellys tissue homogenizer (Bertin Instruments) in protein lysis buffer supplemented with phosphatase and protease inhibitor tablets (Sigma). Afterwards, the protein samples were centrifuged for 15 min at 13000 rpm at 4°C, the supernatant was collected and protein concentration was determined using Pierce (Bio-rad).

4.5.2 Preparation of protein extracts from cells

For subcellular fractionation, medium was removed and cells where washed with ice cold PBS and lysed in cell lysis buffer supplemented with phosphatase and protease inhibitor tablets (Sigma). After incubation for 20 min on ice, samples were collected and centrifuged for 10 min at 13000 rpm at 4 °C and protein concentration was determined using Pierce (Bio-rad).

4.5.3 Western blot analysis

For immunoblot analyses, 4×10^5 cells were seeded in collagen coated 6 well plates (Corning, BioCoat, 354556) and eight hours before stimulation the medium was replaced by fresh medium without EGF. Keratinocytes were stimulated by TNF (VIB Protein Service Facility, Gent, 20 ng ml−1) for different timepoints. To denature proteins, protein extracts (20 µg protein/ 50 µl) were boiled in 1x Laemmli buffer for 10 min at 99°C. Afterwards, the protein samples were separated on 10% SDS-polyacrylamide gel in Western blot running buffer and transferred to PVDF membranes (IPVH00010, Millipore) that where activated by incubation in 100% Methanol for 2 min. The transfer was performed as a wet transfer in Western blot transfer buffer at 30 V for 20 h at 4°C. After the protein transfer, the membranes were blocked with 5% milk in 0.1% PBS-T for 1 h at rt and probed with primary antibodies against the proteins indicated in Table 11 for 16 h at 4°C. Membranes were washed three times with 0.1% PBS-T and incubated with a horseradish peroxidase conjugates secondary antibody (Table 12) for 1 h at rt. The protein bands were visualized using commercial ECL (GE Healthcare) with varying exposure times to chemiluminescent films or using the chemiluminescent system Fusion SOLO S (Vilber).

Table 11: Primary antibodies used for Western blot analysis

Antibody	Company	ID	Host	Dilution
α-p-ERK	Cell Signaling	9101	Rabbit	1:1000
α-ERK	Cell Signaling	9102	Rabbit	1:1000
α-p-IκBα	Cell Signaling	9246	Rabbit	1:1000
α-IκBα	Santa Cruz	Sc-371	Rabbit	1:1000
α-p-JNK	Cell Signaling	9251	Rabbit	1:1000
α-JNK	Cell Signaling	9252	Rabbit	1:1000
α-M1-Ubiquitin	Genentech	1F11/3F5/Y102L	Human	1:1000
α-OTULIN	Cell Signaling	14127	Rabbit	1:1000
α-p-p38	Cell Signaling	9211	Rabbit	1:1000
α-p38	Cell Signaling	9212	Rabbit	1:1000
α-p-p65	Santa Cruz	Sc-71	Rabbit	1:1000
α-p65	Santa Cruz	sc-372	Rabbit	1:1000
α- Tubulin	Sigma	B512	Mouse	1:1000

Table 12: Secondary antibodies used for Western blot analysis

Antibody	Company	ID	Host	Dilution
α-rabbit IgG-HRP	GE Helathcare	NA934V	Goat	1:5000
α-mouse IgG-HRP	GE Helathcare	NA9310V	Sheep	1:5000
α-human IgG-HRP	Sigma	I4506	Human serum	1:2000

4.6 Computer analysis

4.6.1 Software

EndnoteX7

IncuCyte

InstantClue

Leica microscopy Software Leica application suite

Microsoft Office

OMERO

Prism Graphpad

4.6.2 Statistical analysis

Data shown in graphs are mean or mean ± s.e.m. If the data fulfilled the criteria for Gaussian distribution tested by column statistics, one-way ANOVA was performed for statistical analysis, otherwise a nonparametric one-sided Kruskal-Wallis test was chosen. All statistical tests listed in the figure legends were two-sided and were performed using Graphpad Prism. *p<0.05, **p<0.01, ***p<0.005, ****p<0.0001 for all figures.

5. References

1. Akutsu, M., Dikic, I. & Bremm, A. Ubiquitin chain diversity at a glance. *J Cell Sci* **129**, 875-880 (2016).
2. Swatek, K.N. & Komander, D. Ubiquitin modifications. *Cell Res* **26**, 399-422 (2016).
3. Chau, V. *et al.* A multiubiquitin chain is confined to specific lysine in a targeted short-lived protein. *Science* **243**, 1576-1583 (1989).
4. Komander, D. & Rape, M. The ubiquitin code. *Annu Rev Biochem* **81**, 203-229 (2012).
5. Yau, R. & Rape, M. The increasing complexity of the ubiquitin code. *Nat Cell Biol* **18**, 579-586 (2016).
6. Kirisako, T. *et al.* A ubiquitin ligase complex assembles linear polyubiquitin chains. *EMBO J* **25**, 4877-4887 (2006).
7. Dikic, I. & Dotsch, V. Ubiquitin linkages make a difference. *Nat Struct Mol Biol* **16**, 1209-1210 (2009).
8. Fennell, L.M., Rahighi, S. & Ikeda, F. Linear ubiquitin chain-binding domains. *FEBS J* **285**, 2746-2761 (2018).
9. Komander, D., Clague, M.J. & Urbe, S. Breaking the chains: structure and function of the deubiquitinases. *Nat Rev Mol Cell Biol* **10**, 550-563 (2009).
10. Dikic, I., Wakatsuki, S. & Walters, K.J. Ubiquitin-binding domains - from structures to functions. *Nat Rev Mol Cell Biol* **10**, 659-671 (2009).
11. Webster, J.D. & Vucic, D. The Balance of TNF Mediated Pathways Regulates Inflammatory Cell Death Signaling in Healthy and Diseased Tissues. *Front Cell Dev Biol* **8**, 365 (2020).
12. Pasparakis, M. & Vandenabeele, P. Necroptosis and its role in inflammation. *Nature* **517**, 311-320 (2015).
13. Varfolomeev, E. & Vucic, D. Intracellular regulation of TNF activity in health and disease. *Cytokine* **101**, 26-32 (2018).
14. Hayden, M.S. & Ghosh, S. Regulation of NF-kappaB by TNF family cytokines. *Semin Immunol* **26**, 253-266 (2014).
15. Legler, D.F., Micheau, O., Doucey, M.A., Tschopp, J. & Bron, C. Recruitment of TNF receptor 1 to lipid rafts is essential for TNFalpha-mediated NF-kappaB activation. *Immunity* **18**, 655-664 (2003).
16. Hsu, H., Huang, J., Shu, H.B., Baichwal, V. & Goeddel, D.V. TNF-dependent recruitment of the protein kinase RIP to the TNF receptor-1 signaling complex. *Immunity* **4**, 387-396 (1996).
17. Micheau, O. & Tschopp, J. Induction of TNF receptor I-mediated apoptosis via two sequential signaling complexes. *Cell* **114**, 181-190 (2003).
18. Hsu, H., Shu, H.B., Pan, M.G. & Goeddel, D.V. TRADD-TRAF2 and TRADD-FADD interactions define two distinct TNF receptor 1 signal transduction pathways. *Cell* **84**, 299-308 (1996).
19. Hsu, H., Xiong, J. & Goeddel, D.V. The TNF receptor 1-associated protein TRADD signals cell death and NF-kappa B activation. *Cell* **81**, 495-504 (1995).
20. Bertrand, M.J. *et al.* cIAP1 and cIAP2 facilitate cancer cell survival by functioning as E3 ligases that promote RIP1 ubiquitination. *Mol Cell* **30**, 689-700 (2008).
21. Mahoney, D.J. *et al.* Both cIAP1 and cIAP2 regulate TNFalpha-mediated NF-kappaB activation. *Proc Natl Acad Sci U S A* **105**, 11778-11783 (2008).
22. Varfolomeev, E. *et al.* c-IAP1 and c-IAP2 are critical mediators of tumor necrosis factor alpha (TNFalpha)-induced NF-kappaB activation. *J Biol Chem* **283**, 24295-24299 (2008).
23. Haas, T.L. *et al.* Recruitment of the linear ubiquitin chain assembly complex stabilizes the TNF-R1 signaling complex and is required for TNF-mediated gene induction. *Mol Cell* **36**, 831-844 (2009).
24. Gerlach, B. *et al.* Linear ubiquitination prevents inflammation and regulates immune signalling. *Nature* **471**, 591-596 (2011).
25. Ikeda, F. *et al.* SHARPIN forms a linear ubiquitin ligase complex regulating NF-kappaB activity and apoptosis. *Nature* **471**, 637-641 (2011).

26. Tokunaga, F. *et al.* SHARPIN is a component of the NF-kappaB-activating linear ubiquitin chain assembly complex. *Nature* **471**, 633-636 (2011).
27. Tokunaga, F. & Iwai, K. Linear ubiquitination: a novel NF-kappaB regulatory mechanism for inflammatory and immune responses by the LUBAC ubiquitin ligase complex. *Endocr J* **59**, 641-652 (2012).
28. Martens, A. & van Loo, G. A20 phosphorylation controls A20 function. *Nat Immunol* **20**, 1261-1262 (2019).
29. Elliott, P.R. *et al.* SPATA2 Links CYLD to LUBAC, Activates CYLD, and Controls LUBAC Signaling. *Mol Cell* **63**, 990-1005 (2016).
30. Kupka, S. *et al.* SPATA2-Mediated Binding of CYLD to HOIP Enables CYLD Recruitment to Signaling Complexes. *Cell Rep* **16**, 2271-2280 (2016).
31. Martens, A. & van Loo, G. A20 at the Crossroads of Cell Death, Inflammation, and Autoimmunity. *Cold Spring Harb Perspect Biol* **12** (2020).
32. Keusekotten, K. *et al.* OTULIN antagonizes LUBAC signaling by specifically hydrolyzing Met1-linked polyubiquitin. *Cell* **153**, 1312-1326 (2013).
33. Rivkin, E. *et al.* The linear ubiquitin-specific deubiquitinase gumby regulates angiogenesis. *Nature* **498**, 318-324 (2013).
34. Heger, K. *et al.* OTULIN limits cell death and inflammation by deubiquitinating LUBAC. *Nature* **559**, 120-124 (2018).
35. Hrdinka, M. *et al.* CYLD Limits Lys63- and Met1-Linked Ubiquitin at Receptor Complexes to Regulate Innate Immune Signaling. *Cell Rep* **14**, 2846-2858 (2016).
36. Sato, Y. *et al.* Structures of CYLD USP with Met1- or Lys63-linked diubiquitin reveal mechanisms for dual specificity. *Nat Struct Mol Biol* **22**, 222-229 (2015).
37. Kanayama, A. *et al.* TAB2 and TAB3 activate the NF-kappaB pathway through binding to polyubiquitin chains. *Mol Cell* **15**, 535-548 (2004).
38. Wang, C. *et al.* TAK1 is a ubiquitin-dependent kinase of MKK and IKK. *Nature* **412**, 346-351 (2001).
39. Kensche, T. *et al.* Analysis of nuclear factor-kappaB (NF-kappaB) essential modulator (NEMO) binding to linear and lysine-linked ubiquitin chains and its role in the activation of NF-kappaB. *J Biol Chem* **287**, 23626-23634 (2012).
40. Tokunaga, F. *et al.* Involvement of linear polyubiquitylation of NEMO in NF-kappaB activation. *Nat Cell Biol* **11**, 123-132 (2009).
41. Rahighi, S. *et al.* Specific recognition of linear ubiquitin chains by NEMO is important for NF-kappaB activation. *Cell* **136**, 1098-1109 (2009).
42. Ikeda, F., Rahighi, S., Wakatsuki, S. & Dikic, I. Selective binding of linear ubiquitin chains to NEMO in NF-kappaB activation. *Adv Exp Med Biol* **691**, 107-114 (2011).
43. Haas, A.L. Linear polyubiquitylation: the missing link in NF-kappaB signalling. *Nat Cell Biol* **11**, 116-118 (2009).
44. Wu, C.J., Conze, D.B., Li, T., Srinivasula, S.M. & Ashwell, J.D. Sensing of Lys 63-linked polyubiquitination by NEMO is a key event in NF-kappaB activation [corrected]. *Nat Cell Biol* **8**, 398-406 (2006).
45. Woronicz, J.D., Gao, X., Cao, Z., Rothe, M. & Goeddel, D.V. IkappaB kinase-beta: NF-kappaB activation and complex formation with IkappaB kinase-alpha and NIK. *Science* **278**, 866-869 (1997).
46. Mercurio, F. *et al.* IKK-1 and IKK-2: cytokine-activated IkappaB kinases essential for NF-kappaB activation. *Science* **278**, 860-866 (1997).
47. Mitchell, S., Vargas, J. & Hoffmann, A. Signaling via the NFkappaB system. *Wiley Interdiscip Rev Syst Biol Med* **8**, 227-241 (2016).
48. Tang, Y. *et al.* K63-linked ubiquitination regulates RIPK1 kinase activity to prevent cell death during embryogenesis and inflammation. *Nat Commun* **10**, 4157 (2019).
49. Scheidereit, C. IkappaB kinase complexes: gateways to NF-kappaB activation and transcription. *Oncogene* **25**, 6685-6705 (2006).

50. Zarnegar, B.J. *et al.* Noncanonical NF-kappaB activation requires coordinated assembly of a regulatory complex of the adaptors cIAP1, cIAP2, TRAF2 and TRAF3 and the kinase NIK. *Nat Immunol* **9**, 1371-1378 (2008).
51. Senftleben, U. *et al.* Activation by IKKalpha of a second, evolutionary conserved, NF-kappa B signaling pathway. *Science* **293**, 1495-1499 (2001).
52. Kerr, J.F., Wyllie, A.H. & Currie, A.R. Apoptosis: a basic biological phenomenon with wide-ranging implications in tissue kinetics. *Br J Cancer* **26**, 239-257 (1972).
53. Galluzzi, L. *et al.* Molecular mechanisms of cell death: recommendations of the Nomenclature Committee on Cell Death 2018. *Cell Death Differ* **25**, 486-541 (2018).
54. Elmore, S. Apoptosis: a review of programmed cell death. *Toxicol Pathol* **35**, 495-516 (2007).
55. Delanghe, T., Dondelinger, Y. & Bertrand, M.J.M. RIPK1 Kinase-Dependent Death: A Symphony of Phosphorylation Events. *Trends Cell Biol* **30**, 189-200 (2020).
56. Polykratis, A. *et al.* Cutting edge: RIPK1 Kinase inactive mice are viable and protected from TNF-induced necroptosis in vivo. *J Immunol* **193**, 1539-1543 (2014).
57. Berger, S.B. *et al.* Cutting Edge: RIP1 kinase activity is dispensable for normal development but is a key regulator of inflammation in SHARPIN-deficient mice. *J Immunol* **192**, 5476-5480 (2014).
58. Dondelinger, Y. *et al.* Serine 25 phosphorylation inhibits RIPK1 kinase-dependent cell death in models of infection and inflammation. *Nat Commun* **10**, 1729 (2019).
59. Laurien, L. *et al.* Autophosphorylation at serine 166 regulates RIP kinase 1-mediated cell death and inflammation. *Nat Commun* **11**, 1747 (2020).
60. Lafont, E. *et al.* TBK1 and IKKepsilon prevent TNF-induced cell death by RIPK1 phosphorylation. *Nat Cell Biol* **20**, 1389-1399 (2018).
61. Xu, D. *et al.* TBK1 Suppresses RIPK1-Driven Apoptosis and Inflammation during Development and in Aging. *Cell* **174**, 1477-1491 e1419 (2018).
62. Dondelinger, Y. *et al.* MK2 phosphorylation of RIPK1 regulates TNF-mediated cell death. *Nat Cell Biol* **19**, 1237-1247 (2017).
63. Jaco, I. *et al.* MK2 Phosphorylates RIPK1 to Prevent TNF-Induced Cell Death. *Mol Cell* **66**, 698-710 e695 (2017).
64. Menon, M.B. *et al.* p38(MAPK)/MK2-dependent phosphorylation controls cytotoxic RIPK1 signalling in inflammation and infection. *Nat Cell Biol* **19**, 1248-1259 (2017).
65. Newton, K. *et al.* Cleavage of RIPK1 by caspase-8 is crucial for limiting apoptosis and necroptosis. *Nature* **574**, 428-431 (2019).
66. Medema, J.P. *et al.* FLICE is activated by association with the CD95 death-inducing signaling complex (DISC). *EMBO J* **16**, 2794-2804 (1997).
67. Medema, J.P. *et al.* Cleavage of FLICE (caspase-8) by granzyme B during cytotoxic T lymphocyte-induced apoptosis. *Eur J Immunol* **27**, 3492-3498 (1997).
68. Scaffidi, C., Medema, J.P., Krammer, P.H. & Peter, M.E. FLICE is predominantly expressed as two functionally active isoforms, caspase-8/a and caspase-8/b. *J Biol Chem* **272**, 26953-26958 (1997).
69. Darding, M. & Meier, P. IAPs: guardians of RIPK1. *Cell Death Differ* **19**, 58-66 (2012).
70. Dillon, C.P. *et al.* Survival function of the FADD-CASPASE-8-cFLIP(L) complex. *Cell Rep* **1**, 401-407 (2012).
71. Feoktistova, M. *et al.* cIAPs block Ripoptosome formation, a RIP1/caspase-8 containing intracellular cell death complex differentially regulated by cFLIP isoforms. *Mol Cell* **43**, 449-463 (2011).
72. Pop, C. *et al.* FLIP(L) induces caspase 8 activity in the absence of interdomain caspase 8 cleavage and alters substrate specificity. *Biochem J* **433**, 447-457 (2011).
73. Scaffidi, C., Schmitz, I., Krammer, P.H. & Peter, M.E. The role of c-FLIP in modulation of CD95-induced apoptosis. *J Biol Chem* **274**, 1541-1548 (1999).

74. Wachter, T. *et al.* cFLIPL inhibits tumor necrosis factor-related apoptosis-inducing ligand-mediated NF-kappaB activation at the death-inducing signaling complex in human keratinocytes. *J Biol Chem* **279**, 52824-52834 (2004).
75. Luo, X., Budihardjo, I., Zou, H., Slaughter, C. & Wang, X. Bid, a Bcl2 interacting protein, mediates cytochrome c release from mitochondria in response to activation of cell surface death receptors. *Cell* **94**, 481-490 (1998).
76. Gross, A. *et al.* Caspase cleaved BID targets mitochondria and is required for cytochrome c release, while BCL-XL prevents this release but not tumor necrosis factor-R1/Fas death. *J Biol Chem* **274**, 1156-1163 (1999).
77. Li, H., Zhu, H., Xu, C.J. & Yuan, J. Cleavage of BID by caspase 8 mediates the mitochondrial damage in the Fas pathway of apoptosis. *Cell* **94**, 491-501 (1998).
78. Eskes, R., Desagher, S., Antonsson, B. & Martinou, J.C. Bid induces the oligomerization and insertion of Bax into the outer mitochondrial membrane. *Mol Cell Biol* **20**, 929-935 (2000).
79. Wei, M.C. *et al.* tBID, a membrane-targeted death ligand, oligomerizes BAK to release cytochrome c. *Genes Dev* **14**, 2060-2071 (2000).
80. Du, C., Fang, M., Li, Y., Li, L. & Wang, X. Smac, a mitochondrial protein that promotes cytochrome c-dependent caspase activation by eliminating IAP inhibition. *Cell* **102**, 33-42 (2000).
81. Zou, H., Henzel, W.J., Liu, X., Lutschg, A. & Wang, X. Apaf-1, a human protein homologous to C. elegans CED-4, participates in cytochrome c-dependent activation of caspase-3. *Cell* **90**, 405-413 (1997).
82. Zou, H., Li, Y., Liu, X. & Wang, X. An APAF-1.cytochrome c multimeric complex is a functional apoptosome that activates procaspase-9. *J Biol Chem* **274**, 11549-11556 (1999).
83. Wilson, N.S., Dixit, V. & Ashkenazi, A. Death receptor signal transducers: nodes of coordination in immune signaling networks. *Nat Immunol* **10**, 348-355 (2009).
84. Srinivasula, S.M., Ahmad, M., Fernandes-Alnemri, T. & Alnemri, E.S. Autoactivation of procaspase-9 by Apaf-1-mediated oligomerization. *Mol Cell* **1**, 949-957 (1998).
85. Acehan, D. *et al.* Three-dimensional structure of the apoptosome: implications for assembly, procaspase-9 binding, and activation. *Mol Cell* **9**, 423-432 (2002).
86. Vanden Berghe, T. *et al.* Determination of apoptotic and necrotic cell death in vitro and in vivo. *Methods* **61**, 117-129 (2013).
87. Vanden Berghe, T., Linkermann, A., Jouan-Lanhouet, S., Walczak, H. & Vandenabeele, P. Regulated necrosis: the expanding network of non-apoptotic cell death pathways. *Nat Rev Mol Cell Biol* **15**, 135-147 (2014).
88. Degterev, A. *et al.* Chemical inhibitor of nonapoptotic cell death with therapeutic potential for ischemic brain injury. *Nat Chem Biol* **1**, 112-119 (2005).
89. Green, D.R. The Coming Decade of Cell Death Research: Five Riddles. *Cell* **177**, 1094-1107 (2019).
90. O'Donnell, M.A. *et al.* Caspase 8 inhibits programmed necrosis by processing CYLD. *Nat Cell Biol* **13**, 1437-1442 (2011).
91. Moquin, D.M., McQuade, T. & Chan, F.K. CYLD deubiquitinates RIP1 in the TNFalpha-induced necrosome to facilitate kinase activation and programmed necrosis. *PLoS One* **8**, e76841 (2013).
92. de Almagro, M.C. *et al.* Coordinated ubiquitination and phosphorylation of RIP1 regulates necroptotic cell death. *Cell Death Differ* **24**, 26-37 (2017).
93. Zhang, Y. *et al.* RIP1 autophosphorylation is promoted by mitochondrial ROS and is essential for RIP3 recruitment into necrosome. *Nat Commun* **8**, 14329 (2017).
94. Li, J. *et al.* The RIP1/RIP3 necrosome forms a functional amyloid signaling complex required for programmed necrosis. *Cell* **150**, 339-350 (2012).
95. Sun, X., Yin, J., Starovasnik, M.A., Fairbrother, W.J. & Dixit, V.M. Identification of a novel homotypic interaction motif required for the phosphorylation of receptor-interacting protein (RIP) by RIP3. *J Biol Chem* **277**, 9505-9511 (2002).

96. Cho, Y.S. *et al.* Phosphorylation-driven assembly of the RIP1-RIP3 complex regulates programmed necrosis and virus-induced inflammation. *Cell* **137**, 1112-1123 (2009).
97. He, S. *et al.* Receptor interacting protein kinase-3 determines cellular necrotic response to TNF-alpha. *Cell* **137**, 1100-1111 (2009).
98. Zhang, D.W. *et al.* RIP3, an energy metabolism regulator that switches TNF-induced cell death from apoptosis to necrosis. *Science* **325**, 332-336 (2009).
99. Wu, X.N. *et al.* Distinct roles of RIP1-RIP3 hetero- and RIP3-RIP3 homo-interaction in mediating necroptosis. *Cell Death Differ* **21**, 1709-1720 (2014).
100. Zhao, J. *et al.* Mixed lineage kinase domain-like is a key receptor interacting protein 3 downstream component of TNF-induced necrosis. *Proc Natl Acad Sci U S A* **109**, 5322-5327 (2012).
101. Sun, L. *et al.* Mixed lineage kinase domain-like protein mediates necrosis signaling downstream of RIP3 kinase. *Cell* **148**, 213-227 (2012).
102. Murphy, J.M. *et al.* The pseudokinase MLKL mediates necroptosis via a molecular switch mechanism. *Immunity* **39**, 443-453 (2013).
103. Chen, W. *et al.* Diverse sequence determinants control human and mouse receptor interacting protein 3 (RIP3) and mixed lineage kinase domain-like (MLKL) interaction in necroptotic signaling. *J Biol Chem* **288**, 16247-16261 (2013).
104. McQuade, T., Cho, Y. & Chan, F.K. Positive and negative phosphorylation regulates RIP1- and RIP3-induced programmed necrosis. *Biochem J* **456**, 409-415 (2013).
105. Cai, Z. *et al.* Plasma membrane translocation of trimerized MLKL protein is required for TNF-induced necroptosis. *Nat Cell Biol* **16**, 55-65 (2014).
106. Gong, Y.N. *et al.* ESCRT-III Acts Downstream of MLKL to Regulate Necroptotic Cell Death and Its Consequences. *Cell* **169**, 286-300 e216 (2017).
107. Dondelinger, Y. *et al.* MLKL compromises plasma membrane integrity by binding to phosphatidylinositol phosphates. *Cell Rep* **7**, 971-981 (2014).
108. Ros, U. *et al.* Necroptosis Execution Is Mediated by Plasma Membrane Nanopores Independent of Calcium. *Cell Rep* **19**, 175-187 (2017).
109. Petrie, E.J. *et al.* Conformational switching of the pseudokinase domain promotes human MLKL tetramerization and cell death by necroptosis. *Nat Commun* **9**, 2422 (2018).
110. Davies, K.A. *et al.* The brace helices of MLKL mediate interdomain communication and oligomerisation to regulate cell death by necroptosis. *Cell Death Differ* **25**, 1567-1580 (2018).
111. Hildebrand, J.M. *et al.* Activation of the pseudokinase MLKL unleashes the four-helix bundle domain to induce membrane localization and necroptotic cell death. *Proc Natl Acad Sci U S A* **111**, 15072-15077 (2014).
112. Newton, K. & Manning, G. Necroptosis and Inflammation. *Annu Rev Biochem* **85**, 743-763 (2016).
113. Newton, K. & Dixit, V.M. Signaling in innate immunity and inflammation. *Cold Spring Harb Perspect Biol* **4** (2012).
114. Cohen, P., Kelsall, I.R., Nanda, S.K. & Zhang, J. HOIL-1, an atypical E3 ligase that controls MyD88 signalling by forming ester bonds between ubiquitin and components of the Myddosome. *Adv Biol Regul* **75**, 100666 (2020).
115. Akira, S., Takeda, K. & Kaisho, T. Toll-like receptors: critical proteins linking innate and acquired immunity. *Nat Immunol* **2**, 675-680 (2001).
116. Akira, S. TLR signaling. *Curr Top Microbiol Immunol* **311**, 1-16 (2006).
117. Janeway, C.A., Jr. & Medzhitov, R. Innate immune recognition. *Annu Rev Immunol* **20**, 197-216 (2002).
118. Kawai, T. & Akira, S. The role of pattern-recognition receptors in innate immunity: update on Toll-like receptors. *Nat Immunol* **11**, 373-384 (2010).
119. Poltorak, A. *et al.* Defective LPS signaling in C3H/HeJ and C57BL/10ScCr mice: mutations in Tlr4 gene. *Science* **282**, 2085-2088 (1998).

120. Kang, S.M. & Compans, R.W. Host responses from innate to adaptive immunity after vaccination: molecular and cellular events. *Mol Cells* **27**, 5-14 (2009).
121. Takeuchi, O. & Akira, S. Toll-like receptors; their physiological role and signal transduction system. *Int Immunopharmacol* **1**, 625-635 (2001).
122. Takeuchi, O. & Akira, S. MyD88 as a bottle neck in Toll/IL-1 signaling. *Curr Top Microbiol Immunol* **270**, 155-167 (2002).
123. Takeuchi, O. *et al.* Differential roles of TLR2 and TLR4 in recognition of gram-negative and gram-positive bacterial cell wall components. *Immunity* **11**, 443-451 (1999).
124. Gewirtz, A.T., Navas, T.A., Lyons, S., Godowski, P.J. & Madara, J.L. Cutting edge: bacterial flagellin activates basolaterally expressed TLR5 to induce epithelial proinflammatory gene expression. *J Immunol* **167**, 1882-1885 (2001).
125. Hayashi, F. *et al.* The innate immune response to bacterial flagellin is mediated by Toll-like receptor 5. *Nature* **410**, 1099-1103 (2001).
126. Alexopoulou, L., Holt, A.C., Medzhitov, R. & Flavell, R.A. Recognition of double-stranded RNA and activation of NF-kappaB by Toll-like receptor 3. *Nature* **413**, 732-738 (2001).
127. Diebold, S.S., Kaisho, T., Hemmi, H., Akira, S. & Reis e Sousa, C. Innate antiviral responses by means of TLR7-mediated recognition of single-stranded RNA. *Science* **303**, 1529-1531 (2004).
128. Greulich, W. *et al.* TLR8 Is a Sensor of RNase T2 Degradation Products. *Cell* **179**, 1264-1275 e1213 (2019).
129. Heil, F. *et al.* Species-specific recognition of single-stranded RNA via toll-like receptor 7 and 8. *Science* **303**, 1526-1529 (2004).
130. Kruger, A. *et al.* Human TLR8 senses UR/URR motifs in bacterial and mitochondrial RNA. *EMBO Rep* **16**, 1656-1663 (2015).
131. Hidmark, A., von Saint Paul, A. & Dalpke, A.H. Cutting edge: TLR13 is a receptor for bacterial RNA. *J Immunol* **189**, 2717-2721 (2012).
132. Tenev, T. *et al.* The Ripoptosome, a signaling platform that assembles in response to genotoxic stress and loss of IAPs. *Mol Cell* **43**, 432-448 (2011).
133. Ma, Y., Temkin, V., Liu, H. & Pope, R.M. NF-kappaB protects macrophages from lipopolysaccharide-induced cell death: the role of caspase 8 and receptor-interacting protein. *J Biol Chem* **280**, 41827-41834 (2005).
134. Ruckdeschel, K. *et al.* Signaling of apoptosis through TLRs critically involves toll/IL-1 receptor domain-containing adapter inducing IFN-beta, but not MyD88, in bacteria-infected murine macrophages. *J Immunol* **173**, 3320-3328 (2004).
135. Cusson-Hermance, N., Khurana, S., Lee, T.H., Fitzgerald, K.A. & Kelliher, M.A. Rip1 mediates the Trif-dependent toll-like receptor 3- and 4-induced NF-{kappa}B activation but does not contribute to interferon regulatory factor 3 activation. *J Biol Chem* **280**, 36560-36566 (2005).
136. Meylan, E. *et al.* RIP1 is an essential mediator of Toll-like receptor 3-induced NF-kappa B activation. *Nat Immunol* **5**, 503-507 (2004).
137. Kaiser, W.J. & Offermann, M.K. Apoptosis induced by the toll-like receptor adaptor TRIF is dependent on its receptor interacting protein homotypic interaction motif. *J Immunol* **174**, 4942-4952 (2005).
138. Kaiser, W.J. *et al.* Toll-like receptor 3-mediated necrosis via TRIF, RIP3, and MLKL. *J Biol Chem* **288**, 31268-31279 (2013).
139. Cao, Z., Xiong, J., Takeuchi, M., Kurama, T. & Goeddel, D.V. TRAF6 is a signal transducer for interleukin-1. *Nature* **383**, 443-446 (1996).
140. Li, S., Strelow, A., Fontana, E.J. & Wesche, H. IRAK-4: a novel member of the IRAK family with the properties of an IRAK-kinase. *Proc Natl Acad Sci U S A* **99**, 5567-5572 (2002).
141. Ferrao, R. *et al.* IRAK4 dimerization and trans-autophosphorylation are induced by Myddosome assembly. *Mol Cell* **55**, 891-903 (2014).
142. Tan, Y. & Kagan, J.C. Innate Immune Signaling Organelles Display Natural and Programmable Signaling Flexibility. *Cell* **177**, 384-398 e311 (2019).

143. Everts, B. *et al.* TLR-driven early glycolytic reprogramming via the kinases TBK1-IKKvarepsilon supports the anabolic demands of dendritic cell activation. *Nat Immunol* **15**, 323-332 (2014).
144. Hacker, H. *et al.* Specificity in Toll-like receptor signalling through distinct effector functions of TRAF3 and TRAF6. *Nature* **439**, 204-207 (2006).
145. Gabay, C., Lamacchia, C. & Palmer, G. IL-1 pathways in inflammation and human diseases. *Nat Rev Rheumatol* **6**, 232-241 (2010).
146. Cohen, P. & Strickson, S. The role of hybrid ubiquitin chains in the MyD88 and other innate immune signalling pathways. *Cell Death Differ* **24**, 1153-1159 (2017).
147. Zinngrebe, J. *et al.* --LUBAC deficiency perturbs TLR3 signaling to cause immunodeficiency and autoinflammation. *J Exp Med* **213**, 2671-2689 (2016).
148. Sato, Y. *et al.* Specific recognition of linear ubiquitin chains by the Npl4 zinc finger (NZF) domain of the HOIL-1L subunit of the linear ubiquitin chain assembly complex. *Proc Natl Acad Sci U S A* **108**, 20520-20525 (2011).
149. Emmerich, C.H. *et al.* Activation of the canonical IKK complex by K63/M1-linked hybrid ubiquitin chains. *Proc Natl Acad Sci U S A* **110**, 15247-15252 (2013).
150. Boisson, B. *et al.* Immunodeficiency, autoinflammation and amylopectinosis in humans with inherited HOIL-1 and LUBAC deficiency. *Nat Immunol* **13**, 1178-1186 (2012).
151. Peltzer, N. *et al.* HOIP deficiency causes embryonic lethality by aberrant TNFR1-mediated endothelial cell death. *Cell Rep* **9**, 153-165 (2014).
152. Yang, Y. *et al.* Essential role of the linear ubiquitin chain assembly complex in lymphoma revealed by rare germline polymorphisms. *Cancer Discov* **4**, 480-493 (2014).
153. Fennell, L.M. *et al.* Site-specific ubiquitination of the E3 ligase HOIP regulates apoptosis and immune signaling. *EMBO J*, e103303 (2020).
154. Draber, P. *et al.* LUBAC-Recruited CYLD and A20 Regulate Gene Activation and Cell Death by Exerting Opposing Effects on Linear Ubiquitin in Signaling Complexes. *Cell Rep* **13**, 2258-2272 (2015).
155. Elliott, P.R. *et al.* Molecular basis and regulation of OTULIN-LUBAC interaction. *Mol Cell* **54**, 335-348 (2014).
156. Schaeffer, V. *et al.* Binding of OTULIN to the PUB domain of HOIP controls NF-kappaB signaling. *Mol Cell* **54**, 349-361 (2014).
157. Takiuchi, T. *et al.* Suppression of LUBAC-mediated linear ubiquitination by a specific interaction between LUBAC and the deubiquitinases CYLD and OTULIN. *Genes Cells* **19**, 254-272 (2014).
158. Elliott, P.R. & Komander, D. Regulation of Met1-linked polyubiquitin signalling by the deubiquitinase OTULIN. *FEBS J* **283**, 39-53 (2016).
159. Komander, D. *et al.* Molecular discrimination of structurally equivalent Lys 63-linked and linear polyubiquitin chains. *EMBO Rep* **10**, 466-473 (2009).
160. Zhang, J., Clark, K., Lawrence, T., Peggie, M.W. & Cohen, P. An unexpected twist to the activation of IKKbeta: TAK1 primes IKKbeta for activation by autophosphorylation. *Biochem J* **461**, 531-537 (2014).
161. Tokunaga, F. *et al.* Specific recognition of linear polyubiquitin by A20 zinc finger 7 is involved in NF-kappaB regulation. *EMBO J* **31**, 3856-3870 (2012).
162. Verhelst, K. *et al.* A20 inhibits LUBAC-mediated NF-kappaB activation by binding linear polyubiquitin chains via its zinc finger 7. *EMBO J* **31**, 3845-3855 (2012).
163. Polykratis, A. *et al.* A20 prevents inflammasome-dependent arthritis by inhibiting macrophage necroptosis through its ZnF7 ubiquitin-binding domain. *Nat Cell Biol* **21**, 731-742 (2019).
164. Martens, A. *et al.* Two distinct ubiquitin-binding motifs in A20 mediate its anti-inflammatory and cell-protective activities. *Nat Immunol* **21**, 381-387 (2020).
165. Priem, D. *et al.* A20 protects cells from TNF-induced apoptosis through linear ubiquitin-dependent and -independent mechanisms. *Cell Death Dis* **10**, 692 (2019).

166. Wertz, I.E. *et al.* De-ubiquitination and ubiquitin ligase domains of A20 downregulate NF-kappaB signalling. *Nature* **430**, 694-699 (2004).
167. Wertz, I.E. *et al.* Phosphorylation and linear ubiquitin direct A20 inhibition of inflammation. *Nature* **528**, 370-375 (2015).
168. Cockram, P.E. *et al.* Ubiquitination in the regulation of inflammatory cell death and cancer. *Cell Death Differ* **28**, 591-605 (2021).
169. Kumari, S. *et al.* Sharpin prevents skin inflammation by inhibiting TNFR1-induced keratinocyte apoptosis. *Elife* **3** (2014).
170. Rickard, J.A. *et al.* TNFR1-dependent cell death drives inflammation in Sharpin-deficient mice. *Elife* **3** (2014).
171. Peltzer, N. *et al.* LUBAC is essential for embryogenesis by preventing cell death and enabling haematopoiesis. *Nature* **557**, 112-117 (2018).
172. Zeng, C., Xiong, D., Zhang, K. & Yao, J. Shank-associated RH domain interactor signaling in tumorigenesis. *Oncol Lett* **20**, 2579-2586 (2020).
173. Seymour, R.E. *et al.* Spontaneous mutations in the mouse Sharpin gene result in multiorgan inflammation, immune system dysregulation and dermatitis. *Genes Immun* **8**, 416-421 (2007).
174. Sharma, B.R. *et al.* Innate immune adaptor MyD88 deficiency prevents skin inflammation in SHARPIN-deficient mice. *Cell Death Differ* **26**, 741-750 (2019).
175. Wang, K. *et al.* Whole-genome DNA/RNA sequencing identifies truncating mutations in RBCK1 in a novel Mendelian disease with neuromuscular and cardiac involvement. *Genome Med* **5**, 67 (2013).
176. Nilsson, J. *et al.* Polyglucosan body myopathy caused by defective ubiquitin ligase RBCK1. *Ann Neurol* **74**, 914-919 (2013).
177. Boisson, B. *et al.* Human HOIP and LUBAC deficiency underlies autoinflammation, immunodeficiency, amylopectinosis, and lymphangiectasia. *J Exp Med* **212**, 939-951 (2015).
178. Shimizu, S. *et al.* Differential Involvement of the Npl4 Zinc Finger Domains of SHARPIN and HOIL-1L in Linear Ubiquitin Chain Assembly Complex-Mediated Cell Death Protection. *Mol Cell Biol* **36**, 1569-1583 (2016).
179. Fiil, B.K. *et al.* OTULIN restricts Met1-linked ubiquitination to control innate immune signaling. *Mol Cell* **50**, 818-830 (2013).
180. Douglas, T. & Saleh, M. Post-translational Modification of OTULIN Regulates Ubiquitin Dynamics and Cell Death. *Cell Rep* **29**, 3652-3663 e3655 (2019).
181. Zhao, M. *et al.* Non-proteolytic ubiquitination of OTULIN regulates NF-kappaB signaling pathway. *J Mol Cell Biol* **12**, 163-175 (2020).
182. Lee, E.G. *et al.* Failure to regulate TNF-induced NF-kappaB and cell death responses in A20-deficient mice. *Science* **289**, 2350-2354 (2000).
183. Jono, H. *et al.* NF-kappaB is essential for induction of CYLD, the negative regulator of NF-kappaB: evidence for a novel inducible autoregulatory feedback pathway. *J Biol Chem* **279**, 36171-36174 (2004).
184. Damgaard, R.B. *et al.* OTULIN deficiency in ORAS causes cell type-specific LUBAC degradation, dysregulated TNF signalling and cell death. *EMBO Mol Med* **11** (2019).
185. Damgaard, R.B. *et al.* The Deubiquitinase OTULIN Is an Essential Negative Regulator of Inflammation and Autoimmunity. *Cell* **166**, 1215-1230 e1220 (2016).
186. Zhou, Q. *et al.* Biallelic hypomorphic mutations in a linear deubiquitinase define otulipenia, an early-onset autoinflammatory disease. *Proc Natl Acad Sci U S A* **113**, 10127-10132 (2016).
187. Damgaard, R.B. *et al.* OTULIN protects the liver against cell death, inflammation, fibrosis, and cancer. *Cell Death Differ* **27**, 1457-1474 (2020).
188. Verboom, L. *et al.* OTULIN Prevents Liver Inflammation and Hepatocellular Carcinoma by Inhibiting FADD- and RIPK1 Kinase-Mediated Hepatocyte Apoptosis. *Cell Rep* **30**, 2237-2247 e2236 (2020).

189. Nikolaou, K. *et al.* Inactivation of the deubiquitinase CYLD in hepatocytes causes apoptosis, inflammation, fibrosis, and cancer. *Cancer Cell* **21**, 738-750 (2012).
190. van Wijk, S.J.L. *et al.* Linear ubiquitination of cytosolic Salmonella Typhimurium activates NF-kappaB and restricts bacterial proliferation. *Nat Microbiol* **2**, 17066 (2017).
191. Noad, J. *et al.* LUBAC-synthesized linear ubiquitin chains restrict cytosol-invading bacteria by activating autophagy and NF-kappaB. *Nat Microbiol* **2**, 17063 (2017).
192. Damgaard, R.B. *et al.* The ubiquitin ligase XIAP recruits LUBAC for NOD2 signaling in inflammation and innate immunity. *Mol Cell* **46**, 746-758 (2012).
193. Belokhvostova, D. *et al.* Homeostasis, regeneration and tumour formation in the mammalian epidermis. *Int J Dev Biol* **62**, 571-582 (2018).
194. Rognoni, E. & Watt, F.M. Skin Cell Heterogeneity in Development, Wound Healing, and Cancer. *Trends Cell Biol* **28**, 709-722 (2018).
195. Watt, F.M. Mammalian skin cell biology: at the interface between laboratory and clinic. *Science* **346**, 937-940 (2014).
196. Lynch, M.D. & Watt, F.M. Fibroblast heterogeneity: implications for human disease. *J Clin Invest* **128**, 26-35 (2018).
197. Pasparakis, M., Haase, I. & Nestle, F.O. Mechanisms regulating skin immunity and inflammation. *Nat Rev Immunol* **14**, 289-301 (2014).
198. Wallach, D., Kang, T.B. & Kovalenko, A. Concepts of tissue injury and cell death in inflammation: a historical perspective. *Nat Rev Immunol* **14**, 51-59 (2014).
199. Witt, A. & Vucic, D. Diverse ubiquitin linkages regulate RIP kinases-mediated inflammatory and cell death signaling. *Cell Death Differ* **24**, 1160-1171 (2017).
200. Nenci, A. *et al.* Epithelial NEMO links innate immunity to chronic intestinal inflammation. *Nature* **446**, 557-561 (2007).
201. Nenci, A. *et al.* Skin lesion development in a mouse model of incontinentia pigmenti is triggered by NEMO deficiency in epidermal keratinocytes and requires TNF signaling. *Hum Mol Genet* **15**, 531-542 (2006).
202. Pasparakis, M. *et al.* TNF-mediated inflammatory skin disease in mice with epidermis-specific deletion of IKK2. *Nature* **417**, 861-866 (2002).
203. Pasparakis, M., Schmidt-Supprian, M. & Rajewsky, K. IkappaB kinase signaling is essential for maintenance of mature B cells. *J Exp Med* **196**, 743-752 (2002).
204. Kist, M. & Vucic, D. Cell death pathways: intricate connections and disease implications. *EMBO J*, e106700 (2021).
205. Kovalenko, A. *et al.* Caspase-8 deficiency in epidermal keratinocytes triggers an inflammatory skin disease. *J Exp Med* **206**, 2161-2177 (2009).
206. Lee, P. *et al.* Dynamic expression of epidermal caspase 8 simulates a wound healing response. *Nature* **458**, 519-523 (2009).
207. Bonnet, M.C. *et al.* The adaptor protein FADD protects epidermal keratinocytes from necroptosis in vivo and prevents skin inflammation. *Immunity* **35**, 572-582 (2011).
208. Kaiser, W.J., Upton, J.W. & Mocarski, E.S. Receptor-interacting protein homotypic interaction motif-dependent control of NF-kappa B activation via the DNA-dependent activator of IFN regulatory factors. *J Immunol* **181**, 6427-6434 (2008).
209. Rebsamen, M. *et al.* DAI/ZBP1 recruits RIP1 and RIP3 through RIP homotypic interaction motifs to activate NF-kappaB. *EMBO Rep* **10**, 916-922 (2009).
210. Ingram, J.P. *et al.* ZBP1/DAI Drives RIPK3-Mediated Cell Death Induced by IFNs in the Absence of RIPK1. *J Immunol* **203**, 1348-1355 (2019).
211. Lin, J. *et al.* RIPK1 counteracts ZBP1-mediated necroptosis to inhibit inflammation. *Nature* **540**, 124-128 (2016).
212. Jiao, H. *et al.* Z-nucleic-acid sensing triggers ZBP1-dependent necroptosis and inflammation. *Nature* **580**, 391-395 (2020).
213. Tokunaga, F. & Iwai, K. [Involvement of LUBAC-mediated linear polyubiquitination of NEMO in NF-kappaB activation]. *Tanpakushitsu Kakusan Koso* **54**, 635-642 (2009).

214. Smahi, A. *et al.* Genomic rearrangement in NEMO impairs NF-kappaB activation and is a cause of incontinentia pigmenti. The International Incontinentia Pigmenti (IP) Consortium. *Nature* **405**, 466-472 (2000).
215. Zonana, J. *et al.* A novel X-linked disorder of immune deficiency and hypohidrotic ectodermal dysplasia is allelic to incontinentia pigmenti and due to mutations in IKK-gamma (NEMO). *Am J Hum Genet* **67**, 1555-1562 (2000).
216. Dannappel, M. *et al.* RIPK1 maintains epithelial homeostasis by inhibiting apoptosis and necroptosis. *Nature* **513**, 90-94 (2014).
217. Moulin, M. *et al.* IAPs limit activation of RIP kinases by TNF receptor 1 during development. *EMBO J* **31**, 1679-1691 (2012).
218. Anderton, H., Rickard, J.A., Varigos, G.A., Lalaoui, N. & Silke, J. Inhibitor of Apoptosis Proteins (IAPs) Limit RIPK1-Mediated Skin Inflammation. *J Invest Dermatol* **137**, 2371-2379 (2017).
219. de Almagro, M.C., Goncharov, T., Newton, K. & Vucic, D. Cellular IAP proteins and LUBAC differentially regulate necrosome-associated RIP1 ubiquitination. *Cell Death Dis* **6**, e1800 (2015).
220. Peltzer, N., Darding, M. & Walczak, H. Holding RIPK1 on the Ubiquitin Leash in TNFR1 Signaling. *Trends Cell Biol* **26**, 445-461 (2016).
221. Taraborrelli, L. *et al.* LUBAC prevents lethal dermatitis by inhibiting cell death induced by TNF, TRAIL and CD95L. *Nat Commun* **9**, 3910 (2018).
222. Sundberg, J.P. *et al.* Keratinocyte-specific deletion of SHARPIN induces atopic dermatitis-like inflammation in mice. *PLoS One* **15**, e0235295 (2020).
223. Lippens, S. *et al.* Keratinocyte-specific ablation of the NF-kappaB regulatory protein A20 (TNFAIP3) reveals a role in the control of epidermal homeostasis. *Cell Death Differ* **18**, 1845-1853 (2011).
224. Devos, M. *et al.* Keratinocyte Expression of A20/TNFAIP3 Controls Skin Inflammation Associated with Atopic Dermatitis and Psoriasis. *J Invest Dermatol* **139**, 135-145 (2019).
225. Miliani de Marval, P. *et al.* CYLD inhibits tumorigenesis and metastasis by blocking JNK/AP1 signaling at multiple levels. *Cancer Prev Res (Phila)* **4**, 851-859 (2011).
226. Fernandez-Majada, V. *et al.* The tumour suppressor CYLD regulates the p53 DNA damage response. *Nat Commun* **7**, 12508 (2016).
227. Hafner, M. *et al.* Keratin 14 Cre transgenic mice authenticate keratin 14 as an oocyte-expressed protein. *Genesis* **38**, 176-181 (2004).
228. Lawlor, K.E. *et al.* RIPK3 promotes cell death and NLRP3 inflammasome activation in the absence of MLKL. *Nat Commun* **6**, 6282 (2015).
229. Vince, J.E. *et al.* Inhibitor of apoptosis proteins limit RIP3 kinase-dependent interleukin-1 activation. *Immunity* **36**, 215-227 (2012).
230. Chen, Y.E., Fischbach, M.A. & Belkaid, Y. Skin microbiota-host interactions. *Nature* **553**, 427-436 (2018).
231. Legarda, D. *et al.* CYLD Proteolysis Protects Macrophages from TNF-Mediated Auto-necroptosis Induced by LPS and Licensed by Type I IFN. *Cell Rep* **15**, 2449-2461 (2016).
232. Jin, Y.J. *et al.* Epidermal CYLD inactivation sensitizes mice to the development of sebaceous and basaloid skin tumors. *JCI Insight* **1** (2016).
233. Massoumi, R., Chmielarska, K., Hennecke, K., Pfeifer, A. & Fassler, R. Cyld inhibits tumor cell proliferation by blocking Bcl-3-dependent NF-kappaB signaling. *Cell* **125**, 665-677 (2006).
234. Shimizu, Y., Taraborrelli, L. & Walczak, H. Linear ubiquitination in immunity. *Immunol Rev* **266**, 190-207 (2015).
235. Ceccarelli, D.F. *et al.* FAM105A/OTULINL Is a Pseudodeubiquitinase of the OTU-Class that Localizes to the ER Membrane. *Structure* **27**, 1000-1012 e1006 (2019).
236. Zuo, Y. *et al.* Regulation of the linear ubiquitination of STAT1 controls antiviral interferon signaling. *Nat Commun* **11**, 1146 (2020).
237. Sarhan, J. *et al.* Constitutive interferon signaling maintains critical threshold of MLKL expression to license necroptosis. *Cell Death Differ* **26**, 332-347 (2019).

238. Yang, D. *et al.* ZBP1 mediates interferon-induced necroptosis. *Cell Mol Immunol* **17**, 356-368 (2020).
239. Rajewsky, K. *et al.* Conditional gene targeting. *J Clin Invest* **98**, 600-603 (1996).
240. Sauer, B. Inducible gene targeting in mice using the Cre/lox system. *Methods* **14**, 381-392 (1998).
241. Van Hauwermeiren, F. *et al.* Safe TNF-based antitumor therapy following p55TNFR reduction in intestinal epithelium. *J Clin Invest* **123**, 2590-2603 (2013).
242. Newton, K., Sun, X. & Dixit, V.M. Kinase RIP3 is dispensable for normal NF-kappa Bs, signaling by the B-cell and T-cell receptors, tumor necrosis factor receptor 1, and Toll-like receptors 2 and 4. *Mol Cell Biol* **24**, 1464-1469 (2004).
243. Welz, P.S. *et al.* FADD prevents RIP3-mediated epithelial cell necrosis and chronic intestinal inflammation. *Nature* **477**, 330-334 (2011).
244. Newton, K. *et al.* Activity of protein kinase RIPK3 determines whether cells die by necroptosis or apoptosis. *Science* **343**, 1357-1360 (2014).
245. Vlantis, K. *et al.* TLR-independent anti-inflammatory function of intestinal epithelial TRAF6 signalling prevents DSS-induced colitis in mice. *Gut* **65**, 935-943 (2016).
246. Nolte, H., MacVicar, T.D., Tellkamp, F. & Kruger, M. Instant Clue: A Software Suite for Interactive Data Visualization and Analysis. *Sci Rep* **8**, 12648 (2018).

6. Appendix

Acknowledgement

Prof. Dr. Manolis Pasparakis
Thank you for giving me the opportunity to do my Master project in your lab and for trusting me with this very exciting PhD project. I highly appreciate your scientific guidance, sustained encouragement and great interest in the progress of my work during that time. I am grateful for your support and mentoring during the last years!

Ulrike Goebel, Prof. Dr. Alexander Dilthey & Prof. Dr. Ivan Dikic
Many thanks for your precise work and outstanding expertise that contributed to this work!

Lucie Laurien, Trieu-My Van & Vangelis Kondylis
I am very thankful for all your support since my very first internship in this lab and for listening to all the problems that I encountered during my PhD!

Robin Schwarzer & Laurens Wachsmuth
Thank you very much for your supervision, helpful discussions and contribution to this manuscript!

ELza Garreus, Jennifer Kuth, Julia von Rhein, Edeltraud Stade & Claudia Uthoff-Hachenberg
Many thanks for all your help and outstanding technical assistant during the last years but especially thank you for all the inspiring discussions during our breaks!

Silke Röpke, Martin Hafner & Johannes Winkler
Thank you for helping me with administrative, bureaucratic and all kind of problems that came along!

Pasparakis lab
My grateful thanks to all former and current lab members for all the expertise, fruitful scientific discussions and exceptional environment that contributed to this work!

Kevin, meine Familie & Freunde
Vielen Dank für eure bedingungslose Unterstützung! Ohne euren stetigen Zuspruch, eure unerlässlichen Aufmunterungen und eure zahllosen Ablenkungen in den vergangenen Jahren wäre diese Arbeit nicht möglich gewesen!

Erklärung zur Dissertation

Hiermit versichere ich an Eides statt, dass ich die vorliegende Dissertation selbstständig und ohne die Benutzung anderer als der angegebenen Hilfsmittel und Literatur angefertigt habe. Alle Stellen, die wörtlich oder sinngemäß aus veröffentlichten und nicht veröffentlichten Werken dem Wortlaut oder dem Sinn nach entnommen wurden, sind als solche kenntlich gemacht. Ich versichere an Eides statt, dass diese Dissertation noch keiner anderen Fakultät oder Universität zur Prüfung vorgelegen hat; dass sie - abgesehen von unten angegebenen Teilpublikationen und eingebundenen Artikeln und Manuskripten - noch nicht veröffentlicht worden ist sowie, dass ich eine Veröffentlichung der Dissertation vor Abschluss der Promotion nicht ohne Genehmigung des Promotionsausschusses vornehmen werde. Die Bestimmungen dieser Ordnung sind mir bekannt. Darüber hinaus erkläre ich hiermit, dass ich die Ordnung zur Sicherung guter wissenschaftlicher Praxis und zum Umgang mit wissenschaftlichem Fehlverhalten der Universität zu Köln gelesen und sie bei der Durchführung der Dissertation zugrundeliegenden Arbeiten und der schriftlich verfassten Dissertation beachtet habe und verpflichte mich hiermit, die dort genannten Vorgaben bei allen wissenschaftlichen Tätigkeiten zu beachten und umzusetzen. Ich versichere, dass die eingereichte elektronische Fassung der eingereichten Druckfassung vollständig entspricht.

Hannah Schünke

Köln, 18.10.2021

Teilpublikation:

Schünke H, Göbel U., Dikic I., Pasparakis M., OTULIN inhibits RIPK1-mediated keratinocyte necroptosis to prevent skin inflammation in mice. *Nat Commun* **12,** 5912 (2021).